Axotomy-Induced Gene Expression in Rat Brain

I n a u g u r a l - D i s s e r t a t i o n

zur

Erlangung des Doktorgrades der

Mathematisch-Naturwissenschaftlichen Fakultät

der Heinrich-Heine-Universität Düsseldorf

vorgelegt von

Daniel Abankwa

aus Saarbrücken

Düsseldorf 2001

Gedruckt mit der Genehmigung der Mathematisch-Naturwissenschaftlichen Fakultät
der Heinrich-Heine Universität Düsseldorf

Referent: Prof. Dr. Hans Werner Müller

Koreferent: Prof. Dr. Hanns Weiss

Tag der mündlichen Prüfung: 16. November 2001

To my family

Table of Contents

1. SUMMARY

Axotomized CNS neurons do not regenerate spontaneously. Instead, only abortive axon outgrowth up to the lesion site is observed. The reasons for this limited outgrowth capacity are still unknown.

The distal transection of the fornix of the adult rat provides an experimental axotomy model, which allows the investigation of axotomy induced responses. Using this CNS lesion paradigm, part A of this thesis describes the induced molecular changes, which could be detected with histochemical techniques. In addition, the regeneration failure after immediate 2,2'-dipyridyl injection is reported. In part B, cDNA arrays were applied to identify genes, which were differentially expressed within the subiculum upon axotomy, the part of the brain, which contains the projecting neurons of the fornix.

In part A, immunohistochemistry and in situ hybridization were used to study the expression of genes, which were known to be responsive in other axotomy paradigms. Both, GAP-43 and L1 were expressed in the unlesioned subiculum, and their expression pattern was not changed between one day and four weeks after axotomy. The same was true for the calcium binding proteins calbindin d28 and parvalbumin, which were studied at two and three weeks after fornix transection, and also for the transcription factor Sox-10 and the metalloprotease rMDC15. The latter two genes were also expressed at the lesion site upon axotomy, but only Sox-10 was increased in areas, where the axons degenerated.

In addition, GAP-43 and L1 were studied in the fornix stumps, as they were known to be fast anterogradely transported in the axons. Furthermore, the degeneration marker protein clusterin was used to describe the extension of degenerative events. GAP-43 and L1 immunolabeling was found to be increased in the proximal fornix stump in a small ribbon like structure. At later times after axotomy, the expression of L1, clusterin and Sox-10 were found to be increased in degenerating segments of the fornix. The observed molecular changes suggested, that the expression of the genes studied in the subiculum remained unaltered. Moreover, the expression data within the proximal stump and at the lesion site helped to describe the spatio-temporal extension of the degenerative and regenerative events within the fornix.

In part B of this thesis, cDNA arrays were employed to characterize the transcriptional changes within the subiculum upon axotomy on a scale of about 3% of the rat genome. Datasets of sham operated controls were compared to animals displaying (i) degeneration

onset at 1 day, (ii) axonal outgrowth at 7 days and (iii) axon outgrowth arrest at the lesion site at 3 weeks after fornix transection. Therefore, a Microsoft Excel based analysis program was developed, which performed normalization of raw data, differential analysis and identification of genes, which were highly reproduced.

Out of 1185 studied genes 174 were identified to be differentially expressed in the subiculum after axotomy of the postcommissural fornix. Out of these genes, 29, 19 and 17 regulated genes were identified to be highly reproducible at stages (i), (ii) and (iii), respectively. The overall comparison of the regulated genes at stages (i) - (iii) revealed three specific gene expression patterns, but with stages (i) and (iii) sharing 18 (about 10% of all identified) genes. Among these genes were some, which are known to be functionally associated, e.g. with the proteasome, small GTPases, G proteins or the cytoskeleton, suggesting their importance in the cellular response after axotomy.

This genomics approach provides a cautious estimation for the total number of responsive neural genes following axotomy. In addition, it could be shown that the expression pattern during (ii) axonal outgrowth is dynamically changed upon (iii) growth arrest at the lesion site, which raises the question whether feedback mechanisms act retrogradely from the lesion site to change the expression pattern.

Further analysis of identified putative pathways, which could be responsible for axon outgrowth, may provide a completely new basis for the development of new therapies, which might preferentially act on the neuron after axon transection in the CNS.

2. INTRODUCTION

In order to provide profound information for the reader about the current clinical and experimental methods for the treatment of axons injuries and the molecular responses, which could be expected in response to axotomy, this introduction tries to cover these broad scientific fields, by comprehensively reviewing their latest results.

2.1 Axonal regeneration strategies in the adult mammalian CNS.

Axonal and neurite lesions occur in many neurological diseases, like for example Alzheimer's disease (AD), if neuritic plaques and neurofibrillary tangles are formed or during inflammatory processes in multiple sclerosis (MS) (Selkoe, 1999; Trapp et al., 1999; Jeffery et al., 2000). In both AD and MS associated axonal transections could be correlated with increasing mental and physical disabilities. These chronic diseases show manifestation of the full pathology over a longer period of time and it is remarkable that axonal injury was identified as a major cause of the accompanying affections.

In contrast, traumatic axonal lesions that occurs in the brain (Parker et al., 1990) or the spinal cord show an immediate dramatic effect on nervous system functions. Damage to the spinal cord, the major nervous connection from the brain to the body, leads to permanent paralysis. Within a split second all major sensory and motor functions below the site of injury are irreversably affected.

This is a very dramatic fate, especially as there is at present no cure for spinal cord injury (SCI), which would restore all or at least many of its previous functions. Standard clinical procedures comprise surgical decompression and stabilization of the severed spine. However, early start of rehabilitation is considered to be the most important step to regain as many functions as possible (DeVivo et al., 1990). A pharmacological promissing attempt was believed to be done in 1990 when the FDA (Food and Drug Administration in the USA) approved methylprednisolone for acute treatment of SCI. This corticosteroid was beneficial if given within the first eight hours of injury (Green et al., 1980; Seidl, 2000). But recent reports present contraindicating results on the efficacy of methylprednisolone administration (Short et al., 2000; Hurlbert, 2000; Coleman et al., 2000).

Among the 40 spinal cord associated clinical trials, which are listed on www.clinicaltrials.gov (January 2001), only three aimed at functional restoration after SCI (one by rehabilitative treadmill training and two others by either neuromuscular or transcranial electrical

stimulation). Other internet based information resources (like www.centerwatch.com; spinal cord injury information network on www.spinalcord.uab.edu) mentioned the following three more recent studies. A group from Purdue School of Veterinary Medicine and Indiana University School of Medicine, lead by Prof. R. Borgens and Prof. P. Nelson, wants to stimulate axonal outgrowth by extraspinal oscillating electrical fields (Borgens et al., 1987; Borgens et al., 1999). The second study of the Biomedical Research Alliance of New York (BRANY) evaluates the effects of orally administered Fampridine-SR (also known as 4-AP; 4-aminopyridine). This substance is known to block potassium channels, which became exposed after demyelination (Segal et al., 1999). And the last trial, which should be mentioned here, is conducted by the israeli company Proneuron Biotechnologies, which recruits patients for phase one clinical trials to assess the efficacy of activated, autologous macrophage implantation in complete SCI.

The framework for axon regeneration research

If restitution of all functions after SCI wants to be achieved, a complex set of requirements has to be fulfilled. These requirements could be recognized as the ultimate goal in axonal regeneration research, as complete restoration of functions would demand recapitulation of early developmental events in an adult organism. Despite this apparently insurmountable challenge, limited regeneration success has been achieved in a number of experimental cases, which aimed at resolving one or more of the following general requirements for complete regeneration:

1. survival of axotomized neurons
2. stimulation of axonal outgrowth
3. tissue repair at the lesion site
4. correct pathfinding of outgrowing axons
5. functional reinnervation

In addition to these neuronal and axonal repair steps, mechanical stabilization, rehabilitation and muscle stimulation will probably be necessary.

The diversity of the formerly mentioned approaches in the clinical phase originated from a growing number of experimental strategies, which aim at understanding and alleviating the ailments arising after SCI (for review see Caroni, 1997; Olson, 1997; Horner and Gage, 2000; Behar et al., 2000).

Since the early regeneration research of Ramon y Cajal (Ramon y Cajal, 1928), lesions to central axons in mammalia were considered to lead to a permanent loss of function. But

pioneer work by Aguayo and colleagues (Richardson et al., 1980) revived this increasingly popular field in neuroscience. The demonstrated potency for regeneration was nurtured by the notion that regeneration capabilities in adult mammals were not lost, but needed to be stimulated.

The hope that CNS axons could regenerate even in the adult animal was furthermore supported by the regeneration properties found in other animals.

It appeared that there was a hierarchical loss of regeneration capabilities,

phylogenetically:

Lower vertebrates like the zebrafish regenerated most of their spinal axons, and traversion of the lesion site was seen at six weeks after axotomy (Becker et al., 1997). But characteristic reexpression of regeneration associated genes depended on the cell type and the distance of the lesion in the spinal cord (Becker et al., 1998) .

ontogenetically among mammals:

In neonate oppossum spinal tissue neurites regenerate until myelination at postnatal day thirteen (Varga et al., 1995). However, this case could be arguable with respect to postnatal regeneration capabilities, as the apparent long lasting ability for regeneration, could be attributed to the early birth of marsupialia. The reported developmental stage could be better correlated with embryonic stages in placentalia. Nevertheless could developmental changes be correlated with a gradual loss of the CNS regeneration capability.

systemically:

While peripheral nerves do regenerate (Ide, 1996; Fu and Gordon, 1997), only regeneration tendencies are recognized in the CNS. Serotonergic and noradrenergic fibres often diplay marked regeneration efforts, while corticospinal fibres do not (Ramon-Cueto et al., 2000).

Tissue and cell transplantations as experimental treatments

The concept to transplant a permissive PNS-derived substrate into a non-permissive CNS-environment, which was introduced by Aguayo and colleagues (David and Aguayo, 1981; Benfey and Aguayo, 1982) stimulated the development of a series of tissue and cell implantation strategies. Transplanted peripheral nerves were developed further for axonal regeneration, for example by combining them with methylprednisolone application (Chen et al., 1996). The apparently better efficacy of predegenerated peripheral nerves (Dahlin, 1995; Decherchi and Gauthier, 1996; Dubuisson et al., 1997) lead to the discovery, that activated macrophages alone had an unrecognized potential to create a permissive environment and suppport lesion repair processes, thus allowing extensive axonal regeneration (Rapalino et al.,

1998). The importance of macrophage infiltration after axotomy is further supported by data from a *Xenopus* tadpole optic nerve crush paradigm, where regeneration is found after massive invasion of macrophages in the lesion site (Wilson et al., 1992).

Another variant of these cell transplantation approaches was the implantation of olfactory ensheathing cells, which were recognized as a cell type with features of both, peripheral Schwann cells and central oligodendrocytes (Li et al., 1998; Ramon-Cueto et al., 2000). Grafting of embryonic tissue (Reier et al., 1983; Schnell and Schwab, 1993; Itoh et al., 1999) and the recent embryonic stem cell implantations (McDonald et al., 1999) resulted in a certain degree of functional recovery accompanied by some axonal elongation. But to date it is not clear, which shared or unique features of these therapeutic approaches should be persued for future studies.

Application of neurotrophic substances

Cellular implants have the advantage to respond in multiple ways to the complex environment that they are placed in. They can migrate into the host tissue, therby often forming traces which could be followed by regrowing axons (Ramon-Cueto et al., 1998; Weidner et al., 1999). As a response to their environment many of the above mentioned cell types are also able to secrete neurotrophins (Schober et al., 1998; Ramon-Cueto and Avila, 1998; Meier et al., 1999). Neurotrophins were known to have neurite promoting and guidance effects in vitro (Campenot, 1994), as well as effects on neuronal survival. Therefore, it was not long until neurotrophins alone were applied to treat experimental spinal cord lesions in vivo (Schnell et al., 1994). But the effects on recovery are still not completely understood. Treatment of adult rat spinal cords with brain-derived neurotrophic factor (BDNF) stimulated hindlimb activity, with sprouting of cholinergic fibres only at the lesion site without long distance regeneration (Jakeman et al., 1998). In similarity to these results, neurotrophin-3 (NT-3) containing collagen gels attracted proximal axons, but did not result in elongation caudally to the lesion (Houweling et al., 1998), while others were able to demonstrate a correlation of neurotrophin stimulated axonal outgrowth at the dorsal root entry zone with functional recovery (Ramer et al., 2000).

Unfortunately, clinical trials have also revealed side effects of neurotrophin treatment, such as pain and weight loss (Olson, 1993). Thus strategies were developed, such as the implantation of genetically manipulated fibroblasts (Nakahara et al., 1996; Grill et al., 1997; Liu et al., 1999a), Schwann cells (Tuszynski et al., 1998) and neural stem cells (Liu et al., 1999b),

which created experimental cellular tools for long lasting, low dose application of neurotrophins.

Neutralization of inhibitory molecules at the lesion site

Another mainstream of regeneration research followed the early work of Ramón y Cajal and initial transplantation results, which demonstrated the inhibitory nature of the lesion site and the white matter in the mammalian CNS. Neutralization of the inhibitory effect of CNS white matter was demostrated for the first time by the administration of the M-type immunoglobulin IN1 (Caroni and Schwab, 1989), which lead to axonal regeneration and functional recovery (reviewed by Tatagiba et al., 1997). This concept to neutralize myelin resident inhibitors stimulated new experimental therapeutic approaches. Disruption of myelin by x-ray irradiation (Savio and Schwab, 1990; Kalderon and Fuks, 1996) and by immunological means (Keirstead et al., 1995; Huang et al., 1999) both proved that myelin removal could enhance regeneration.

Reports on cloning of the IN1 antigen, Nogo-A, promised to provide more insight into the axon inhibitory mechanisms associated with this myelin resident protein (GrandPre et al., 2000; Chen et al., 2000; Prinjha et al., 2000). Surprisingly, these reports revealed that the inhibitory aminoterminal domain of the membrane anchored Nogo-A was localized to the cytoplasmic face of the oligodendrocyte plasma membrane. But an additional small extracellular fragment of the protein was also shown to possess growth cone collapse activity. Nogo was identified to belong to the family of reticulon proteins, which are associated with the endoplasmic reticulum (GrandPre et al., 2000). But none of the extracellular fragments of the other reticulon family members displayed a collapsing activity, like it was recognized for Nogo isoforms. Investigations by Fournier et al., lead to the isolation of the corresponding glycosylphosphatidylinositol-linked receptor for this extracellular fragment, which might present a new target for the development of agents, which promote axonal outgrowth (Fournier et al., 2001).

Although the inhibitory nature of CNS white matter is widely accepted, some reports demonstrated surprising results, showing a permissiveness of this apparently hostile substrate. Neuroblasts grafted into the striatum (Wictorin et al., 1990) or adult dorsal root ganglia (DRG) neurons microimplanted directly into the corpus callosum or fimbria (Davies et al., 1997) extended their axons for considerable distances along or within the white matter. This apparent contradiction to the aforementioned approaches could, on the one hand, be explained by myelin geometry, upon which its permissive or inhibitory nature could rely on (Pettigrew

and Crutcher, 1999). Neurons cultured on native cryostatsections of mature rat CNS tissue, were found to extend their neurons preferentially on grey matter. But interestingly, white matter appeared to support neurite outgrowth, if neurites elongated parallel to existing myelinated tracts, but not nonparallel outgrowth.

On the other hand it could be shown that elongating axons stop or turn at presumptive barriers consisting of chondroitinsulphate proteoglycans (CSPGs) (Davies et al., 1997). These extracellular matrix (ECM) proteins were found to be expressed at axon lesion sites (Stichel et al., 1995b; Lausberg, 2000) and were shown to inhibit neurite outgrowth in vitro (Fawcett and Asher, 1999). CSPGs are produced or induced by fibroblasts, astrocytes and macrophages (Fitch and Silver, 1997), interestingly, with the latter cells being also axon regeneration stimulating in other experimental paradigms (Rapalino et al., 1998). Targeting of CSPG inhibition with CSPG degrading matrix metalloprotease, MMP-2, was successful in vitro (Zuo et al., 1998), while in vivo the transected fornix did not regenerate after chondroitinase treatment (Lausberg, 2000). The composition of the ECM at the lesion site is influenced by a complex array of inflammatory cytokines, which are known to stimulate reactive gliosis (Logan et al., 1994) or induce ECM formation, like TGF-β1, which upregulates tenascin synergistically with basic fibroblast growth factor (bFGF) (Smith and Hale, 1997). Other effectors like interferon-γ acted against scarring, but did not increase axonal outgrowth (DiProspero et al., 1997).

As axons grow out along axonal guidance cues during development, either by attractive or inhibitory means, the expression of such molecules at CNS lesion sites was analysed. Indeed, the repulsion mediating proteins semaphorin 3A (Pasterkamp et al., 1999) and EphB3 (Miranda et al., 1999) were found to be expressed at several CNS lesion sites, either within fibroblasts or white matter resident astrocytes and grey matter motor neurons, respectively, and might therefore be involved in axonal outgrowth inhibiton.

In addition to this potential role in barrier formation, correct expression of guidance cues along the former pathways is a prerequisite for successful target reinnervation. In some cases existing guidance cues were followed by grafted cells. Transplanted into adult rat striatum, human telencephalic neuroblasts followed major myelinated axon tracts up to their putative target regions in the substantia nigra, the pontine nuclei and the cervical spinal cord (Wictorin et al., 1990). Similar results were obtained with human dopaminergic neurons, which were also grafted into the rat brain and specifically extended tyrosine-hydroxylase positive fibres into the nigro-striatal pathway up to the deafferented striatum (Stromberg et al., 1992).

Expression of attractive guidance cues, such as L1 and PSA-NCAM along regenerated tracts (Aubert et al., 1998; Weidner et al., 1999) also served as a template for artificial bridges. Bridges are especially important to traverse a gap in the severed spinal cord, and were shown, to consist of synthetic sheaths, filled with viable Schwann cells (Xu et al., 1999; Steuer et al., 1999) or consist solely of modified polymers (Woerly et al., 1999; Holmes et al., 2000), which could also be enriched with neurotrophic growth factors, like NT-3 (Houweling et al., 1998).

Neuroprotective and -replacement treatments

Although loss of projecting motor neurons in the cerebral cortex is not a major concern after SCI, motor neuron loss at the lesion site within the spinal cord could be observed after chronic cervical cord compression and decompression (Harkey et al., 1995). Moreover, secondary tissue damage is known to further complicate injuries (Lu et al., 2000). Neuroprotection is the primary prerequisite after lesion to the optic nerve. Apoptotic loss of retinal ganglion cells upon axotomy was treated with a number of anti apoptotic interventions, such as expression of the anti apoptotic protein p35 (Kugler et al., 1999), injection of aurintricarboxylic acid into the eye (Heiduschka and Thanos, 2000) or cataractogenic lens injury (Fischer et al., 2000). Expression of the proto-oncogene bcl-2 was shown to be anti apoptotic, by protecting red nucleus neurons after cervical axotomy (Zhou et al., 1999) and regeneration stimulatory for axotomized retinal ganglion cells (Chen et al., 1997). Additional knowledge on the preservation of neurons was gathered by studying neurodegenerative diseases, where neurotrophins or synthetic analogues were successful in preventing neuronal loss (Skaper and Walsh, 1998).

Neuron replacement with neuronal (Brustle and McKay, 1996; Whittemore, 1999) or embryonic stem cells (McDonald et al., 1999) was also applied after spinal injury. The small population of mitotically active neuronal stem cells, which wer also found in the human dentate gyrus (Eriksson et al., 1998), could serve as a reservoir for autologous neuron replacement in the future. Especially in primates these cells are sparse. Therefore, it was very important to find stem cells from the bone marrow (Woodbury et al., 2000) or embryonic stem cells (Lee et al., 2000b), which could be differentiated into neurons. Adaptation of these cells to the local environment could be advantageous for transplantation (Gaiano and Fishell, 1998). Whether these neurons would be able to extend long axons down the spinal cord remains to be shown.

In conclusion, many different experimental strategies for neuroreplacement, neuroprotection and stimulation of axonal outgrowth have contributed to the understanding of nervous system functions in the axotomy disease state. Although limitted functional recovery was often described, not all examples conclusively demonstrated that the improvements completely rely on the treatment and its postulated effects (Horner and Gage, 2000). This could in part be attributed to the difficulty to dissociate beneficial effects of the therapeutic intervention from accompanying spontaneous plastic changes. Likewise, improved sensoric and motoric abailities could not always be strictly correlated to the length of regenerated axons. Only a few studies demonstrated loss of functions, which were gained by the therapy, after relesioning. Nevertheless, the existing array of therapeutic approaches will hopefully be valuable in the development of new therapies for a variety of lesions to central nervous system axons.

2.2 Insight into the molecular machinery involved in axon outgrowth

Axon outgrowth in the developing organism is a highly complex task. The complexity of synaptic connections in the brain easily outnumbers the number of possible instructions directly encoded in an organism's genome. Therefore this complex network must be realized in a molecular structure and interaction-based code. This chapter intends to provide an overview over general aspects of signal transduction from the growth cone membrane down to the cytoskeleton. Special emphasis will be put on signalling mechanisms during growth cone turning, the collapse response and axotomy induced molecular responses. In additon, important families of guidance proteins will be briefly introduced.

2.2.1 Second messenger cascades activated during growth cone turning, collapse, and after axotomy

Calcium

The importance of calcium as a second messenger in the eucaryotic cell is well established (Berridge, 1998; Berridge et al., 2000), but its fundamental role in growth cone navigation is still elusive (Goldberg and Grabham, 1999). In an *Xenopus* embryonic spinal cord explant model the increase of the number of calcium transients could be associated with axon stalling or retraction, and were most remarkably at presumptive pathway choice points (Gomez and

Spitzer, 1999). As it is conceived that filopodia sense guidance cues during growth cone navigation, they should be the first transducing structures of extracellular guidance information. Indeed, in vitro experiments demonstrated that individual filopodia increased their number of calcium transients upon stalling (Gomez et al., 2001). In contrast to the complete growth cone, calcium influx through non voltage-gated channels was not amplified in filopodia by internal calcium stores. But, depending on the substrate, a consecutive global rise of the calcium level within the growth cone core demonstrated the trigger function of filopodial calcium influx. Moreover, a repulsive turning response could be induced by elevating filopodial calcium transients on one side of the growth cone by a step gradient in the substrate. This in vitro behaviour could represent an example of similar choice point responses in the *Xenopus* spinal cord explant model.

The increase in the number of calcium transients corresponds well with the observed effects of known axon repellents (increase of calcium) and attractants (decrease of calcium). Calcium release from intracellular stores and influx through (probably L-type) membrane calcium channels was required for netrin-1 induced attraction, while blocking one or both of these calcium sources resulted in repulsion. This attractive response triggered by high-level calcium, as opposed to repulsion by low-level calcium signals could indeed provide complementary guidance elements (Hong et al., 2000). Similar results were obtained in experiments using focal laser-induced photolysis (FLIP) of caged calcium within the growth cone. Here, repulsion of the growth cone away from the side where calcium was elevated was found, while (overall extracellular and) intracellular calcium levels were low. The increased calcium transients during axon stalling the spinal cord explant model (Gomez and Spitzer, 1999) could result in increased calcineurin activity, which dephosphorylates GAP-43 and thus decreases actin polymerisation (Lautermilch and Spitzer, 2000). On the opposite, attraction of the growth cone to the side of induced calcium elevation was observed, if overall calcium was high, suggesting low and high threshold activation of downstream molecules (Zheng, 2000). The adjustment of the intracellular calcium level would therefore be critical for the attractive or repulsive response of the same guidance cue.

Guidance mechanisms involving calcium apparently become further complicated, if the stimulus history of the growth cone response is taken into account. Laminin induced turning or electrically induced growth cone collapse rendered growth cones insensitive to a second identical stimulus. This phenomenon was shown to be associated with calcium/calmodulin-dependent protein kinase II (CaMKII) (Diefenbach et al., 2000). One explanation for this

decreased collapse sensitivity could be the above mentioned setting of the intracellular calcium level, which could be decicive for an attractive or repulsive response.
Therefore, the simple correlation of high calcium levels and no transients resulting in attraction and low calcium levels with many transients, resulting in repulsion, with subsequent disensitization is an attractive one. But as opposed to growth cone behaviour, high amplitude and high frequency calcium transients, implicated in neuronal migration, enhanced cell movement (Komuro and Rakic, 1998). Molecular models explaining these apparently similar behaviours unambigously need to be defined.

Cyclic nucleotides

Growth cone navigation becomes even more complex, if cyclic-adenosinemonophosphate (cAMP) associated effects are considered. Decreasing extracellular (and concomitantly intracellular) calcium, increases the advance of elongating neurites, but renders them insensitive to attractive molecules, such as brain derived neurotrophic factor (BDNF), which is signalling through a cAMP/protein kinase A (PKA) dependent pathway. Under standard calcium conditions, addition of a cAMP competitor, PKA inhibitor or an overall decrease in the cAMP level resulted in a switch of the turning response induced by certain attractive guidance molecules, such as netrin-1, from attraction to repulsion. On the other hand, PKA activation or cAMP increase enhanced attractive turning (Ming et al., 1997; Song et al., 1997). Netrin-1 interaction with adenosine receptor A2b was shown to be required for netrin-dependent axonal outgrowth. This G protein coupled receptor was identified as a DCC (deleted in colorectal cancer) interacting receptor, thus implicating DCC only indirectly into netrin-mediated axonal outgrowth. Activation of A2b to stimulate cAMP accumulation, could provide a missing link for guidance molecule induced changes in cAMP levels (Corset et al., 2000). But these data were recently compromised by a report, showing that netrin-1 binding to DCC derepresses cytoplasmic domain multimerization of the receptor. Furthermore, the cytoplasmic P3 domain was shown to be required for this self-association of the cytoplasmic DCC domain and sufficient for function of DCC as a chemoattractant (Stein et al., 2001).
In similarity to the cAMP associated switch response, attractive or repulsive guidance molecules displayed dependence on cyclic guanosinemonophosphate (cGMP) levels. But this pathway was shown to be independent of extracellular calcium levels and activation of cGMP signalling resulted in a switch from repulsion to attraction (Song et al., 1998).
In conclusion, these results demonstrated that growth cone navigation is critically regulated by intracellular calcium and cyclic nucleotide levels. These levels may depend on neuron

type, neuron age and also the path an axon has already traveled. Whether levels of intracellular calcium or cyclic nucleotides vary to the same extend in vivo, as it has been demonstrated in vitro remains to be shown.

Growth cone collapse

Another well known neurite response, the growth cone collapse, was correlated with a rise in intracellular calcium in some cases (Loschinger et al., 1997), while others clearly demonstrated independence from calcium levels within the growth cone (Ivins et al., 1991). This apparent contradiction may depend on the developmental stage of the studied neurites, as only adult rat DRG or chick RGC neurons were found to display a long lasting collapse response with concomitant calcium rise, while their embryonic counterparts collapsed only transiently, with only small calcium elevations (Bandtlow and Loschinger, 1997). Like during guidance events, different signalling pathways, involving small GTPases or phopholipase A2 and lipoxygenase, could be responsible for the collapse response (Kuhn et al., 1999; de La Houssaye et al., 1999). In the end, the collapse signalling cascades were shown to converge on cytoskeletal rearrangments. Filamentous actin depolymerization was found to be a characteristic molecular result of the collapse response, with the microtubule network only being rearranged (Fan et al., 1993; Kuhn et al., 1999).

The relatedness of guidance mechanisms and growth cone collapse became apparent for cultured retinal ganglion cells. Outgrowing pioneering axons extended lateral extensions hundreds of micrometers away from their tip, after ephrin or mechanically induced collapse, and likewise accompanying axons were induced to defasciculate at the same distance (Davenport et al., 1999).

Calcium induced molecular cascades after axotomy

Reinduction of growth cones a few hundred micrometers away from the collapsing axon tip, strikingly resembles the observed morphological changes upon axotomy of *Aplysia* neurons. If these neurons were axotomized, a brief, sharp rise of intracellular calcium to about 1000 μM (resting level is around 0.1 μM) was observed at the severed axon tip. But within minutes the membrane resealed and no further calcium influx was observed. Subsequently a new growth cone was formed within ten minutes at about 100 μm from the transection site. This region collocalized with an area, where calcium concentrations were raised to 300-500 μM. Elevation of calcium up to this level anywhere along the severed or unsevered axons was sufficient to induce growth cone formation (Ziv and Spira, 1997). Moreover this calcium

rise was sufficient to trigger a localized proteolytic activity, which was already known for its ability to induce growth cones. Within about an hour, proteolytic activity reached its maximum and cytoskeletal alterations were manifested.

Submembraneous, heterotetrameric spectrin/fodrin was shown to be one of the targets of proteolytic cleavage (Gitler and Spira, 1998). Spectrin is especially important for membrane associated cytoskeleton organization and signalling. This is already suggested by its multiple binding domains, which interact with many important cytoskeletal components, such as actin or ankyrin and possibly signalling molecules via its Src-homology-3 (SH3) domain (Pinder and Baines, 2000). Spectrin, actin and calmodulin were also directly associated with calcium dependent membrane transport during axonal regeneration (Koenig et al., 1985).

The mentioned axotomy induced events are further supported by data, which also emphasize the necessity of calcium influx and proteolytic activity for membrane resealing and subsequent axon dedifferentiation in cultured rat septal neurons (Xie and Barrett, 1991). Moreover, it was pointed out that microtubule disassembly was also necessary for membrane resealing. In all of these studies, proteolytic activity was associated with the calcium/calmodulin activated, heterodimeric cystein endopeptidase calpain.

This family of proteases is known to cleave spectrin and microtubule associated protein 2 (MAP2) isoforms (Johnson et al., 1991). The crucial role for calpains in mediating also cytotoxic effects was recently demonstrated. Physiological activation of cyclin-dependent kinase 5 (cdk 5) by its neuron specific activator p35 is required for neurite outgrowth. But upon calcium or amyloid β-peptide stimulation, p35 is cleaved to p25, which in turn upregulates cdk5 activity and mislocalization. As a result tau becomes hyperphosphorylated, the cytoskeleton disrupted and apoptosis is initiated. Cleavage of p35 to p25 depends upon calpain activity, placing this protease in the center of calcium induced cytoskeletal alterations in acutely axotomized neurons and during chronic Alzheimer's disease (AD) (Lee et al., 2000a).

Therefore, the mechanisms leading to calpain induced neurotoxicity in AD could possibly also affect axotomized neurons and may contribute to the distance related effects of axotomy induced cell death in some neuronal populations.

2.2.2 Major families of guidance molecules

The pivotal role and general importance of second messengers in transducing molecular informations to the cytoskeleton has been described above. Alterations in second messenger levels are thought to be initiated my interactions of guidance molecules at the growth cone membrane. These membrane associated proteins belong to the best studied proteins, which are invoved during axonal outgrowth and have more comprehensively been reviewed by Goodman (Goodman, 1996), Tessier-Lavigne and Goodman (Tessier Lavigne and Goodman, 1996), and Müller (Mueller, 1999).

Pioneers of neurite growth associated proteins

Cell adhesion molecules (CAMs) belonging to the immunoglobulin superfamily were among the first transmembrane proteins to be implicated in axonal outgrowth. Three major members of that family, NCAM, N-cadherin and L1, were shown to signal via their homo- and heterophilic trans interaction (between membranes of different cells) induced cis clustering (within the same membrane) with fibroblast growth factor (FGF) receptors. Stimulation of the CAM/FGF pathway results in calcium influx via N- and L-type calcium channels and production of inositol phosphate. Furthermore G_i- and G_o-type G proteins participate in the activation of second messenger production, probably by interaction of the $\beta\gamma$ subunit with the pleckstrin homology (PH) domain of phospholipase C γ (PLC γ) (Viollet and Doherty, 1997).

Whether CAM mediated growth responses are attractive or inhibitory may depend on their extracellular binding partners. Heterophilic interaction of L1 with laminin initially lead to growth cone collapse, but then supported neurite outgrowth, while interaction with a chondroitinsulphate proteoglycan (CSPG) was inhibitory. The presence of an RGD-motif in L1 was shown to specifically recognize several integrin heterodimers.

In addition to the mentioned participation in signalling events, L1 could directly influence cytoskeletal changes. The highly conserved cytoplasmic binding site for ankyrin, indirectly links L1 to the spectrin-actin cytoskeleton, and appears to be crucial for L1 function. The importance of the cytoplasmic tail is further supported by mutation data within this region, which lead to severe brain malformations (Hortsch, 1996; Brummendorf et al., 1998).

L1 activity could furthermore be modulated by phosphorylation of serine 1181 and 1152 by casein kinase II and p90 rsk, an S6 kinase, respectively. Possible tyrosine phosphorylation of L1 may also be regulated by the intracellular domain of the phosphacan CSPG, RPTP ζ/β , a

receptor type protein tyrosine phosphatase (Burden Gulley et al., 1997), illustrating the multiple interactions which have to be concidered in mechanistic guidance models.

Among various other pioneering growth associated proteins, such as NCAM, integrins, low affinity NGF receptor, c-src (a non receptor tyrosine kinase) (Skene, 1989), actin and tubulin (McKerracher et al., 1993b; Bisby and Tetzlaff, 1992) and c-jun (Herdegen et al., 1993; Herdegen et al., 1997), GAP-43 is one of the best known and studied.

This protein was identified as a protein, which is highly upregulated and axonally transported upon sciatic nerve transection (Skene and Willard, 1981), its role during axonal outgrowth has been intensively studied. GAP-43 alone is neither sufficient, nor necessary for axonal outgrowth, but its supportive effect for axonal sprouting has been demonstrated. But also other proteins could be equally important, like CAP-23, which has similar biochemical characteristics.

Although GAP-43 upregulation is often associated with a potential for regeneration, a strict correlation between axotomy and neuronal GAP-43 induction cannot be found. Transection of the central branch of dorsal root ganglia (DRG) does not increase GAP-43 levels, if lesions are made far from the soma. GAP-43 also appears to be important during development, where high perinatal GAP-43 levels decrease until adulthood (reviewed in Caroni, 1997). But mRNA and protein are still widely distributed in the adult brain (Benowitz et al., 1988; Yao et al., 1992).

These data have not established GAP-43 as a primary determinant of axon outgrowth. Therefore a more generalized perspective could be generated by taking its biochemical properties into account. The aminoterminus of GAP-43 activates G_o and G_i proteins, of which the α and β subunits are enriched in growth cone membranes. But G protein activation was shown to retard axon outgrowth, which raises a conflict between the observed GAP-43 induction and its stimulating effect on G proteins (Strittmatter et al., 1992). A solution to this apparent contradiction could be seen in the palmitoylation of GAP-43, which blocks G protein activation and could also alter GAP-43 localization. The IQ motif of GAP-43, which is shared by members of the calpacitin family, and mediates calmodulin binding in the absence of calcium, is also involved in GAP-43 function. GAP-43 is a major substrate of protein kinase C (PKC) isoforms in the growth cone, and phophorylation by PKCs abolishes calmodulin binding. The calcium/calmodulin activated phophatase calcineurin, on the other hand, decreases the level of phosphorylated GAP-43 (reviewed in Benowitz and Routtenberg, 1997). Phosphorylated GAP-43 stabilizes F-actin (He et al., 1997) and localizes to growth cone lamellae.

Semaphorins

The semaphorin family of membrane bound or secreted chemotropic proteins was founded by collapsin (renamed to Sema3A), which induces growth cone collapse. Many members of this protein family have since been identified and implicated in axon guidance and patterning, but also in skeleton and heart formation during development. The phylogenetically highly conserved aminoterminus is characterized by the 500 amino acids containing the semaphorin domain with several conserved sequence stretches. The family has been subdivided into seven classes, with the first two containing invertebrate semaphorins. Within the five vertebrate classes, comprising 20 members, the class specific carboxyterminus determines, whether semaphorins are secreted (class three), transmembrane (classes four to six) or GPI-anchored (class seven).

The cytosol facing carboxy terminals might also be involved in signalling (reviewed in Fujisawa and Kitsukawa, 1998), as for example SemaVib was shown to interact with the SH3 domain of c-src (Eckhardt et al., 1997). The repulsive actions of Sema3A are known to depend on furin convertase processing, which might therefore introduce the first level of axon repulsion modulation (Mark et al., 1997). The Sema3A induced collapse response stimulates endocytosis in growth cones. Endocytosis associated vacuoles at sites of altered F-actin organization contained the Sema3A receptors neuropilin-1 and plexin (mentioned below), and the Sema3A signalling molecule rac1 (Fournier et al., 2000).

Apart from mediating repulsion, like in the case of Sema3A, semaphorins are also known to mediate neurite attraction. Sema3C and Sema-1 mediated attraction was found in vertebrates (Bagnard et al., 1998) and in invertebrates (Wong et al., 1999), respectively. But the observed guidance responses depend on an increasing gradient, as neither Sema3C mediated attraction, nor Sema3A mediated repulsion could be observed, if axons grew along decreasing semaphorin concentrations (Bagnard et al., 2000). Moreover, neurites from the same cell could respond in an opposite fashion towards a gradient of the axon repellent Sema3A. This semaphorin is suggested to be distributed in a gradient within the developing cortex (Polleux et al., 1998). Axons were shown to grow out along a decreasing Sema3A gradient, while dendrites of the same pyramidal cells moved upwards, requiring both Sema3A and neuropilin-1. In this case, asymmetrical distribution of soluble guanylate cyclase, being high at the apical side of the differentiating pyramidal cell, could explain the different behaviour of dendrites and axons towards cGMP gradients.

The extend of Sema3A contribution to cortex patterning, though, is still not understood. As class four semaphorins are generally distributed throughout the developing brain, and

members of class three are more restricted to distinct brain regions, it is difficult to dissociate the contribution of different semaphorins to brain patterning (Mark et al., 1997). Especially during cortex development additional modulation of semaphorin interactions by glycosaminogycans (Franken, 2000) make the molecular network more puzzling. Persistent expression during adulthood, like for example of Sema3A, in the subiculum, the lateral entorhinal area and some other brain regions (Giger et al., 1998), raise the question of the function of continued semaphorin expression in the adult brain.

Semaphorin receptors and associated proteins

The discovery of class three specific semaphorin receptors, neuropilin-1 (NP-1) and neuropilin-2 (NP-2) might help to unravel part of the function of spatially and temporally overlapping semaphorin expression. The structure of these membrane associated proteins suggests multiple activities. The extracellular part is built by three unique domains with similarities to other known proteins, such as for example brain morphogenic proteins (BMPs). NP-1 deficient mouse mutants have a similar embryonic phenotype in the PNS, as Sema3A deficient mutants. NP-1 binds Sema3A with high affinity and is required for the Sema3A induced collapse response. Two other class three semaphorins are bound by NP-1, Sema3C and the former Sema IV. In contrast to NP-1, NP-2 only binds to the latter two semaphorins, but not to Sema3A. This adds to the complexity of semaphorin mediated actions during development (reviewed in Fujisawa and Kitsukawa, 1998).

In the case of Sema3A, Plexin 1 (Plex 1) was shown to enhance binding of Sema3A to NP-1 and induces a different biological effect in cells, than Sema3A and NP-1 alone (Takahashi et al., 1999). Plexin is furthermore required to transduce the Sema3A signal to the cytoskeleton and certain semaphorins are also able to bind directly to Plex 1. Signal transduction to the cytoskeleton involves the small GTPase Rac 1, and the family of collapsin response mediator proteins (CRMPs) (Nakamura et al., 2000). Early reports on the collapse response also included trimeric G proteins in semaphorin signalling pathway (Goshima et al., 1995).

The TOAD/Ulip/CRMP (TUC) family of neuronal proteins may modulate the intracellular action of at least semaphorin signalling. Committment to a neuronal phenotype in the developing brain, in PC 12 cells and neuroblastomas is accompanied by the upregulation of members of this family (Quinn et al., 1999).

The expression of CRMPs in the brain is developmentally regulated, with generally high expression during perinatal stages. The proteins rCRMP-1 and rCRMP-2 are continued to be expressed in the adult rat brain in certain regions, while rCRMP-3 and rCRMP-4 are

downregulated until adulthood. This is especially striking for rCRMP-4 expression in hippocampal pyramidal cells (Wang and Strittmatter, 1996). In the PNS, all four CRMPs are continued to be expressed in dorsal root ganglia.

Following axotomy of the sciatic nerve, rCRMP-2 is reinduced in adult sciatic motor neurons in the spinal cord, suggesting a role of this protein during neurite extension (Minturn et al., 1995). But the molecular mechanisms of action and biochemical properties of CRMPs are still largely unknown.

Cytosolic CRMPs were found in heterotetramers (Wang and Strittmatter, 1997), while membrane association may be accounted for by an association with the plasma membrane oxidoreductase (PMO) complex of recycling vesicles and the synaptic plasma membrane. In PMO complexes, CRMP was found to be associated with glyceraldehyde-3-phosphate (GAPDH) isoforms, enolase-γ and aldolase C (Bulliard et al., 1997). How and if these properties of CRMPs contribute to axon guidance and cytoskeletal remodelling remains to be shown.

Finally, another aspect of semaphorin associated axon guidance was associated with vesicle trafficking, namely the dependence of guidance efficacy on their oligomerization state. Like the increase in endocytosis (Fournier et al., 2000), this feature is shared with the ephrin family. In analogy to ephrin B ligands (mentioned below), which interact with PDZ containing proteins PICK 1 and GRIP, thereby organizing ion channels and ephrin B ligands into membrane clusters or lipid rafts, semaphorins could interact in a similar fashion, as one of the vertebrate semaphorins has been shown to interact with a PDZ protein, too (Puschel, 1999).

The Eph-family of receptor tyrosine kinases and their ephrin ligands

The Eph receptor family of receptor tyrosine kinases (RTK) and their cognate ligands, the ephrins, are implicated in many developmental processes, such as angiogenesis, cell migration and establishment of topographic projections in the brain.

The extracellular aminoterminal globular domain of the Eph receptors constitutes the pimary ligand binding domain, while the carboxyterminal cytoplasmic tail forms the tyrosine kinase domain in most cases. According to the membrane association of the ephrins, and their binding specificity, both receptors and ligands were divided into two subclasses. Ephrin-A ligands (five genes) are membrane associated via their glycosylphosphatidyl-inositol anchor and ephrin-B ligands (three genes) are transmembrane proteins. Their corresponding receptors have been designated EphA, of which eight genes are known, and EphB (six genes). The

family is evolutionary well conserved. Within the subclasses Eph-receptor and ephrin-ligand interaction is quite promiscuous.

Activation by autophosphorylation of the Eph-receptors is only seen, if ephrins are applied in a clustered form. The underlying cascade initiated by this stimulation is still largely unknown, but two classes of directly interacting proteins of the Eph receptors are likely to play a role in this context. The adapter proteins SLAP, Grb 2 and Grb 10, and the SH2 domain containing enzymes, like src tyrosine kinase and PLCγ, were reported to interact with Eph receptors. Moreover cis interactions of Eph receptors with L1 might be important in certain developmental events (reviewed in Zisch and Pasquale, 1997; Frisen and Barbacid, 1997; Orioli and Klein, 1997).

Eph receptor activation is generally thought to be responsible for the repulsive nature of Eph-ephrin interactions during axonal outgrowth. Gradients of ephrins are known to be repulsive for Eph expressing axons in vitro (stripe assay) and complementary distribution of receptors and ligands support this interaction during establishment of important topographic projections, as shown for the retinotectal system and during muscle innervation by motor neurons.

A graded expression of EphA5 in the hippocampus and subiculum was implicated in the topographic organization of the septohippocampal projection (Zhou et al., 1994; Zhou, 1997), and is very likely also involved in the establishment of subicular projections (see 2.3), as a hypothalamic gradient of EphA5 ligands was reported as well (Zhang et al., 1996). But additional contribution to subicular projections by other members of the Eph/ephrin mediated axon guidance system is likely, for example by EphA4, which was immunolocalized to the fornix (Martone et al., 1997).

Recent results suggest a role for ephrin-B ligands in transducing signalling. Bidirectional signalling was shown to be necessary to restrict cell intermingling, which could be important for hindbrain formation (Mellitzer et al., 1999). Adding to the functional complexity, different splice isoforms of EphA7, which lack the kinase domain, contributed to an adhesive, rather than repulsive interaction of cells expressing the truncated and full length form of EphA7 and unaltered ephrin-A5 during neurulation (Holmberg et al., 2000).

Another important requirement during the maturation of the developing brain is the elimination of mistargeted projections and synaptic refinements. Localization of Eph receptors and their ligands to PDZ protein containing synaptic membrane specializations (Hsueh and Sheng, 1998; Torres et al., 1998; Bruckner et al., 1999) and ephrin dependent

pruning of hippocampal axons (Gao et al., 1999), both suggest a role of the Eph receptors during refinement of connections.

Repulsion and/or pruning may involve cleavage of ephrins ligand by metalloproteases of the ADAM (A Disintegrin And Metalloprotease) family. Multivalent or clustered EphA3 receptors triggered surface cleavage of ephrin-A2 in neuroblastoma cells. The metalloprotease Kuzbanian/ADAM 10 (Kuz) was able to complex ephrin-A2. Furthermore, medial hippocampal neurons, which are repelled by ephrin-A2 were shown to retract from GFP-ephrin-A2 fusion protein expressing cells on a time scale (of about 30 minutes), which was similar to in vitro proteolytical processing of ephrin-A2 by Kuz. Retraction was tyrosine kinase dependent and fluorescence containing vesicles could be visualized within retracting axons, suggesting an endocytotic internalization of cleaved ephrin-A2 (Hattori et al., 2000).

The action of netrins on axonal outgrowth

(reviewed in Tessier Lavigne and Goodman, 1996; Goodman, 1996; Mueller, 1999)

The aminoterminal two thirds of netrins are partially homologous to laminin, while the basic rest of the protein is conserved among the netrins and is known to bind heparin and heparansulphate proteoglycans. Two vertebrate netrin homologues of the *C. elegans* UNC-6 are known, which are likewise secreted from floor plate glial and neuronal cells in the developing nervous system. Again high sequence conservation among vertebrate and invertebrate netrins suggests an important biological role of these molecules.

Indeed, proper netrin function is required for correct formation of commissural connections in all species studied so far. They were furthermore implicated in guidance of corticofugal axons and retinal axons in the optic disc. The bifunctionality to induce both attractive and repulsive responses in axons appears to be mediated by interaction with different netrin binding receptors.

The transmembrane UNC-40 receptor, identified in *C. elegans*, has two homologues in vertebrates, DCC (deleted in colorectal cancer) and neogenin, and the homologous Frazzled in *Drosophila*. Antibody perturbation experiments suggest that DCC mediates netrin attraction. Netrin hereby appears to derepress multimerization of DCC cytoplasmic tails (Stein et al., 2001).

If DCC is coexpressed with members of the UNC-5 family, axons are repelled by netrin. UNC-5 thus appears to be dominant over DCC in mediating netrin induced axon repulsion. Three vertebrate homologues of the *C. elegans* unc-5 gene are known, UNC-5H1, UNC-5H2 (for UNC-5 homologue 1 and 2) and UNC-5H3/RCM (for rostral cerebellar malformation).

UNC-5 proteins are transmembrane proteins with a large cytoplasmic domain, which is likely to transmit extracellular netrin interactions into the cytoplasm. Again nothing further is known about the associated signalling pathways, except that they could result in altered cAMP levels.

Netrin associated guidance can be modulated in vivo. Attractive netrin interaction with DCC is known to be increased by a proteinaceous netrin-synergizing activity (Galko and Tessier-Lavigne, 2000b). This activity could be mimicked by hydroxamate metalloprotease inhibitors. Furthermore, application of these inhibitors prevented DCC ectodomain shedding in transfected chinese hamster ovary cells (Galko and Tessier-Lavigne, 2000a). The ADAM metalloprotease MIG-17 is required for migration of distal tip cells in *C. elegans* and genetically interacts with UNC-6, the *C. elegans* netrin homologue (Nishiwaki et al., 2000), and might therefore be a candidate for the ectodomain shedding protein.

Concluding remarks

Increasing information on axon guidance associated protein families, has resulted in a remarkable gain of knowledge about nervous system wiring in the past few years. This list reported here is still far from being complete and some guidance families had to be neglected in this introduction.

For example the recently identified receptor for the extracellular domain of the neurite outgrowth inhibitor, Nogo, might be a founder of a new family of guidance proteins. These data raise questions on the mechanism, of how a comparatively small (66 amino acids; Nogo-66) extracellular portion of a protein, and in addition the intracellular part, too, can both exert their inhibitory effects (Fournier et al., 2001). This Nogo-66 receptor (NgR) has novel features, with closest structural homology to slit1-3 and the acid labile subunit of the insulin-like growth-factor binding protein complex.

In addition, an ingenious gene trap approach to detect secreted or transmembrane proteins that contribute to axon patterning in the nervous system, by analysing a zoo of transgenic mice phenotypically, identified known and novel genes as being important for axonal guidance (Leighton et al., 2001).

Though classical biochemical and genetic approaches are still very powerful to identify new guidance molecules and also some of their interaction partners, they fail to detect the highly complex downstream signalling machinery in the growth cone. The recent availability of genomics techniques enabled researchers to quantify the expression of known and unknown genes on a genomic scale (DeRisi et al., 1997). Coexpression analysis in clusterograms helped

to visualize thousands of genes, which are expressed together in different or similar experimental contexts (Eisen et al., 1998). Coregulation of genes suggests a necessity of these genes or group of genes in the studied biological context. It can also be used to assign potentially new functions to known and unknown genes and proteins, thus providing candidate lists of genes that could be studied further by biochemical, pharmacological or genetic means (Marcotte et al., 1999a; Marcotte et al., 1999b).

Therefore, recent advances in genomics could provide new insights into the machinery that governs directed axonal outgrowth.

2.3 The lesion model of the axotomized postcommissural fornix

The subicular complex is part of the hippocampal formation. Other main anatomical components of the HIF are the dentate gyrus, the fields of the cornu ammonis (CA) and the entorhinal area. The subiculum can be further subdivided into subiculum proper, pre- and parasubiculum (Björklund and Hökfelt, 1987; Amaral and Witter, 1995).

Main inputs to the subiculum are received from CA1 and the entorhinal area, with the first also projecting to the latter. Pre- and parasubiculum also weakly project to the subiculum proper and bilaterally to the entorhinal area via the dorsal hippocampal commissure. Likewise the subiculum proper projects to the entorhinal and perirhinal area, as well as to pre- and parasubiculum, completing this complex intrahippocampal network centered around the subiculum. All these projections are topographically organized.

The fornix is the main extrahippocampal output of the subicular complex, employing glutamate and neurotensin as neurotransmitters. It projects unidirectional and topographically highly organized to the mammillary body in the diencephalon (Shibata, 1989; Allen and Hopkins, 1989; Schroeder et al., 1989). The subicular fibres project bilaterally to the mammillary body, wheras presubiculum derived fibres were shown to project in part only ipsilaterally to the lateral mammillary nucleus (Shibata, 1989). Within pre- and parasubiculum only a distinct set of neurons projects to the mammillary body only, while another set projects to the entorhinal area (Donovan and Wyss, 1983). The topographical organization of subico-mammillary projections is summarized in figure 1.

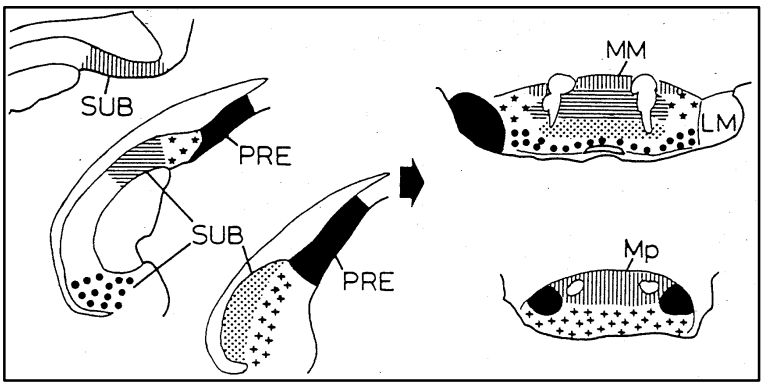

Figure 1. Topography of subicular projections to the mammillary body. Interconnected areas are labeled identically. Note that the medial mammillary nucleus (MM) and the posterior mammillary nucleus (Mp) are almost exclusively connected to the dorsal (septal) parts of the subiculum (SUB). Projections from the presubiculum (PRE) reach the MM ipsilaterally, while the Mp is afferented bilaterally. Taken from Shibata, 1989.

It appears that more cells in the dorsal two thirds of the subiculum project to the mammillary body. This topography is in agreement with the proximo-distal (transverse) topographic organization axis (Fig. 2). It is important to note that projections from subicular neurons from the proximal half (closer to CA1) to the mammillary body, entorhinal area and septum appear to arise at least in part as collaterals.

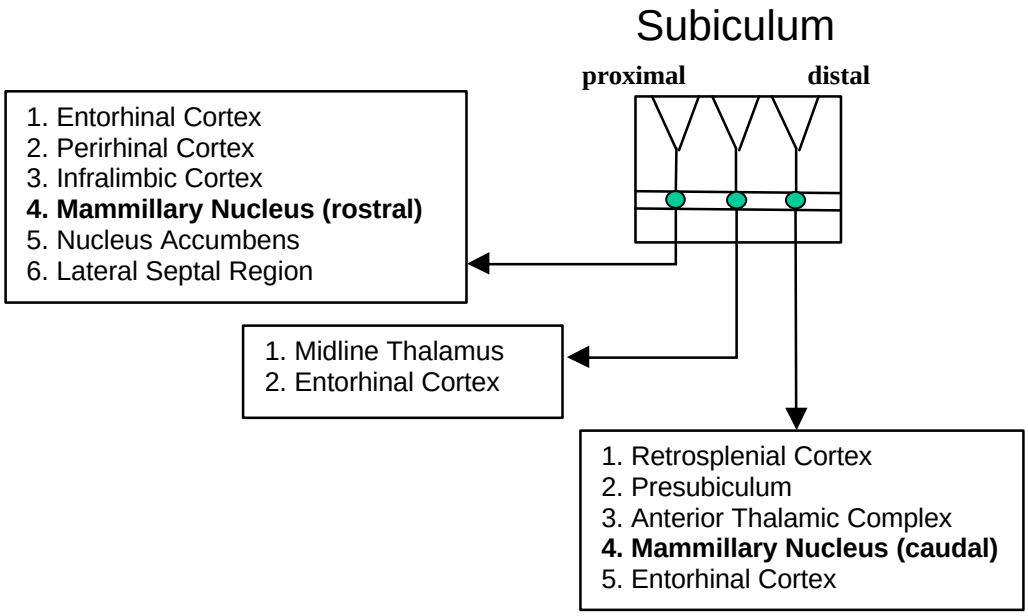

Figure 2. Summary diagram illustrating the transverse organization of subicular connections. Note that different transversal parts (proximal and distal) of the subiculum innervate distinct structures, except for the entorhinal cortex and the mammillary nucleus. Instead, an additional topographic organization axis is revealed for the mammillary nucleus (bold) as compared to figure 1. Taken from Amaral and Witter, 1995.

The postcommissural fornix gives also rise to two other tracts. The medial corticohypothalamic tract, diverging just ventral to the anterior commisure and runs to the hypothalamus (arcuate nucleus, ventromedial nucleus, ventral premammillary nucleus, basomedial parts of the lateral hypothalamic area). The second is the subicolothalamic tract, which connects the subiculum to the midline and anterior groups of the thalamus. Projections to the midline group are also topographically highly organized, as the dorsal subiculum projects preferentially to the nucleus interanteromedialis, the dorso-ventral subiculum to the nucleus reuniens and the ventral subiculum to the paraventricular nucleus. A ventral pathway running via the amygdala to the hypothalamus was also described, but does not run within the fornix (Kohler, 1990). A reciprocal connection running from the supramammillary nucleus to the subicular complex is not found within the postcommissural fornix (Schroeder et al., 1989). The subicular input from the premammillary nucleus of the hypothalamus projects via the amygdala (Amaral and Witter, 1995; Canteras and Swanson, 1992).

The column of the fornix is the remaining part of the postcommissural fornix that, after the divergence of the medial corticohypothalamic tract and the subicolothalamic tract travels on to the mammillary body. Unilateral transection of this part of the fornix therefore exclusively affects subicular neurons projecting ipsilaterally to the mammillary body, as collaterization does not occur until close to the mammillary body (Schroeder et al., 1989), leaving the unsevered contralateral subiculum and fornix as a possible internal control (Fig. 3).

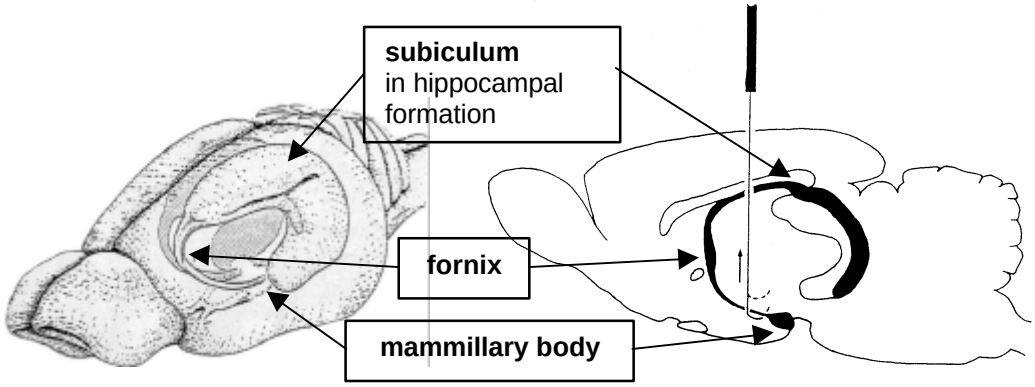

Figure 3. Three dimensional model of the adult rat brain (left) and the lesion model of the postcommissural fornix (right). The black structure in the lesion model shows the subiculum in the hippocampal formation projecting via the postcommissural fornix to the mammillary body. The scouten wire knife transecting the postcommissural fornix close to the mammillary body is also shown.

After unilateral fornix transection no obvious functional deficits were observed. Other studies reported on minor deficits in spatial working memory processing after bilateral transection (Tonkiss and Rawlins, 1992). In general, effects on behavioural and learning tasks can be expected, as the fornix is a component of the Papez circuit, which is important for learning, motivation, emotion and reproductive physiology (Fig. 4).

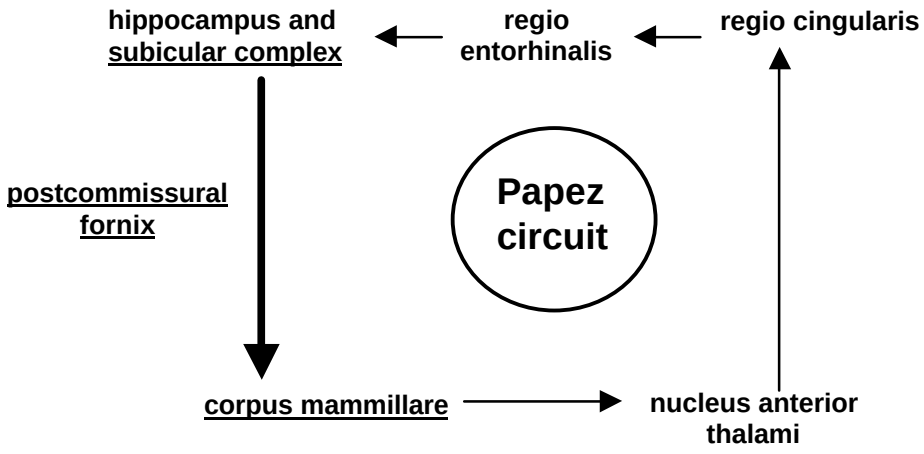

Figure 4. The Papez circuit. Major anatomical components are shown. The postcommissural fornix is printed as a bold arrow, connecting the subicular complex with the mammillary body. See text for further reference.

2.4. Aim of this thesis

While axons of the peripheral nervous system (PNS) can regenerate after being lesioned, central nervous system (CNS) axons cannot do so. The reasons for the chronic loss of motor and sensory projections are still poorly understood. In order to develop new therapies for CNS axon injuries, it is therefore important to understand the molecular mechanisms that are responsible for the limited regeneration capacity in the CNS.

In previous work, the CNS axotomy model of the transected postcommissural fornix was used to study the axotomy induced molecular reactions at the lesion site, which were associated with an altered glial and extracellular matrix response (Stichel and Mueller, 1994; Stichel and Muller, 1994; Lips et al., 1995; Stichel et al., 1995a; Stichel et al., 1995b). Furthermore, Schwann cell suspension grafts and basement membrane inhibiting treatments of the lesion site have been described, which stimulated axonal outgrowth (Stichel et al., 1996; Stichel et al., 1999b,).

Within this thesis, the axotomy induced response within the subiculum, which contains the projecting neurons of the postcommissural fornix, was intended to be studied during (i) degeneration onset, (ii) spontaneous axonal outgrowth, (iii) axonal outgrowth arrest at the lesion site and (iv) during stimulated regeneration. Therefore, in a first series of experiments the expression of a limited number of marker proteins within the subiculum and at the lesion site should be characterized. The postlesional distribution of regeneration and degeneration associated proteins and genes should be described by immunohistochemistry and in situ hybridization, respectively.

After this initial histological characterization of the subiculum and of the fornix stump, a genomics approach using cDNA arrays should be applied to study the expression of 1185 genes in the subiculum during the above mentioned stages.

The combination of histological and genomics techniques may help to answer the following questions:

Is the neuronal transcriptom altered upon axotomy?

Is the expression pattern during axon outgrowth maintained after growth arrest at the lesion?

Is there a genetic regeneration or axon outgrowth program within neurons that is induced upon axotomy? Which transcription factors become activated to govern such a program?

Is the expression pattern identical during axon sprouting and induced axonal regeneration?

3. MATERIALS AND METHODS

3.1 Animal surgery

3.1.1 Animals

Adult male Wistar rats (190-210g) were subjects for experimental postcommissural fornix transection. Animals were bread within the animal facility (Tierversuchsanlage, TVA) of the Heinrich-Heine-University, Düsseldorf and kept under specific pathogen free conditions until surgery. They were maintained in a temperature (21°C) and humidity (50+/- 5%) controlled animal housing, on a 12h light/dark cycle. Dry and pelleted animal food (Fa. Ssniff) and water (pH 2), was available ad libitum.

3.1.2 Transections of the postcommissural fornix

Animals were preanaesthetized with the inhalative Ethrane^{TM}, followed by deep anaesthesia with an intraperitoneal injection of a mixture of Ketavet (Pharmacia/Upjohn) /Rompun (Bayer) (90 mg/kg and 5 mg/kg, respectively). They were then secured in a stereotaxic frame and the left postcommissural fornix was unilaterally transected at a distance of about 1 mm proximal to the target, using a Scouten wire knife, as described in (Stichel et al., 1995a). The guidance canula of the tungsten wire knife was lowered stereotactically into the brain (for applied stereotactic coordinates, see below) lateral to the left fornix. The wire was extended for 3 mm in a semicircle ventral to the tract. Then the knife with the extended wire was withdrawn for 3 mm to cut the fornix. Finally, the wire was retracted and the guidance canula of the knife was removed. In sham operated animals the surgery was identically performed, except for the extension of the tungsten wire. Therefore, the fornix was not cut in sham operated animals, but only a stab wound remained.

All of the surgical interventions and pre/postsurgical animal care were provided in compliance with the German Animal Protection law.

Applied stereotactic surgery coordinates were optimized as compared to (Stichel et al., 1995a), in order to make sure that the tract was properly cut:

anterior	+ 5.8
ventral 1, knife extension	+ 9.2
ventral 2, knife retraction	+ 6.2
lateral	+ 2.0

3.1.3 Injection of DPY

Immediately after transection, animals received a topical injection (1.6-2.4 µl) of either 2,2'-dipyridyl (DPY; Sigma) diluted in sterile physiological salt (NaCl) solution. Substances were slowly pressure injected (injection time 10 min) directly into the lesion site via a pulled-glass micropipette coupled to a microsyringe. The micropipette tip remained in place for 5 min before withdrawal.

3.2 Tissue preparation

3.2.1 Tissue preparation for histochemistry

After appropriate survival times, lesioned rats were killed by an overdose of Ethrane™ and either the complete brain or the separated hemispheres were quickly removed and immediately frozen in isopentane between -45 and -55°C for about 30 s.

As some antibodies required perfusion-fixed tissue, a series of animals was injected with an overdose of a mixture of Ketavet™ (Pharmacia/Upjohn) /Rompun™ (Bayer) (90 mg/kg and 5 mg/kg, respectively) intraperitoneally, and perfused transcardially with 0.01 M PBS at pH 7.4, followed by 4% paraformaldehyde in 0.1 M PB at pH 7.4 for 10 min. The brain was removed and placed in 4% paraformaldehyde in 0.1 M PB at pH 7.4 overnight , followed by cryoprotection for one day in 30% sucrose, both at 4°C. After cryoprotection brains were again frozen in isopentane as described above.

Serial sagittal or coronal sections (10 µm) were cut on a cryostat and thaw-mounted on slides coated with 0.1% 3-aminopropyl triethoxysilane or on super-frost plus slides. Sections were air dried at room temperature an then stored at -20°C until further use.

3.2.2 Tissue preparation for total RNA isolation

Animals were sacrificed and brains were removed and frozen as described above (3.2.1). In order to verify the completeness of the transection, lesioned hemispheres were first sagittally cut up to the lesion site and then trimmed in the coronal plane up to the subiculum in a cryostat at -20°C. Subicular tissue was recognized by its anatomical position and excised with a scalpel along anatomical landmarks, provided by white matter areas. Alternating trimming and excision yielded about 10 mg of subicular tissue per animal. Two dissected subiculi were sufficient for total RNA isolation, which was then used for the consecutive steps for one cDNA array hybridization.

3.3 Histochemical staining procedures

3.3.1 Immunohistochemistry

After fixation with either acetone (-20°C, 10 min) or 4% paraformaldehyde in 0.1 M PB at pH 7.4 (-4°C, 10 min) sections were dehydrated in ethanol (50/70/90/100/100%) and then incubated in 0.15% H_2O_2 in methanol (room temperature, 10 min) to block endogenous peroxidase activity. Non-specific binding was blocked by incubation in 0.01 M PBS with 3% normal horse or normal goat serum. Then, serial sections were incubated with one of the primary antibodies (see table below) diluted in PBS (4°C, overnight) and rinsed in PBS the next day, followed by incuabtion with an appropriate biotinylated or fluorophor labeled secondary antiserum (see table below). After washing with PBS, slides were incubated at room temperature for 45 min with an avidin-biotinylated peroxidase complex (Vector Laboratories) according to the manufactures protocol, washed again with PBS and then reacted with a solution of freshly thawn diaminobenzidine (0.07%; Sigma) in 0.1 M PB as a chromogen. For enhancement of immunohistochemical staining a silver intensification method was performed as described (Stichel et al., 1990). Sections were coverslipped in mounting medium DPX (Merck). Fluorescence labeling was performed in analogy, but with incubation of a fluorophor labeled secondary antibody (see table below). Sections were coverslipped with Vectashield (Vector Laboratories).

Table 1. Antibodies, dilutions and conditions employed.

name/host	dilution	fixation	supplier
goat **anti-mouse IgG2a** Texas Red™(**TXRD**)-labeled	1:50 (20µg/ml)	see primary antibody	Southern Biotechnology Associates
goat **anti-mouse IgG1** Fluorescein (**FITC**)-labeled	1:50	see primary antibody	Southern Biotechnology Associates
horse **anti-mouse**	1:150	see primary antibody	Vector
goat **anti-rabbit**	1:200	see primary antibody	Vector
anti-rat **clusterin** mouse monoclonal IgG, 1mg/ml	1:100 10µg/ml	paraform-aldehyde	Upstate Biotechnology, Lake Placid
anti-**parvalbumin** mouse monoclonal	1:2000	paraform-aldehyde	Sigma Immunochemicals
anti-**calbindin d** (28 kD) mouse monoclonal IgG1	1:5000	paraform-aldehyde	Sigma Immunochemicals
anti-phosphorylated neurofilaments (**P*an*-A*xonal* M*arker***) mouse monoclonal IgG1	1:2000	acetone; paraform-aldehyde	Affiniti research products
anti-mouse **L1** rabbit polyclonal, 1.6mg/ml	1:5000	acetone; paraform-aldehyde	Prof. F. Rathjen, MDC Berlin
anti-rat **GAP-43** mouse monoclonal IgG2a	1:60,000	acetone; paraform-aldehyde	Sigma

3.3.2 Non-radioactive in situ hybridization

Native cryostat sections were thawed and air dried at room temperature for 10 min, followed by fixation (3.7% paraformaldehyde in PBS), pretreatment by incubation in proteinase K (1µg/ml in PBS) at 37°C for 10 min, acetylation (0.25% (v/v) acetic acid anhydride in 0.1 M triethanolamin, pH 8.0) at room temperature for 10 min and prehybridization (50% formamide, 2xSSC) for 2h at the respective hybridization temperature. After prehybridization, sections were hybridized overnight at the indicated hybridization temperature (see table below) with digoxigenin-labeled probes diluted to indicated concentrations in hybridization solution (50% formamide, 1xDenhardts, 20mM TrisHCl pH 8.0, 5mM EDTA pH 8.0, 300mM NaCl, 10% (w/v) dextran sulfate 500.000). The sections were then washed in the prehybridization solution at the hybridization temperature for 90 min, followed by treatment with RNAse A (20µg/ml in 0.5 M NaCl, 10 mM Tris pH 8.0, 1 mM EDTA pH 8.0) at 37°C for 20 min. The sections were washed again and digoxigenin detection was carried out following the manufacturer's instruction (Roch BM). In general, all buffers and solution were treated with diethyl-pyrogencarbonate (DEPC) if RNAse contamination had to be avoided.

Table 2. In situ hybridization conditions and employed riboprobes. All probes were rat specific, unless otherwise indicated.

name of probe	dilution (ng/ml)/ T_{Hyb} (°C)	frament of cDNA	promotor for sense	template source/comment
rMDC15	250/60	bp 15-560	T7	RT-PCR cloned in pBKSII
L1/NILE	300/55	XhoI/BamHI (1.3 kb)	T7	Dr. M. Jung, Konstanz pBIIKS
GAP-43	200/55	EcoRI/HindIII ΔAvaI (750 bp)	T7	Dr. M. Jung, Konstanz pGEM-3
Sox-10	500/60	NcoI/EcoRV (a) BamHI/NcoI (s)	(T7) SP6	Dr. P. Küry, Düsseldorf pZL1
CRMP-4	125/60	bp 708-1710	T3	Dr. S. Franken, Bonn pBIIKS
SGK_6	250/60	bp 1794-2487	T3	RZPD UI_p953A2037Q2+Q5 pT7T3D-Pac mod1
SGK_14	500/60	bp 1439-2487	T7	RZPD UI_p953D1116Q2+Q5 pT7T3D-Pac mod1
GIP	250/60	complete (ca. 640 bp)	T7	RZPD UI_p953K2253Q2+Q5 pT7T3D-Pac mod1
FAK	250/65	bp 2580-3280	T7	RT-PCR cloned in pBKSII
JNK1/2	250/65	bp 743-1443 (of JNK2)	T3	RT-PCR cloned in pBKSII
cofilin	65/60	bp 48-683	T3	RT-PCR cloned in pBKSII

3.4 cDNA array hybridization and analysis

3.4.1 Radioactive hybridization on Clontech Atlas^{TM} rat 1.2 filter arrays

The following steps were necessary in order to generate radioactive cDNA, which was hybridized onto the cDNA arrays:

1. total RNA needed to be isolated out of the subicular tissue
2. the RNA was then reverse transcribed into cDNA, incorporating radioactive nucleotides
3. Clontech AtlasTM rat 1.2 filter arrays were hybridized with the radioactive cDNA

Total RNA was extracted out of two subiculi to provide one RNA-pool, which was further used for one cDNA array hybridization, according to the manufactures protocol (RNeasy, Qiagen). Briefly, subicular tissue (about 10mg) was disrupted in denaturating buffer RLT using a polytron, followed by further disruption and homogenization with QIAshredder (Qiagen). Total RNA was eluted from the columns with RNase free water, digested with DNase I according to the instructions of the supplier (Roche BM), followed by its removal. The concentration of the total RNA was determined by measuring the absorbance at 260 nm in a spectrophotometer.

Reverse transcription was carried out using the reagents and the protocol supplied by the cDNA array manufacturer (Clontech). Briefly, 5 μg of total RNA were reverse transcribed using the array specific rat 1.2 CDS primer mix of the manufacturer, a nucleotide mix, replenished by α-^{32}PdATP and MMLV reverse transcriptase.

After activation of the nylon filter cDNA arrays in 0.5% SDS, they were prehybridized in hybridization solution at 68°C for at least 30 min. Then, the denatured radioactive cDNA was added and incubation was continued overnight at 68°C in rotating hybridization flasks. The next day, the hybridized cDNA arrays were extensively washed and wrapped in plastic covers for exposition to the phosphorimager screens for 3-5 days.

3.4.2 Image acquisition and analysis

Phosphorimager screens, which were exposed to the cDNA arrays were scanned (BAS-1500 reader, Fuji) and digitalized images (resolution 100μm, 8 bit) of the hybridized radioactivity on the filter cDNA arrays were further analysed using the image analysis software AIDA Array Metrix 3.0 (Raytest). Within the image analysis software a predefined array-grid could be laid over the hybridized cDNA spots and automatically positioned over the signal centers. Then the background area was defined locally. With a hybridization-signal spot diameter of

1.4 mm, the local background ring of 0.2 mm width was placed at a distance of 0.5 mm away from the spot border. These parameters appeared well adapted, as no interference of surrounding strong signals (spill-over) or scoring of too weak signals was anymore observed. Background subtracted and area normalized expression data were then exported into text files, which were then analysed in Microsoft Excel.

3.4.3 Analysis of raw expression data and generation of results

The Excel matrices, which were used for the analysis were developed within this thesis and can be found stored on a website (http://www.ulb.uni-duesseldorf.de/diss/mathnat/2001/abankwa/). Two types of matrices were compiled, the first performing individual comparisons of target (F) and control (K) hybridization data (comparison matrix); and the second analysed the reproducibility of each gene within an ensemble of comparison matrices, which belonged to the same postlesional stage (reproducibility matrix).

Comparison matrices were composed of four Excel table-leaflets. Two of these contained background subtracted data of the respective target (F-leaflet, with number of experiment) and control (K with number), which were analysed with respect to signal intensity. In addition expression data were normalized on these leaflets. Background subtracted signals were imported from the text files generated in AIDA Array Metrix 3.0 into the respective leaflet. Some of these signals (about 30-35%) had negative values, due to comparatively high background. The average signal intensity of the remaining positive signals was then calculated and used for signal intensity threshold definition and normalization of the genes. Only those genes, which had a (background-subtracted) signal intensity of at least 5% of the average signal intensity (signal threshold) were further compiled. They were normalized with the average signal intensity and with the expression signal for GAPDH (coordinate G27). It has to be pointed out right here, that the GAPDH normalization was not suitable, as this gene was regulated. Furthermore, the means of many measurements is generally more stable against random fluctuations, than a single measurement, what appeared to be very critical in this kind of analysis. The third Excel table leaflet compiled the ratio of the normalized expression data of the target (F) compared to the control (K) data. A given gene was further analysed, only if its expression was changed at least by a factor of 2. Genes, which were upregulated in F compared to K, received a positive value, while downregulated genes received a negative value, which was calculated as the ratio: -(F-expression/K-expression). The differentially expressed genes as revealed by comparison of two cDNA array expression datasets were then summarized on a fourth leaflet, which indicated expression levels below

the signal threshold ("thresh"), changes in the expression, which were below a factor of 2 ("minor") and the regulation values (REG) of differentially expressed genes. As for each of the three postlesional stages, six pairs of independent cDNA array hybridizations were performed, 6(F)x6(K) comparison matrices could be calculated for each stage.

The ensemble of 36 comparison matrices for each stage was then further analysed in a second type of Excel matrix, which compared the results of these matrices in order to identify significantly reproduced genes. For each gene, the number of significant up- or downregulations among the ensemble of comparison matrices was calculated. Then the absolute value of the difference of the number of up- (POS) minus downregulated (NEG) events was calculated, which can be recognized as the netto number of reproductions of a given gene into one regulation direction (RVal). This value was calculated for all genes, providing an average of the value (avRVal) and respective standard deviation (SD) for an ensemble of comparison matrices. These values were used to calculate two thresholds, which were decisive, whether a gene was selected for the final result list. The lower threshold (+2SDcutoff) was calculated as the avRVal+2*SD, while the higher threshold (+3SDcutoff) was calculated in analogy as avRVal+3*SD.

Genes, which had RVals greater than the +2SDcutoff were considered to be sufficiently reproducible, while those with RVals greater than the +3SDcutoff were considered to be highly reproducible. The representation of all genes versus their respective RVals produced a diagram, which appeared like a spectrum and was therefore termed the reproducibility spectrum. Highly reproducible genes have high peaks within these representations, while low peaks correspond to small RVals. In addition, the average regulation value (avREG) was calculated for each of the identified genes.

4. RESULTS

Part A: Calcium homeostasis is very critical for neuronal survival and axon pathfinding, as it was introduced in chapter 2.2. Therefore, the postlesional expression of two calcium binding proteins, calbindin d28 and parvalbumin was studied at three different postlesional intervals by using immunohistochemistry (chapter 4.1).

Within chapter 4.2 the distribution of rMDC15 (metalloprotease/disintegrin/cysteine-rich), a member of the ADAM (a disintegrin and metalloprotease)-family of metalloproteases, collapsin response mediator protein (CRMP)- 4 and Sox-10, a high mobility group protein and transcription factor of neural development, was revealed after fornix transection by using in situ hybridization.

In chapter 4.3, the expression of rMDC15- and Sox-10 mRNA was characterized at the lesion site. Furthermore, both histological techniques were used in order to determine the time points after axotomy, when stage (i) degeneration onset, (ii) axonal outgrowth and (iii) axonal growth arrest at the lesion site could be observed. Therefore, the spatiotemporal expression pattern of GAP-43 and L1 was analysed, using in situ hybridization and immunohistochemistry within the axotomized subiculum. These axon outgrowth associated proteins were known to be anterogradely transported within the axon. Therefore, their distribution within the proximal stump was described in relation to the neurofilament marker pan-axonal marker (PAM) and the degeneration associated protein clusterin at one day (1d), five days (5d), seven days (7d), two (2w) and four weeks (4w) post lesion (PL) by using immunohistochemistry.

Chapter 4.4 will treat the failure of a therapeutic approach, which was formely described to be highly efficacious to stimulate axon outgrowth.

Part B: A genomics approach was then undertaken to identify differentially expressed genes within the subiculum at the afore determined three characteristic postlesional stages (chapter 4.5). Commercially available cDNA filter arrays (Clontech Atlas^{TM} rat 1.2) were applied to analayse the expression of 1185 rat genes.

For each stage, highly reproducible lists of differentially expressed genes were identified, which were assembled into patterns that revealed known and novel features of axonal outgrowth in general. The cellular distribution of selected genes was assessed by using in situ hybridization.

Negative controls for all histological reactions can be found in the Appendix.

Part A

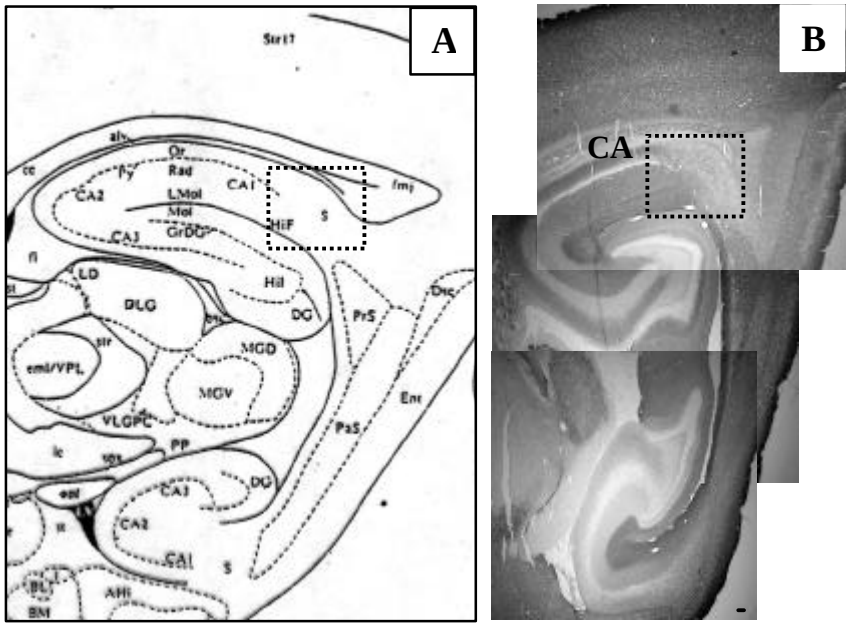

Figure 5. A sagittal view on the left caudal part of the adult rat brain. The schematic representation in (A) displays the sagittal plane of the brain, where dorsal and ventral subiculum could be studied (taken from Paxinos and Watson, 1982). The corresponding part of the brain is shown in the GAP-43 immunohistochemistry (B). Boxes in (A) and (B) show similar regions within the two representations. In the following figures of the subiculum, only the dorsal aspects of the subicular region will be displayed, as it was always found to be representative for the whole subiculum. Selected abbreviations are CA1, CA1 region of the hippocampal formation; cc, corpus callosum; alv, alveus; DG, dentate gyrus; S, subiculum; PrS, presubiculum; PaS, parasubiculum; HiF, hippocampal formation. Scale bar in (B), 100 μm.

4.1 Distribution of calbindin and parvalbumin in the subiculum after fornix transection

Calbindin immunoreactivity was found within principal neurons of CA1, but not in subicular neurons in the unlesioned control (Fig. 6 A and B). Only the dense neuropilar network was found to be labeled, while the neuronal cell bodies were spared. This labeling pattern was maintained at 2w PL (Fig. 6 C) and 3w PL (Fig. 6 D). Occasional labeling of presumably interneurons, like in figure 6 D could also be found within the control and at 2w PL.

On the contrary, parvalbumin positive cells could be identified within the unlesioned control subiculum (Fig. 6 E and F), but also at 2w PL (Fig. 6 G) and 3w PL (Fig. 6 H). Labeling characteristics of the parvalbumin antibody and the distribution of the positive cells suggested interneuronal labeling. Again, the dense neuropilar network within the subiculum was immunopositive for parvalbumin (Fig. 6 E-H). Qualitative comparisons of the overall labeling pattern and the number of neurons suggested that the distribution of parvalbumin positive structures was not changed at postlesional intervals 2w PL and 3w PL, as compared with the unlesioned control.

In conclusion, the labeling patterns and intensities of neither calbindin, nor parvalbumin positive structures were changed at 2w or 3w PL, as far as it could be detected by immunohistochemistry.

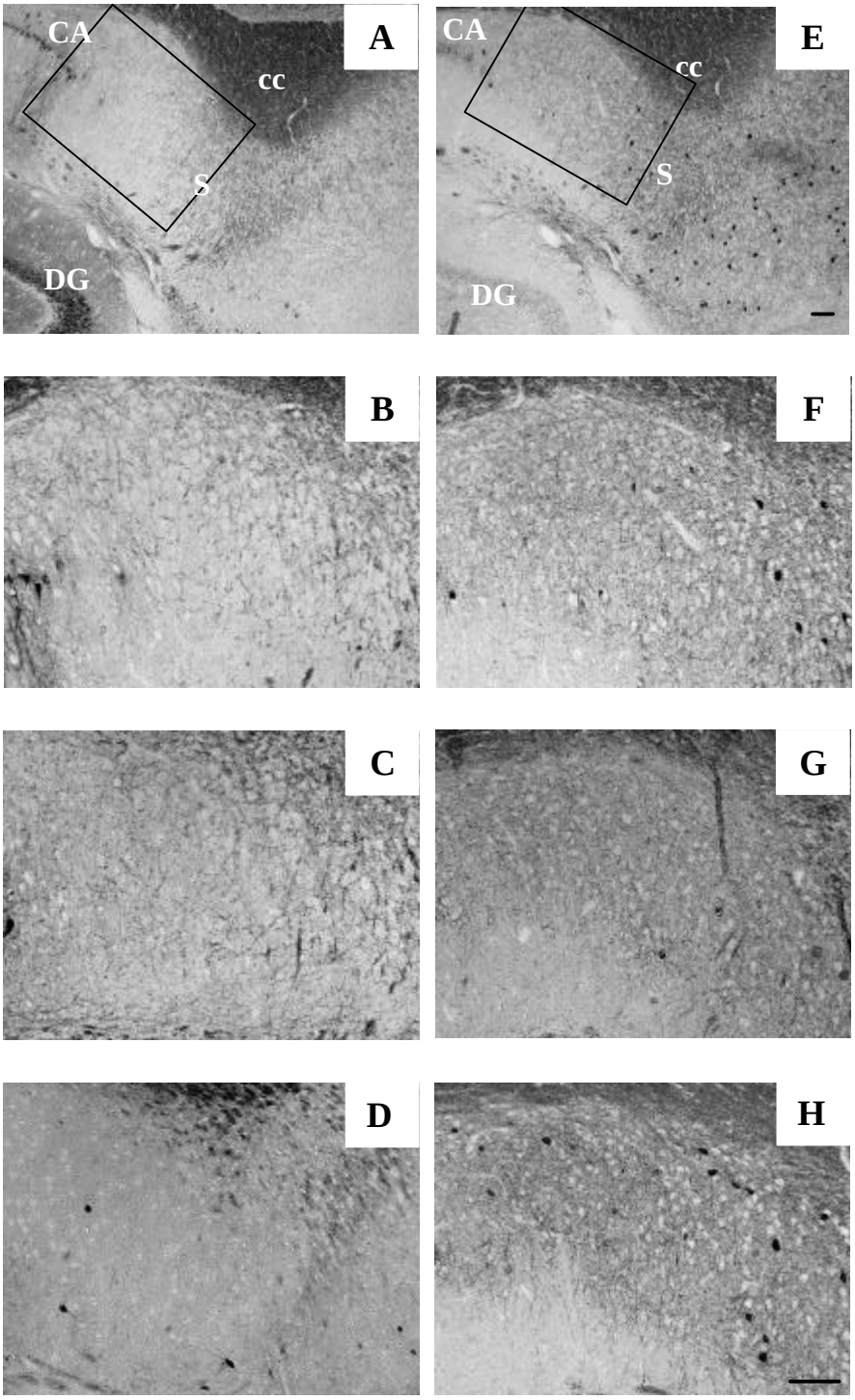

Figure 6. Expression of calbindin (A-D) and parvalbumin (E-H) in the subiculum revealed by immunohistochemistry. Panels A, B and E, F show the distribution of calbindin and parvalbumin in the unlesioned subiculum (n=4), respectively. Immunoreactivities at 2w PL (C, G; n=2) and 3w PL (D, H; n=2) are shown. The boxes in A and E circumscribe the areas shown at high power magnification in B and F, respectively. Panels C, D and G, H show similar areas, like those that are boxed. CA1, beginning of CA1 region of the hippocampus; cc, corpus callosum; DG, dentate gyrus; S, dorsal aspect of subicular complex. Scale bars 100 μm.

4.2 Distribution of rMDC15, CRMP-4 and Sox-10 in the subiculum after fornix transection

4.2.1 Expression of rMDC15 within the subiculum characterized by in situ hybridization

The expression of rMDC15 transcripts within the subiculum was studied with specific cRNA probes by non radioactive in situ hybridization. The unlesioned control displayed only moderate labeling (Fig. 7 A). Neither labeling pattern nor overall intensities within the whole subiculum appeared to be altered at neither postlesional time (Fig. 7 B, C and D). The apparently weaker labeling in figure 7 C was only true for this small aspect of the dorsal subiculum, which was kept within the panel in analogy to the regions selected for figures 7 A, B and D, while the overall labeling was similar to the control. Labeling preferentially over grey matter areas, with only few scattered labeling over white matter areas (see upper parts of Fig. 7 B, C and D), was suggestive for a preferentially neuronal expression of rMDC15.
In conclusion, the in situ hybridization labeling pattern and intensity of rMDC15 remained unchanged at 1d, 7d and 2w PL within the axotomized subiculum.

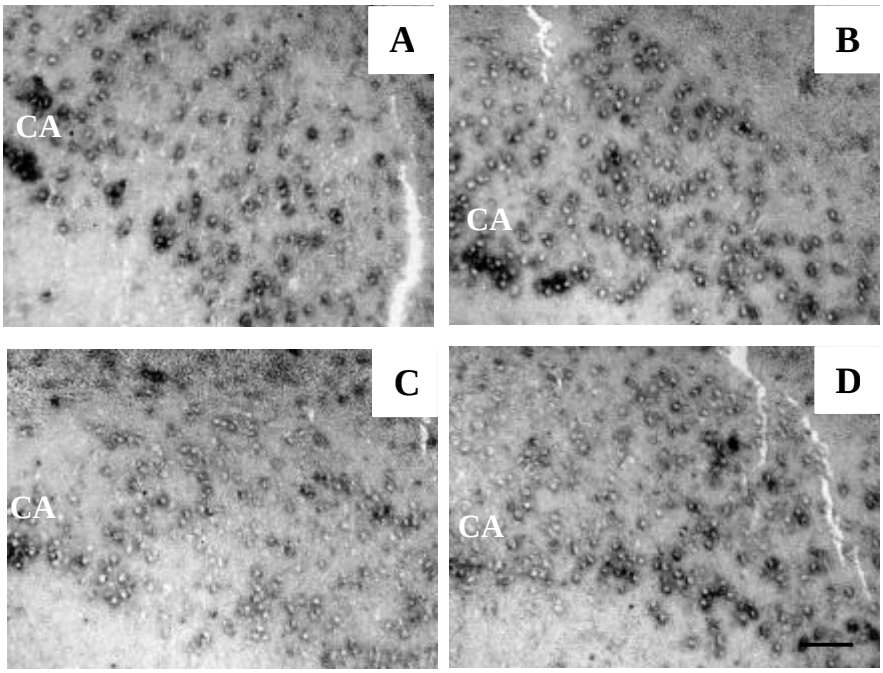

Figure 7. Expression of rMDC15/Disintegrin in the dorsal subiculum revealed by in situ hybridization. Non radioactive in situ hybridization of a probe specific for rMDC15/Disintegrin moderately labeled subiclular cells in the unlesioned control (A; n=1), at 1d PL (B; n=2), 7d PL (C; n=2) and 2w PL (D; n=2). Note the about equal distribution and labeling intensities (A-D). CA1, beginning of CA1 region of the hippocampus. Scale bar 100 μm.

4.2.2 Expression of CRMP-4 within the subiculum characterized by in situ hybridization

No induction of CRMP-4 transcript could be found within the axotomized subiculum at 1d PL by using non radioactive in situ hybridization (Fig. 8 B). Therefore no specific hybridization signals could be identified, neither in the unlesioned control (Fig. 8 A) nor at 1d PL (Fig. 8 B). The same was true for postlesional times 7d (n=2) and 4w (n=2). A sufficiently high concentration of the cRNA probe was used, as could be demonstrated by specific labeling of the developing rat cortex at P0 (Fig. 8 C). The concentration employed here, was twice as much as it would have been needed for an identical labeling patter like in figure 8 C. Therefore, hybridization with the sense probe at the same concentration resulted in some faint labeling of the tissue (Fig. 8 D).

In conclusion, neither the unlesioned, nor the axotomized subiculum expressed CRMP-4 transcripts, as far as it could be detected by in situ hybridization.

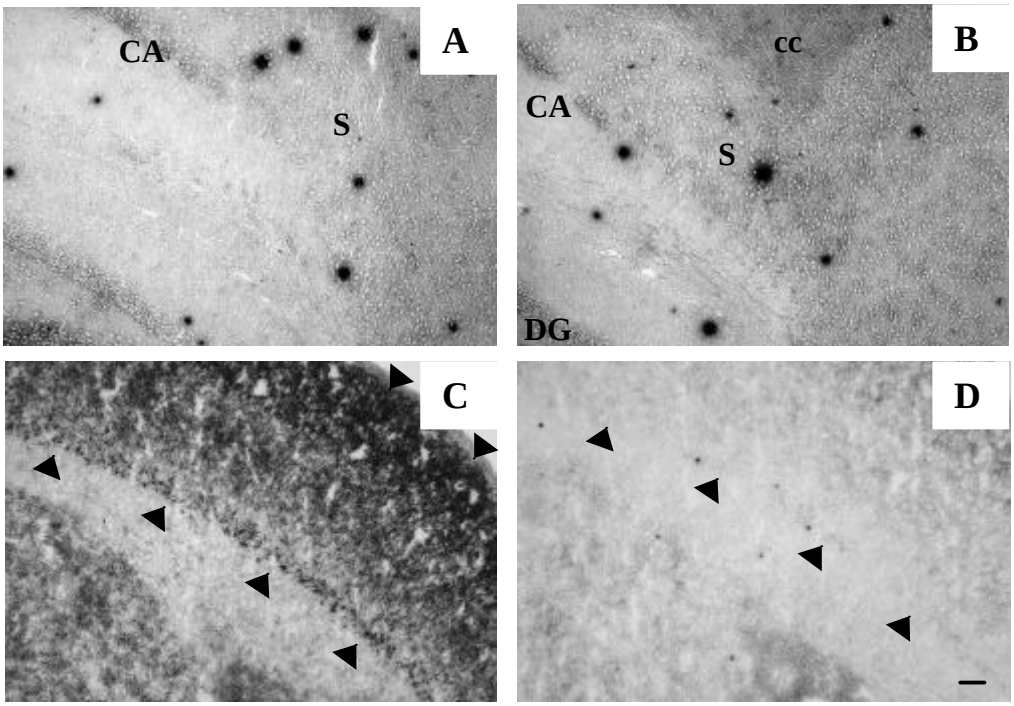

Figure 8. Expression of CRMP-4 in the dorsal adult subiculum and in the P0 cortex revealed by in situ hybridization. Non radioactive in situ hybridization of a probe specific for CRMP-4 did not label subicular cells, neither in the unlesioned control (A; n=1), nor at 1d PL (B; n=2). For comparison, the probe specifically labeled the developing cortex at P0, if the same cRNA probe concentration was used as for the adult brain (C). Both the antisense (A-C) and the sense control (D) were used at a concentration twice as high, as needed for stringent labeling. Thus, some background labeling can be seen with the sense control on an adjacent section (D). Dark spheric dots in (A) and (B) are unspecific precipitates. Arrowheads confine the cortical layers (in C, D). CA1, beginning of CA1 of the hippocampus; cc, corpus callosum; DG, dentate gyrus; S, dorsal aspect fo the subicular complex. Scale bar 100 µm.

4.2.3 Expression of Sox-10 within the subiculum characterized by in situ hybridization

In situ hybridization with a Sox-10 specific riboprobe preferentially labeled white matter areas, like the corpus callosum (cc) in figure 9 A-D. Only scarce labeling over the grey matter could be found (visible especially in Fig. 9 A and C). But none of the principal neurons within the CA1 or the subiculum appeared to be labeled, neither in the unlesioned control, nor at 1d, 7d or 2w PL (Fig. 9 A, B, C or D, respectively). Preferential distribution of Sox-10 positive cells over white matter areas and the small diameter of the cells (Fig. 9 B, inset), suggested labeling of glial cells, probably oligodendrocytes, or subpopulations thereof.

In conclusion, non radioactive in situ hybridization revealed that the expression pattern of Sox-10 remained unchanged at 1d, 7d and 2w PL.

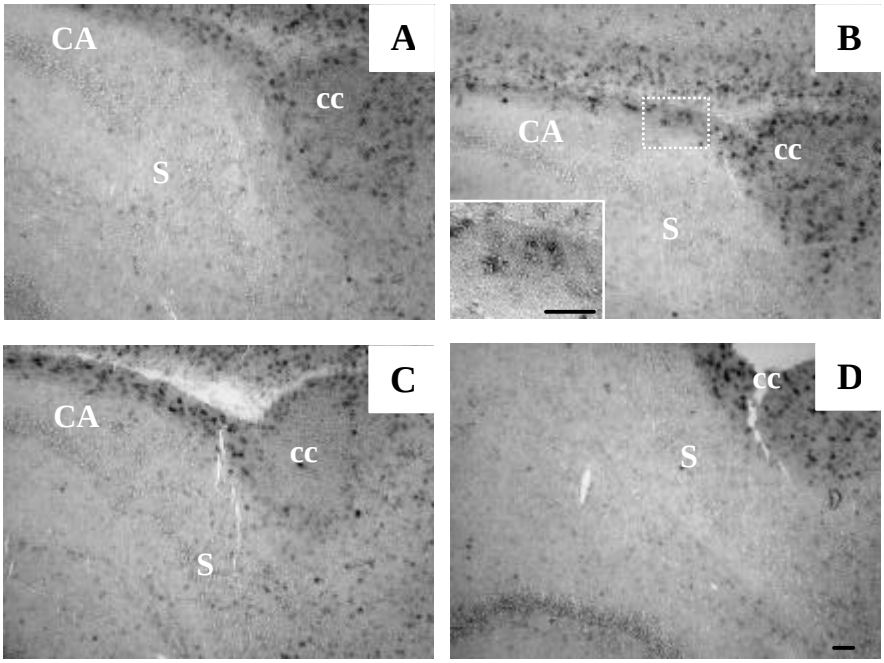

Figure 9. Expression of Sox-10 in the dorsal subiculum revealed by in situ hybridization. Non radioactive in situ hybridization of a probe specific for Sox-10 only scarcely labeled subicular cells, but none of them appeared to be a principal neuron (A-D). But cells of the corpus callosum, cc, were labeled within the unlesioned control (A; n=1), at 1d PL (B; n=3), 7d PL (C; n=3) and at 2w PL (D; n=3). Inset in (B) shows magnification of the boxed area in (B). Note preferential labeling over white matter areas. CA1, beginning of CA1 of the hippocampus; cc, corpus callosum; DG, dentate gyrus; S, dorsal aspect of the subicular complex. Scale bars 100 μm.

4.3 Postlesional distribution of regeneration and degeneration associated genes within the subiculum and the fornix stumps

4.3.1 Expression of GAP-43 and L1 within the subiculum characterized by in situ hybridization and immunohistochemistry

Expression of GAP-43 mRNA and protein within the subiculum

Cells, which were moderately labeled with a GAP-43 specific cRNA probe, were found widespread throughout the unlesioned subiculum (Fig. 10 A). Non radioactive in situ hybridization revealed subicular labeling preferentially over grey matter areas, while the corpus callosum was not labeled (Fig. 10 A). Distribution and labeling intensities were similar in the unlesioned control, at 1d, 7d and 2w PL (Fig. 10 A-D, respectively). Distribution and shape of positive cells (inset Fig. 10, B) suggest labeling of pyramidal neurons of the subiculum.

The corresponding GAP-43 immunolabeling was found at different intensities within the regions of the unlesioned subiculum (Fig. 5). A characteristic transition from a more intensive neuropillar labeling in the CA1 region to a less intensive labeling of the dorsal subiculum could be seen within the unlesioned control and at all postlesional times (CA1 in Fig. 11 A-D). Apparently no neuronal cell bodies were immunopositive for GAP-43, as pyramidally shaped cell bodies were spared from labeling (Fig. 11 A-D). Neuropilar labeling intensities were about equal in the unlesioned control (Fig. 11 A) and at 1d, 7d and 4w PL (Fig. 11 B, C, D, respectively). Therefore, no induction of GAP-43 immunoreactivity could be found within neurons at none of the postlesion times studied. Likewise, the neuropilar labeling pattern remained unchanged.

In conclusion, GAP-43 was constitutively expressed in unlesioned and axotomized subicular neurons, but exclusive labeling of the subicular neuropil suggests, that GAP-43 protein was not detectable within the neuronal cell bodies. Neither the neuronal, nor the neuropilar labeling pattern was changed at 1d, 7d or 4w PL.

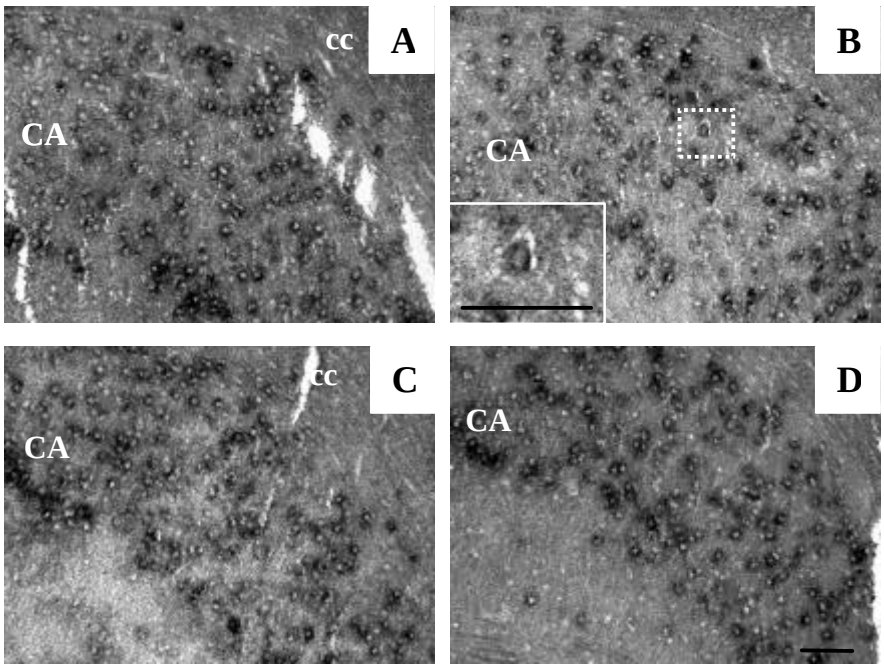

Figure 10. Expression of GAP-43 in the dorsal subiculum revealed by in situ hybridization. Non radioactive in situ hybridization of a probe specific for GAP-43 moderately labeled subicular cells in the unlesioned control (A; n=2), at 1d (B; n=2), 7d (C; n=2) and 2w PL (D; n=1). High power magnification of the boxed area in (B) is shown in the inset in (B). Note the pyramidal shape of the labeled cell (inset in B). CA1, beginning of CA1 region of the hippocampus; cc, corpus callosum. Scale bars 100 μm.

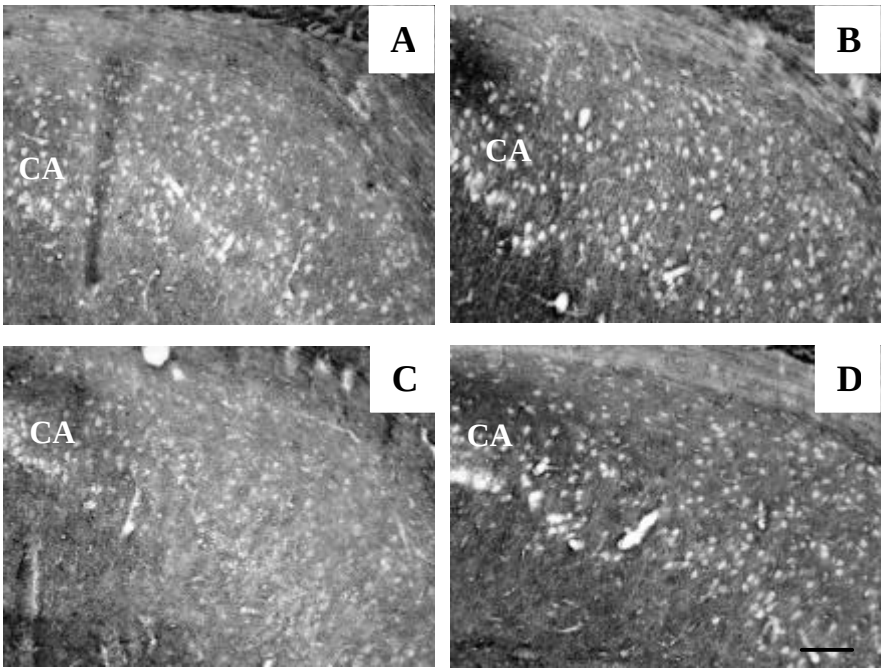

Figure 11. Expression of GAP-43 in the dorsal subiculum revealed by immunohistochemistry. GAP-43 immunoreactivities in the unlesioned control (A; n=2), at 1d (B; n=4), 7d (C; n=4) and 4w PL (D; n=4) are shown. Note the about equal neuropilar labeling, with neuronal cell bodies being spared (i.e. left white). CA1, beginning of CA1 region of the hippocampus. Scale bar 100 µm.

Expression of L1 mRNA and protein within the subiculum

In analogy to the GAP-43 labeling patterns, in situ hybridizations for rat L1 revealed widespread labeling of subicular cells, but only over grey matter areas in the unlesioned control (Fig. 12 A), at 1d, 7d and 2w PL (Fig. 12 B, C and D, respectively). Here, distribution and labeling intensities were about equal, suggesting that L1 mRNA localization and levels did not change after axotomy. Again, the pyramidal cell shape of labeled L1 positive cells suggested localization of the transcript to pyramidal neurons (inset in Fig. 12 B).

L1 immunoreactivity revealed dense labeling of the subicular neuropil, but again with pyramidal neurons being spared in the unlesioned control and at 1d, 7d and 4w PL. (Fig. 13 A-D, respectively). Thus, L1 protein was also not induced within subicular neurons to a level detectable by immunohistochemistry after axotomy of the postcommissural fornix .

In conclusion, rat L1 transcripts were constitutively expressed within the unlesioned subicular neurons and no further induction or repression could be detected after axotomy. L1 immunoreactivity was found in the subicular neuropil, but not in neurons, and this labeling pattern remained unaffected by the axotomy.

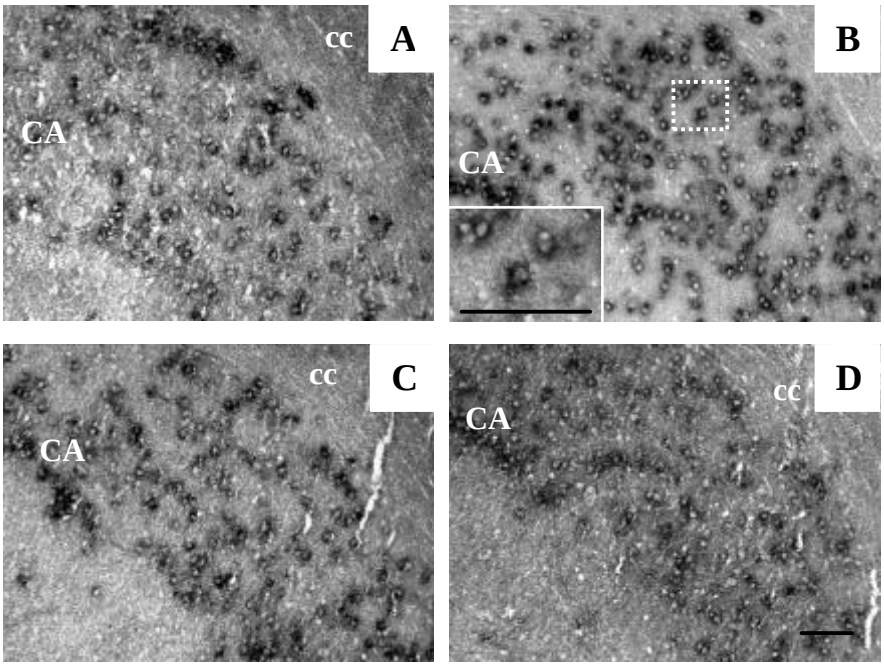

Figure 12. Expression of rat L1 in the dorsal subiculum revealed by in situ hybridization. Non radioactive in situ hybridization of a probe specific for rat L1 moderately labeled subicular cells in the unlesioned control (A; n=2), at 1d (B; n=2), 7d (C; n=2) and 2w PL (D; n=1). High power magnification of the boxed area in (B) is shown in the inset in (B). Note the pyramidal shape of the labeled cell (inset in B). CA1, beginning of CA1 region of the hippocampus; cc, corpus callosum. Scale bars 100 μm.

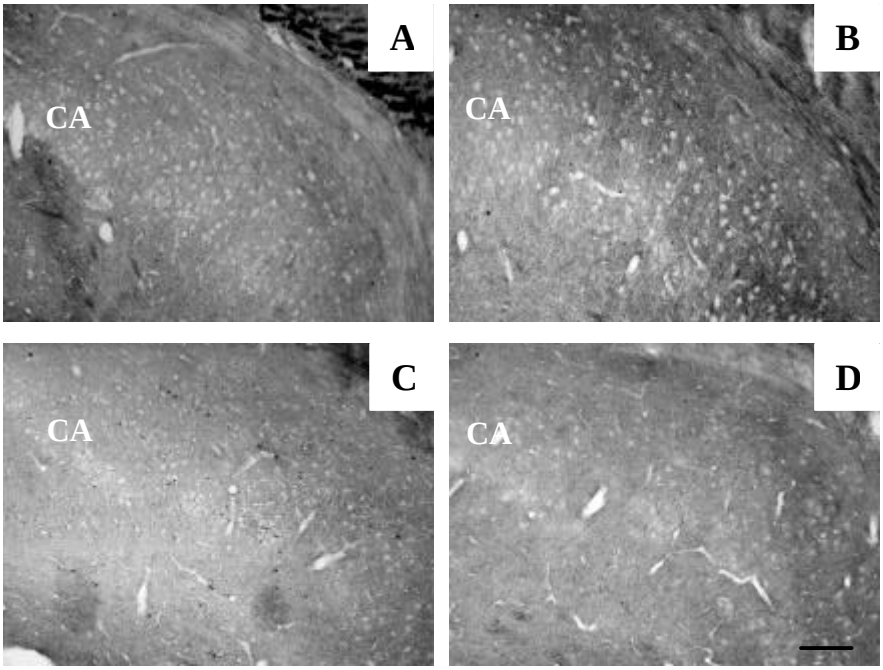

Figure 13. Expression of L1 in the dorsal subiculum revealed by immunohistochemistry. L1 immunoreactivities in the unlesioned control (A; n=2), at 1d (B; n=4), 7d (C; n=4) and 4w PL (D; n=4) are shown. Note the almost equal neuropilar labeling, with neuronal cell bodies being spared (i.e. left white). CA1, beginning of CA1 region of the hippocampus; cc, corpus callosum. Scale bar 100 µm.

4.3.2 Expression of rMDC15 and Sox-10 within the fornix stumps characterized by in situ hybridization

Expression of rMDC15 mRNA within the fornix stumps

In situ hybridization with a rMDC15 specific riboprobe revealed widespread and intensive expression of rMDC15 within the hypothalamus. The distribution of the labeled cells was very uniform, therefore the trajectory of the fornix could not be determined in the unlesioned control (Fig. 14 A). At 1d PL, both the proximal and distal stump appeared to be slightly less labeled close to the lesion, while the surrounding neuropil displayed a similar distribution of rMDC15 expressing cells as the control (Fig. 14 B). At 7d PL, ubiquitous expression of rMDC15 has returned to control levels, apart from the small unlabeled area around the lesion (Fig. 14 C). One week later, the lesion site could hardly be recognized, while the uniform expression pattern looked almost like in the control (Fig. 14 D).

In conclusion, rMDC15 was widely expressed within the unlesioned hypothalamus and after fornix axotomy. Expression over both, the proximal and distal stump of the fornix, appeared to be slightly reduced at 1d PL, but returned back to normal intensity and distribution at 7d and 2w PL.

Expression of Sox-10 mRNA within the fornix stumps

Sox-10 mRNA expression was found within the myelinated unlesioned fornix tract, suggesting glial labeling. The surrounding neuropil was only scarcely positive, as could be shown with the Sox-10 specific in situ hybridization (Fig. 14 E). At 1d PL, only the proximal stump was positive up to its tip (arrowheads in Fig. 14 F), while the remaining area within the proximal stump up to the lesion site was less intensively labeled. The distal stump was positive for Sox-10 (Fig. 14 F, inset). At 7d PL, the proximal stump remained positive, and labeling within the distal stump and at the lesion site was even more increased (Fig. 14 G and inset, respectively). By the time that the fornix reached the lesion site (see 4.3.3), at 2w PL, the Sox-10 expression level has subsided to normal levels within the distal stump, and remained at the control level in the proximal stump (Fig. 14 H, inset and H, respectively).

In conclusion, in situ hybridization with a Sox-10 specific riboprobe revealed preferential expression of the transcript within the fornix tract, with the surrounding neuropil being less labeled. After onset of distal degeneration at 5d PL (see 4.3.3), the distal fornix stump was labeled even more intensively, than in the unlesioned control. At 2w PL this increased labeling of the distal stump returned to control levels again.

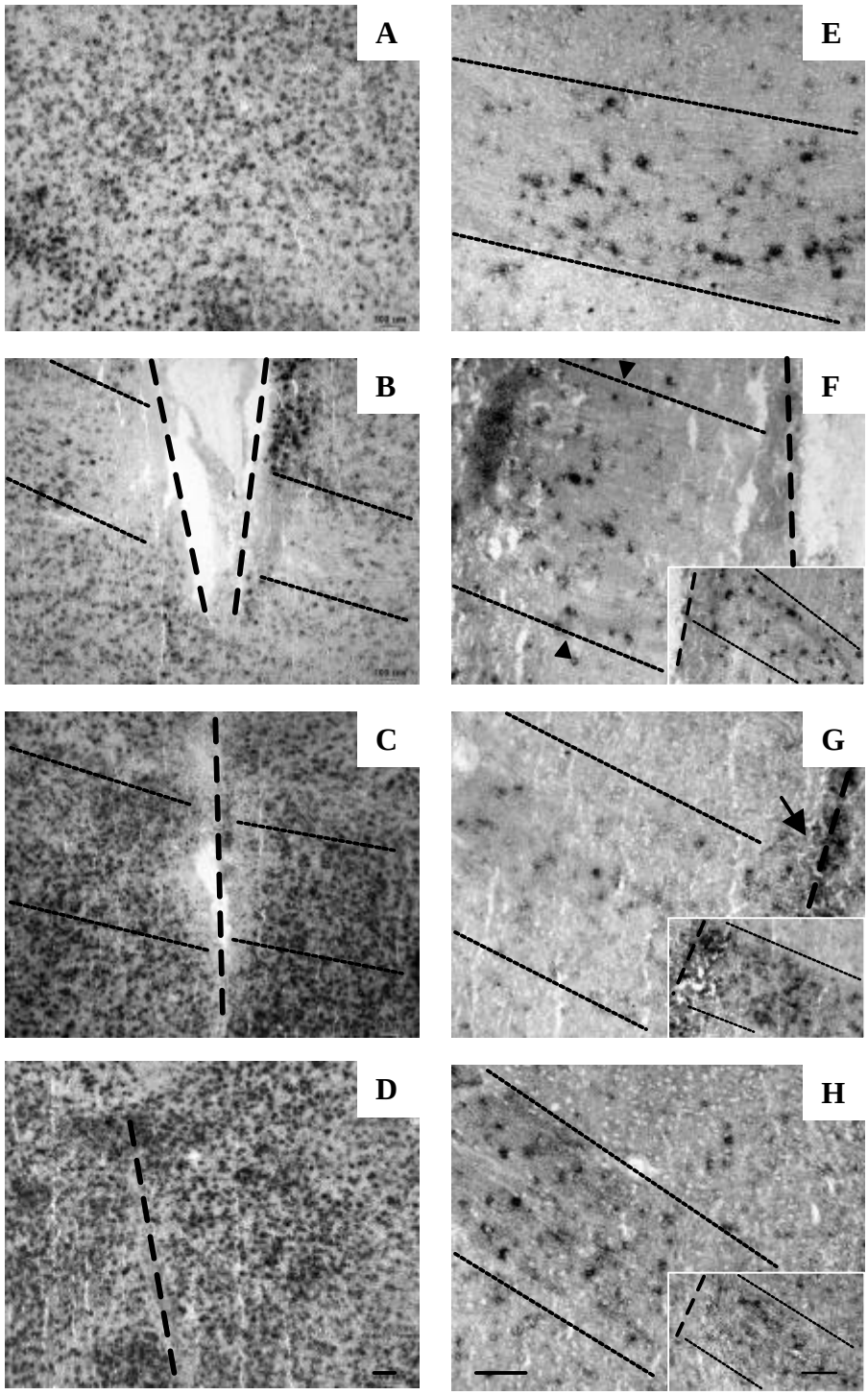

Figure 14. Expression of rMDC15 and Sox-10 within the perilesional area revealed by in situ hybridization. Non radioactive in situ hybridizations of the perilesional area with cRNA probes specific for rMDC14 (A-D) and Sox-10 (E-H) are shown in the control (A, E; n=1), at 1d (B, F; n=3), 7d (C, G; n=3) and 2w PL (D, H; n=3). The trajectory of the fornix is marked by horizontal dotted lines, as far as it could be recognized. Localization of the lesion site is indicated by the vertical dotted lines. The insets in (F, G, H) show Sox-10 labeling of the distal fornix stump. Arrowheads in (F) indicate the position of the tip of the proximal fornix stump. Note the increased labeling intensity for Sox-10 at the lesion site (arrow in G) and within the distal stump at 7d PL (inset in G). Scale bars 100 μm.

4.3.3 Expression of PAM, GAP-43, L1 and clusterin within the fornix stumps characterized by immunohistochemistry

Immunoreactivities in the unlesioned control fornices

The unlesioned fornix was intensively labeled by PAM-immunohistochemistry, which labels neurofilaments, appearing darker than the surrounding tissue and the mammillary body (Fig. 15 A). Other myelinated tracts were equally intensively labeled, while the neuropilar labeling pattern was generally brighter. In contrast, GAP-43 labeling was only weak over the myelinated fornix, while the surrounding neuropil appeared darker (Fig. 15 B). However, the displayed labeling intensity was identified to clearly correspond to a GAP-43 positive immunoreactivity, as compared to other myelinated tracts, which were described to be GAP-43 negative. L1 immunostaining revealed the unlesioned fornix to be slightly more intensively labeled than the surrounding neuropil (Fig. 15 C), while immunoreactivity for clusterin was only scarce over the tract, while higher in the surrounding neuropil (Fig. 15 D). The distribution and shape of clusterin positive cells suggested glial labeling within the neuropil.

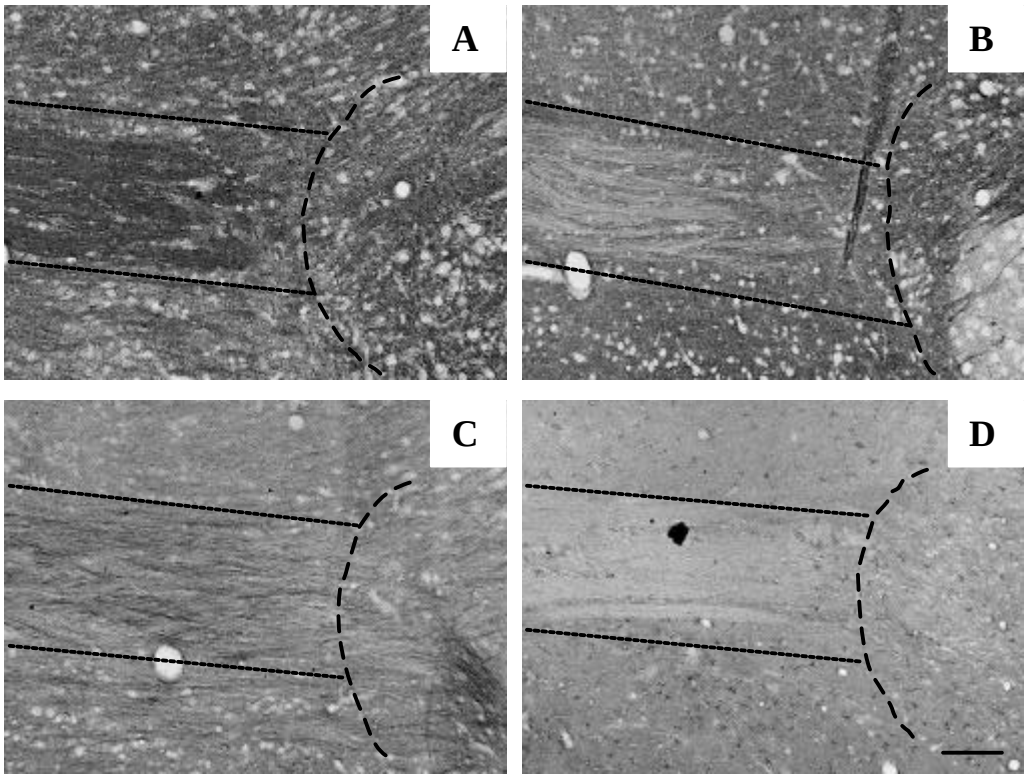

Figure 15. Distribution of PAM, GAP-43, L1 and clusterin in the unlesioned fornix revealed by immunohistochemistry. Specific immunoreactivities of antibodies against PAM (A; n=3), GAP-43 (B; n=3), L1 (C; n=2) and clusterin (D; n=1) within the fornix (confined by horizontal dotted lines) and the surrounding hypothalamic tissue, including the mammillary body (confined by bent dotted lines) are shown on adjacent sections. Scale bar 100 µm.

Immunoreactivities in the transected fornix stumps at one day post lesion

The transected fornix stumps remained at the lesion site at 1d PL. Up to about 400-600 µm proximal from the lesion site, immunoreactivities for PAM, GAP-43, L1 and clusterin remained at control levels (Fig. 16 A-D), while this was not true closer to the lesion site. At a distance of about 400 µm proximal to the lesion, immunoreactivities for PAM, GAP-43 and L1 appeared to be increased, as compared to the surrounding tissue and adjacent parts of the tract (arrowheads in Fig. 16 A-C, respectively). Confocal microscopy revealed spherical structures within the immediate proximal stump (closer than 400 µm to the lesion site), which were positive for GAP-43 only (Fig. 17 B, C), while at greater distances from the lesion site, similar spherical structures were positive for both PAM and GAP-43 (Fig. 17 A-C).

The immediate proximal stump, close to the lesion site (arrows in Fig. 16 A-D), was generally labeled more heterogenously, than the most proximal parts of the stumps. This area later degenerated (mentioned below), which was already recognizable, by an increased immunolabeling for clusterin (Fig. 16 D). Clusterin immunoreactivity was punctually increased within the immediate proximal stump, but also in individual fibres.

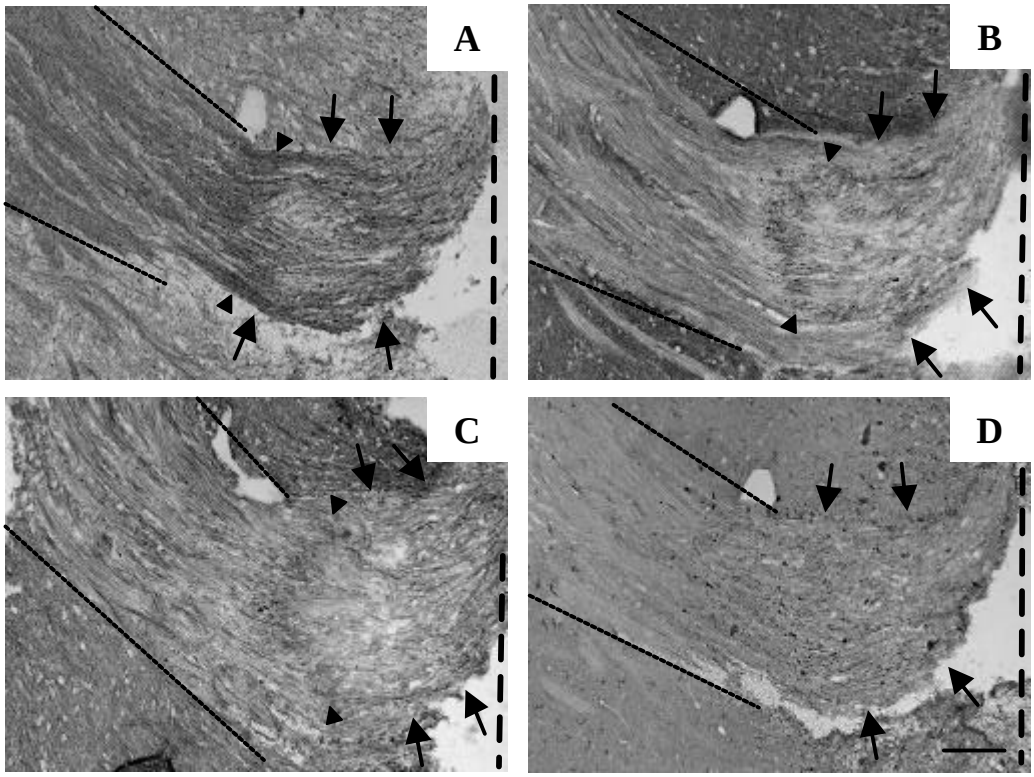

Figure 16. Distribution of PAM, GAP-43, L1 and clusterin in the lesioned fornix at 1d PL revealed by immunohistochemistry. Specific immunoreactivities of antibodies against PAM (A; n=3), GAP-43 (B; n=3), L1 (C; n=3) and clusterin (D; n=3) within the fornix (confined by horizontal dotted lines) and the surrounding hypothalamic tissue are shown on adjacent sections. The lesion site appears to the right (horizontal dotted lines). Note the remaining immunolabelings of proximal fornix fibres close to the lesion site (arrows), which are proximally confined by increased immunoreactivities for PAM, GAP-43 and L1 (arrowheads in A, B, C, respectively). Scale bar 100 μm.

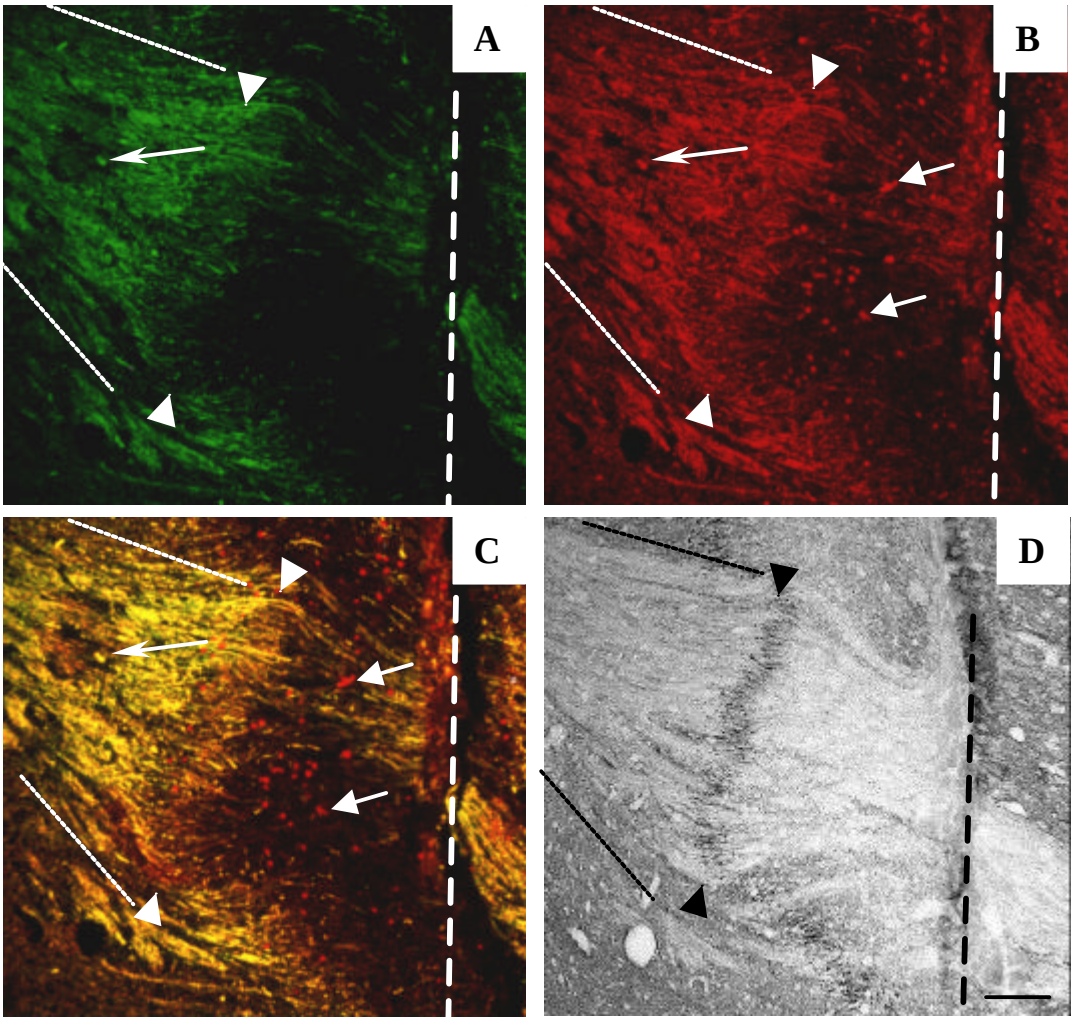

Figure 17. PAM and GAP-43 immunoreactivity of the transected proximal fornix stumps at the lesion site by fluorescence- and DAB-immunohistochemistry at 1d PL. Confocal microscopy of the double-labelled fornix is shown with specific immunoreactivities for PAM (green, A; n=3), GAP-43 (red, B; n=3) and double exposure for these proteins (C). GAP-43 DAB-immunostaining of an adjacent section is displayed for comparison (D). The proximal fornix stump is confined by horizontal dotted lines, while the lesion site to the left is indicated by vertical dotted lines. Note the increased immunoreactivity within the proximal fornix stump in D (arrowheads) being less apparent in the fluorescent labelings (A-C), while they in turn more sensitively reflect PAM and GAP-43 distribution. Thus GAP-43 only positive spherical structures can be recognized in (B) and (C) (normal arrows) up to about 400 µm proximal to the lesion site, which are not positive for PAM. On the other hand, there are spheres further proximally, which are positive for both GAP-43 and PAM (thin arrows in A-C).

Immunoreactivities in the transected fornix stumps at five days post lesion

As mentioned above, proximal axons within the immediate area (closer than 400 µm) of the lesion site apparently degenerated and retracted up to about 500-600 µm from the lesion site (arrowheads in Fig. 18). Both PAM and GAP-43 immunoreactivities were lost distal from this retraction boundary (arrows in Fig. 18 A, B). The proximal tip of the tract displayed some characteristic bulbuous or beadlike structures, which were PAM-positive (Fig. 18 A). The loss of axons could also be recognized within the distal fornix stump, as revealed by loss of control-like PAM immunoreactivity over the tract (inset in Fig. 18 A). Furthermore, both L1 and clusterin immunoreactivities were increased within the area, where axons appeared to be lost (Fig. 18 C, D and insets therein), but not beyond the retraction boundary at about 500-600 µm.

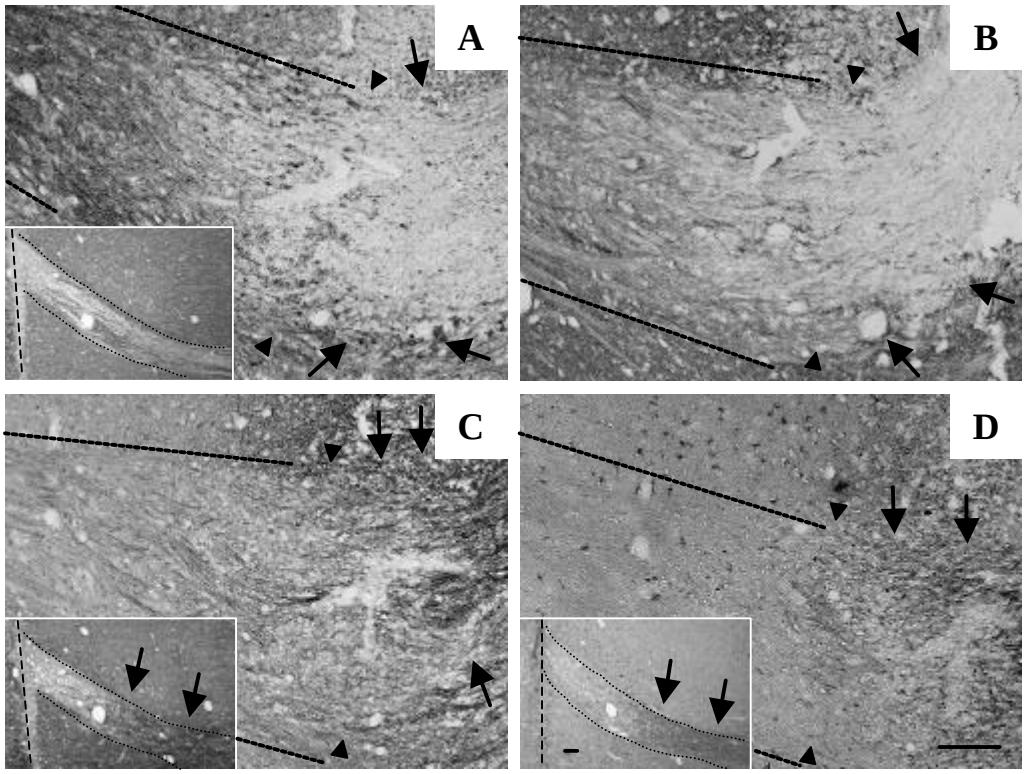

Figure 18. Distribution of PAM, GAP-43, L1 and clusterin in the lesioned fornix at 5d PL revealed by immunohistochemistry. Specific immunoreactivities of antibodies against PAM (A; n=3), GAP-43 (B; n=3), L1 (C; n=3) and clusterin (D; n=3) within the fornix (confined by horizontal dotted lines) and the surrounding hypothalamic tissue are shown on adjacent sections. The lesion site (vertical dotted lines visible only in insets) would appear to the right. Note the approximate tip of the tract (arrowheads in A-D). Furthermore axons within the arrow confined areas (arrows in A-D) have almost completely lost PAM and GAP-43 immunoreactivities (A, B), but display increased reactivities for L1 and clusterin (C, D), what is especially apparent wihin the distal stumps (arrows in insets of C and D), where axons of the distal stump degenerated, too (inset in A). Scale bars 100 µm.

Immunoreactivities in the transected fornix stumps at seven days post lesion

At seven days post lesion immunoreactivities of the proximal stump for PAM, GAP-43 and L1 were almost back to control levels up to about 100-200 µm from the lesion site, indicating an outgrowing proximal stump (Fig. 19 A-C). Concurrent with the outgrowth, increased clusterin immunoreactivity was reduced to an area extending from the lesion site up to about 200 µm proximal to the lesion site (Fig. 19 D). The distal stump has now completely lost its PAM and GAP-43 immunoreactivities (insets in Fig. 19 A and B), while increased immunoreactivities for both L1 and clusterin could still be found within the most proximal and distal parts of the distal stumps (arrows in insets in Fig. 19 C and D).

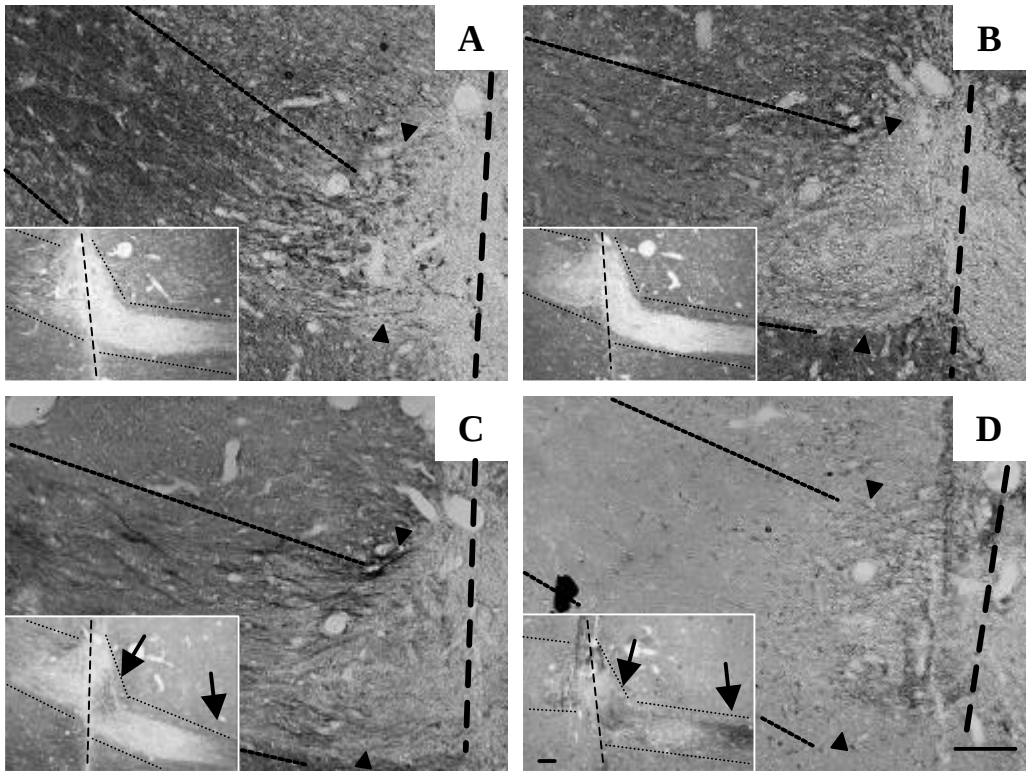

Figure 19. Distribution of PAM, GAP-43, L1 and clusterin in the lesioned fornix at 7d PL revealed by immunohistochemistry. Specific immunoreactivities of antibodies against PAM (A; n=3), GAP-43 (B; n=3), L1 (C; n=3) and clusterin (D; n=3) within the fornix (confined by horizontal dotted lines) and the surrounding hypothalamic tissue are shown on adjacent sections. The lesion site is indicated by a vertical dotted line to the right (in insets A-D in the center). Note the approximate tip of the tract (arrowheads in A-D), which is now close to the lesion. Furthermore, the distal stump displays increased labeling for L1 and clusterin, now close to the lesion site (arrows in insets of C and D, respectively), while immunolabeling for PAM and GAP-43 is lost (insets in A and B, respectively). Scale bars 100 μm.

Immunoreactivities in the transected fornix stumps at two and four weeks post lesion

Immunoreactivities for PAM, GAP-43 and L1 were back to the normal pattern in the proximal stump by 2w PL (Fig. 20 A-C, respectively), what could even better be recognized at 4w PL (Fig. 21 A-C, respectively). Axons remained here within their former pathway and were not seen to circumvent or bypass the lesion site. Only clusterin immunoreactivities were still slightly increased within the lesion site and within the distal tract at 2w PL (Fig. 20 D and inset in D), apparently within glial cells as could be inferred from size and shape of positive cells in (inset in Fig. 20 D). This increased clusterin immunoreactivity of the perilesional area was almost back to control levels at 4w PL (Fig. 21 D).

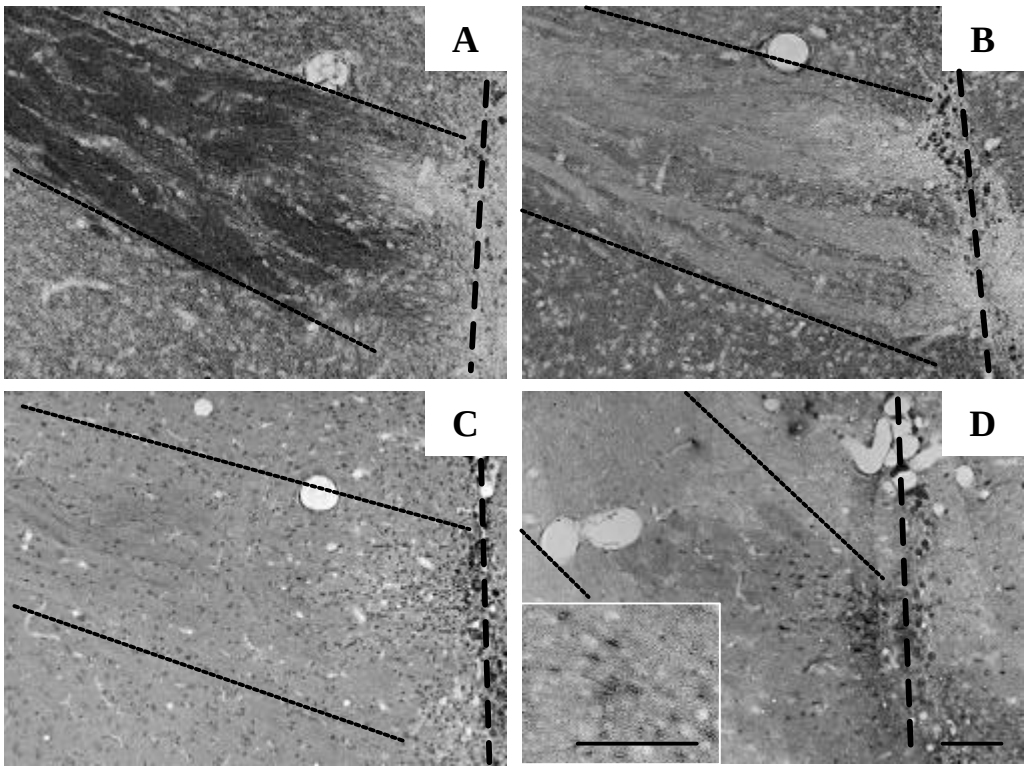

Figure 20. Distribution of PAM, GAP-43, L1 and clusterin in the lesioned fornix at 2w PL revealed by immunohistochemistry. Specific immunoreactivities of antibodies against PAM (A; n=3), GAP-43 (B; n=3), L1 (C; n=3) and clusterin (D; n=3) within the fornix (confined by horizontal dotted lines) and the surrounding hypothalamic tissue are shown on adjacent sections. The lesion site is indicated by a vertical dotted line to the right. Note the labeling pattern for PAM (A), GAP-43 (B) and L1 (C) being back to control levels in the proximal stump, up to the lesion site (compare with Fig. 15), while clusterin immunoreactivity is still increased at the lesion site (D). Inset in (D) shows magnification of clusterin positive cells from the distal stump. Scale bars 100 µm.

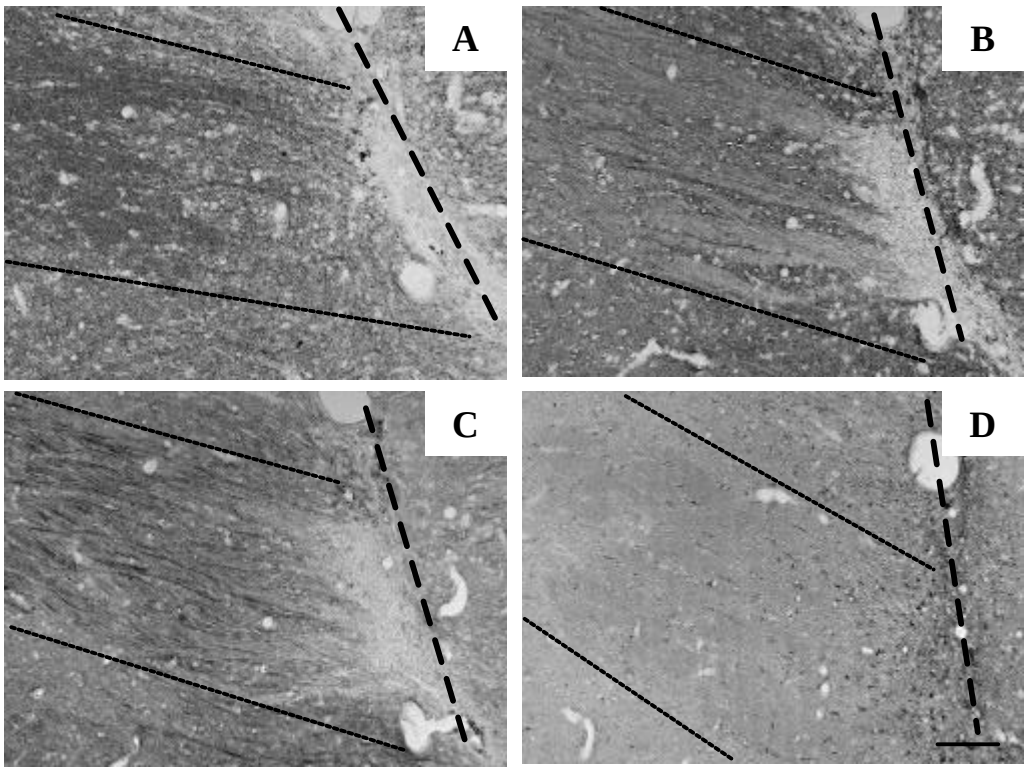

Figure 21. Distribution of PAM, GAP-43, L1 and clusterin in the lesioned fornix at 4w PL revealed by immunohistochemistry. Specific immunoreactivities of antibodies against PAM (A; n=3), GAP-43 (B; n=3), L1 (C; n=2) and clusterin (D; n=3) within the fornix (confined by horizontal dotted lines) and the surrounding hypothalamic tissue are shown on adjacent sections. The lesion site is indicated by a vertical dotted line to the right. Note the labeling pattern for PAM (A), GAP-43 (B) and L1 (C) being back to control levels in the proximal stump up to the lesion site, with the latter being almost unlabeled. Clusterin immunoreactivity at the lesion site is now almost back to control level (D). Scale bars 100 μm.

Conclusion of the degenerative and regenerative events within the fornix between 1d and 4w PL

At 1d PL the transected fornix stumps remained at the lesion site, but already displayed molecular and morphological reorganizations at about 400 µm proximal from the lesion site, which were followed by the degeneration and retraction of the proximal stump to about 600 µm at 5d PL. Concurrent with the degeneration of the tip of the proximal stump, the distal stump degenerated, too, apparently from distal (at 5d PL) to proximal, up to the lesion site (at 7d PL).

Degenerative events within the transected fornix stumps could generally be recognized by a decrease of PAM and GAP-43 and an increase of L1 and clusterin immunoreactivities.

By 7d PL axons started to regrow within their former pathway and approached the lesion site up to about 200 µm, finally having reached it at 2w PL. At least until 4w PL axons of the proximal stump remained at the lesion site, without bypassing it (see Figure 22 for schematic overview).

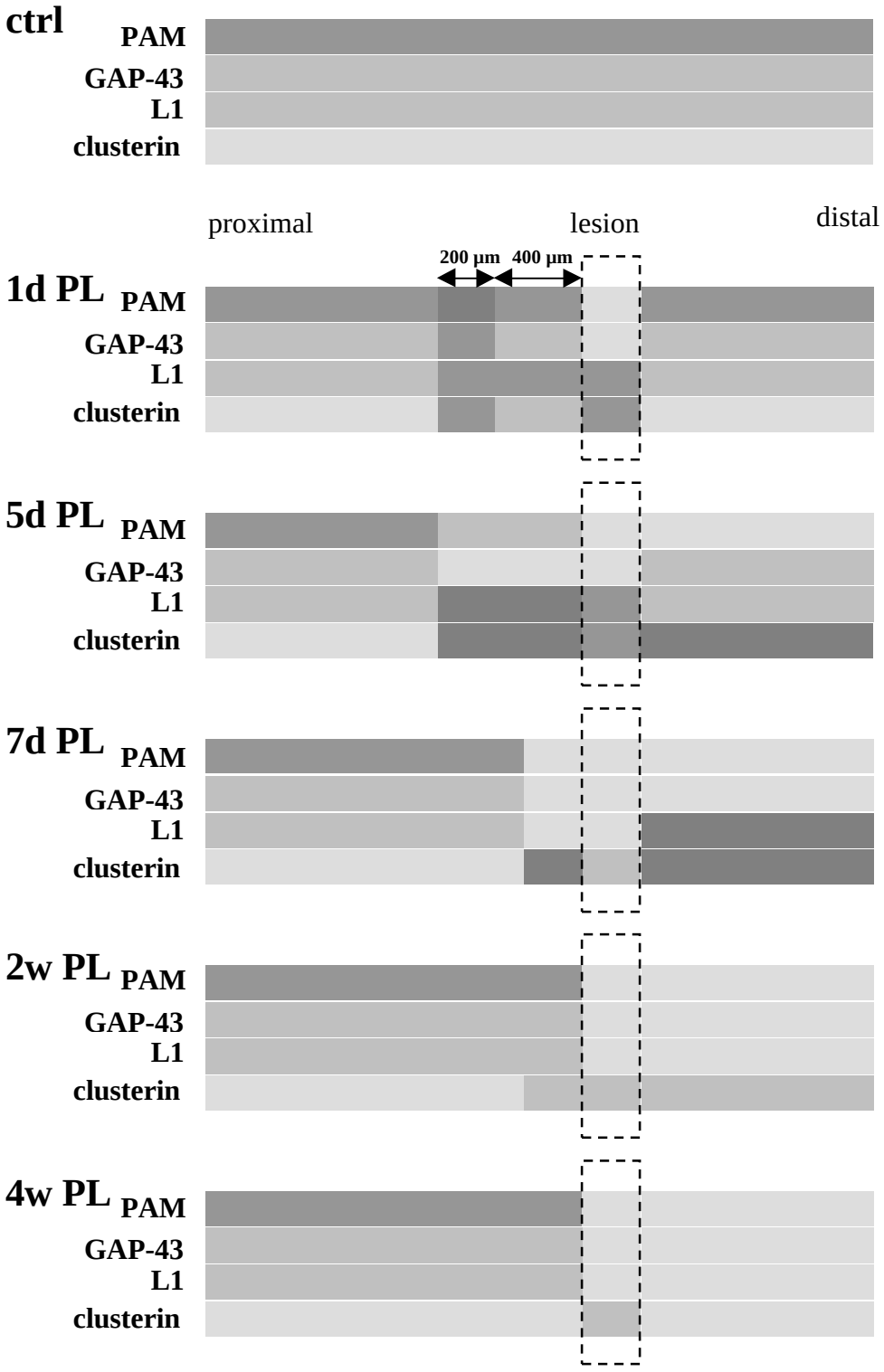

Figure 22. Schematic summary of the relative immunoreactivities within the postcommissural fornix after axotomy. Investigated post lesion (PL) times and proteins are indicated to the left. The lesion area is boxed, with the proximal stump to the left and the distal to the right. Relative immunoreactivities are encoded in grey scales, trying to maintain the approximate intensity relationships within each labeled fornix tract and among the different proteins studied.

4.4 Regeneration failure after immediate DPY injection

In order to study the molecular responses during stage (iv) of CNS axon regeneneration by similar means as described in the chapters before, the fornix regeneration paradigm described by Stichel et al. (Stichel et al., 1999a; Stichel et al., 1999b) was intended to be employed.
The Fe^{2+}-chelator 2,2'-dipyridyl (DPY) which inhibits proly-4-hydroxylase, a crucial enzyme for collagen IV biosynthesis was injected into the lesion site, as it was previously described (Stichel et al., 1999a; Stichel et al., 1999b). This component was shown to interfere with collagen IV deposition within the basement membrane of the lesion site. This treatment was demonstrated to be highly efficacious, leading to axonal regeneration with outgrowth of axotomized axons beyond the lesion site in at least 50% of cases (Stichel et al., 1999a; Stichel et al., 1999b).
After unilateral fornix transection, DPY injected animals were sacrificed after between two and four weeks post lesion. Surgery parameters were adapted to ensure complete fornix transection, while leaving the mammillothalamic tract unsevered (Fig. 23). The slight enlargement of the lesion site was compensated by applying a higher volume and/or concentration of the injected components, than previously reported (Stichel et al., 1999a; Stichel et al., 1999b).
Pan-axonal marker (PAM) labeled cryosections were then screened for regenerating fornix fibres in the lesion site and in the distal portion of the tract, as it was also done previously (Stichel et al., 1999a; Stichel et al., 1999b). Moreover, these labelings revealed both the correct size of the lesion and the position of the injection site with respect to the lesion. Alltogether 88 animals were treated (table 3). Immunohistochemical analysis revealed spontaneous sprouting of the proximal stump of the transected postcommissural fornix up to the lesion site, as it could be observed in untreated animals (4.3). But none of the animals displayed regenerating and PAM-positive axons within or distal to the lesion site (Fig. 23).
In conclusion, immediate DPY injection into the lesion area was not sufficient to promote axonal regeneration in the fornix.

DPY-treated animals

88 altogether	**2w**	**3w**	**4w**
amount/**substance**		**DPY**	
1.6 µl, 10 mM	8	2	8
2x 0.8 µl, 10 mM	2		4
2x 1.2 µl, 10 mM			7
2x 1.2 µl, 15 mM	16		
1.6 µl, 15 mM	7		
2.0 µl, 15 mM	8	10	
2.0 µl, >15 mM	8	8	
sum of column	49	20	19

Table 3. DPY-treated animals.

The table displays post lesion times until animals were sacrificed, the amount of the injected substance and the respective number of treated animals. In none of the 88 treated animals could regenerating fornix axons be identified within or distal from the lesion site.

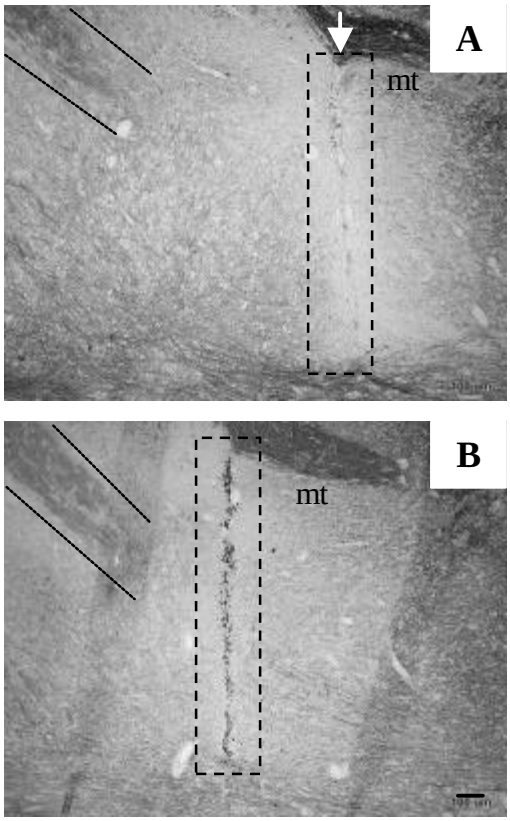

Figure 23. Immunohistochemical labeling of the ventral hypothalamus at the lesion site with anti-PAM antibody. Labeled tissue from a DPY treated animal, sacrificed 4w PL (A) and an untreated animal at 2w PL (B) are shown. Note the lesion site (boxed) extending dorsally up to the mammillothalamic tract (mt). The fornix approaches from the left (confined by dotted lines). The injection site in (A) would appear just dorsal from the top of the lesion site (white arrow), but is not visible in this section. The fornix stump cannot be recognized to immediately contact the lesion site within this plane. Scale bar 100 µm

Part B

4.5. Identification of differentially expressed subicular genes with cDNA arrays and the distribution of selected genes after fornix transection

Genes, which were differentially expressed after postcommissural fornix transection, were identified by analysing hybridization patterns of cDNA arrays. Datasets, which were employed for the analysis will be deposited on a Heinrich-Heine-University website (http://www.ulb.uni-duesseldorf.de/diss/mathnat/2001/abankwa/).

This chapter first introduces the employed methodology, which was established for cDNA array hybridzation data analysis within this thesis. Then, the results of hybridization experiments are presented. Identified genes and their associated values, which characterize reproducibility and differential expression are displayed in individual result tables for all three postlesional stages, (i) degeneration onset at one day post lesion (1d PL), (ii) axonal outgrowth at seven days post lesion (7d PL) and (iii) axonal growth arrest at the lesion site three weeks post lesion (3w PL). The calculated values in these tables are explained and compared.

In addition, sufficiently reproduced genes are listed in appendices A-C. Highly reproducible and sufficiently reproduced genes were assembled in functional groups. These groups were then aligned along the postlesional stages, to visualize stage specific overall and group activities. Prominent features of the assembled differential expression pattern are outlined, which demonstrate that the generated results are very consistent and are therefore of biological importance. Furthermore, verifying calculations and a verifying analysis of a foreign dataset are described.

Finally the distribution of some identified genes within the subiculum, was analysed by in situ hybridization.

4.5.1 Data analysis procedure for cDNA array hybridization experiments

In general, the analysis of raw expression data, which were generated in DNA array hybridization experiments comprise:

(a) background subtraction from the hybridized array-DNA spots

(b) Normalization of significant signal intensities (i.e. those being above a hybridization intensity threshold) against a reference value. This reference should correspond to the total quantity of hybridized cDNA (respectively isolated RNA, respectively isolated target tissue).

(c) Identification of regulated genes, which were differentially expressed, by at least a factor of between two and three, in the target state, as compared to the control.
(d) Selecting regulated genes, which are reproducible.

According to this general procedure, the here applied parameters will be described in the following chapter and the procedure, which was used for selection and identifcation of highly reproducible, differentially expressed genes is outlined.

(A) **Background subtraction** was initially performed using global background areas. Therefore three regions on the filter images were chosen, which represented the average background level. Alternatively each hybridized cDNA spot has its individual background area at a defined distance around it.
Radioactive hybridization with phosphorous-32 labeled cDNAs, is associated with localized scattering of radiation, which leads to a scattering of comparatively strong hybridized signal spots into areas of other spots on the images. This is not unusual, but requires accurate filtering for this signal spill over. This filtering was best performed by using local rings around each hybridized spot for individual background subtraction. This step of the analysis procedure was realized within the image analysis software AIDA Array Metrix (see 3.4.2). The area normalized and background subtracted raw expression data were then further compiled in Excel (see 3.4.3).

(B) Background subtracted expression data were normalized with a value, which represented a stable measure of the total hybridized radioactive cDNA. Therefore, the average spot-signal intensity (i. e. the sum of all positive signals, devided by the number of positive signals) was chosen for **normalizing expression data**. This approach generally requires a high number of hybridized genes and similar hybridization patterns of target (F, for fornix axotomy at a specific survival time) and control (termed K, sham operations, knife not extended), what was in agreement with the experiments described here. Nevertheless, normalization with a frequently used biological reference value, the GAPDH signal, was performed in parallel for comparison reasons. The outcome of the analysis with GAPDH for example at stage (i) is shown in figure 24. The diagram visualizes that comparatively high variations of the GAPDH signal, lead to insufficient sensitivity for the identification of reproducible genes.

(C) Within each comparison matrix the normalized expression data of every gene of a target hybridization (F) was compared with the respective value of a control hybridization (K). Expression levels had to be altered by at least a factor of =2 to be considered significantly regulated. For each postlesional stage, 36 such comparison matrices were calculated, at each stage forming an ensemble of **camparison matrices**. The positive regulation values (avREG) in the tables indicate the respective avREG-fold induction, while the negatives indicate the respective -avREG-fold repression, averaged over all significant regulation events for each gene within a stage specific ensemble of comparison matrices (see 4.5.2).

(D) High **reproducibility** was the final criterion to select genes at each experimental condition (stages (i) to (iii)). The high number of six pairs of independent experiments, with each pair comprising one target (F) and one control (K) hybridization, was performed at each stage in order to identify regulated genes. By comparing all F- with all respective K-hybridizations for each condition, the maximum number of 36 comparison matrices was used. Thus natural fluctuations in gene expression, slight variations in the isolated tissue or in any of the consecutive biochemical steps, could be better taken into account. Random fluctuations should lead to an about equal number of up- and downregulations. Such genes were therefore not selected. On the other hand would confident changes of the expression pattern be visible by a high number of reproductions of significant regulation events (i.e. being above the signal threshold and regulated by a factor =2). The absolute difference between the number of significant inductions and repressions of each gene, thus served as a measure for reproducibility. This difference could be understood as the netto reproduction and was abbreviated RVal, for reproduction value.
Plotting this RVal against the genes investigated, produced diagrams like in figure 24, which could be recognized as a reproducibility spectrum of analysed genes.

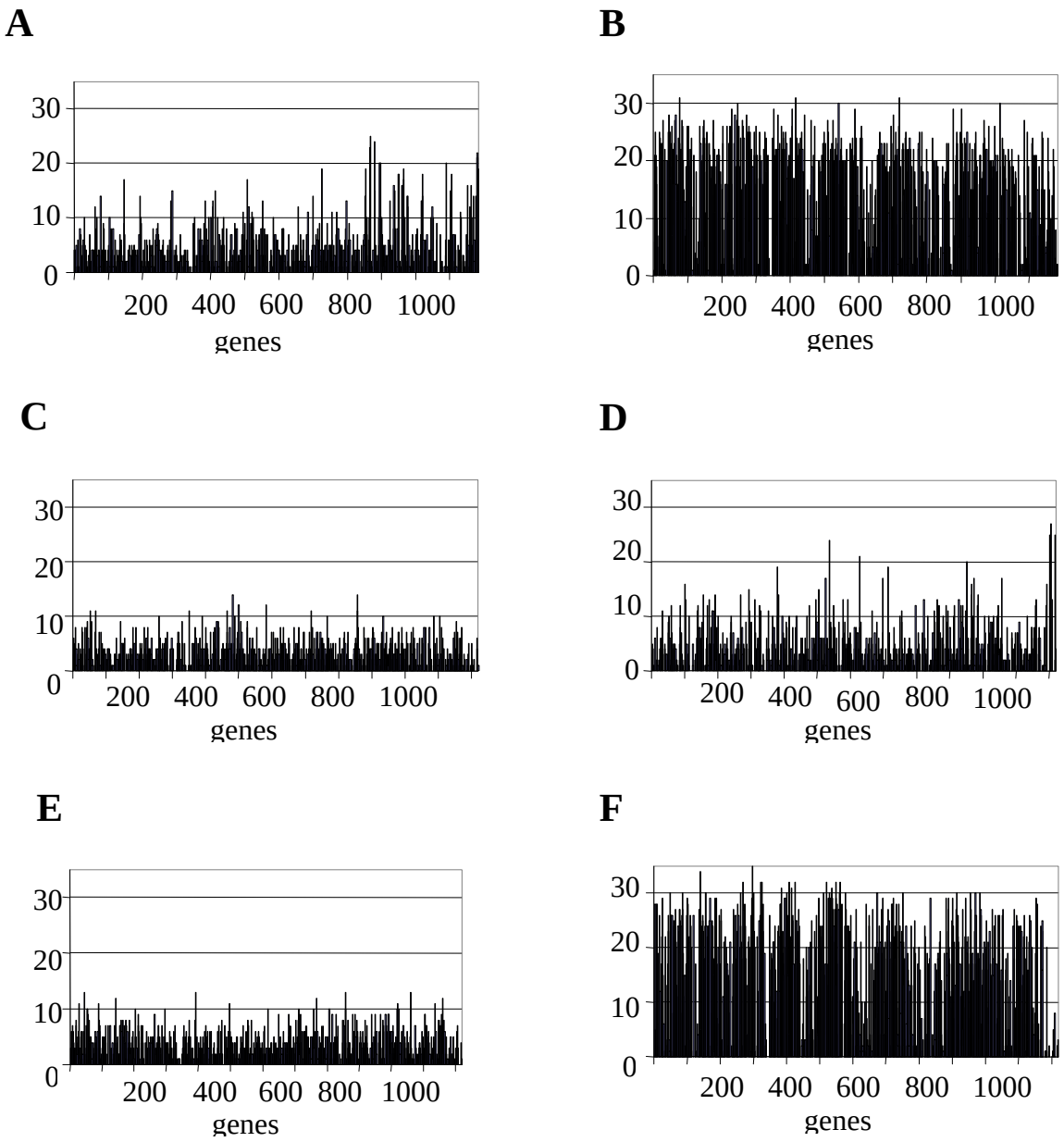

Figure 24. Reproducibility spectrum for analysed genes at stage (i), (ii) and (iii). The netto reproduction is shown on the y-axis versus the running number of the genes for stage (i) (A, B), (ii) (C, D), (iii) (E, F). Left diagrams (A, C, E): If genes were normalized with the average signal intensity, enough sensitivity could be achived. Right diagrams (B, D, F): Normalization with GAPDH resulted in high fluctuations. See text for further reference.

4.5.2 Identification of highly reproducible, differentially expressed genes at three different post lesion times

The following three result-lists contain highly reproducible genes, which were identified at one day, seven days or three weeks post lesion.

Identified genes had an RVal, which was larger than the +3SDcutoff-value, which was calculated by the average RVal (avRVal) of all genes at a given stage plus three times its standard deviation (SD). An analogous cut-off or reproducibility threshold value (+2SDcutoff) was calculated by adding only two times the SD to the avRVal.

Genes which had an RVal between the +2SDcutoff and the +3SDcutoff were less reproducible, but were still regarded as confidential, as will be outlined further below. The respective genes can be found listed in the appendices A-C and were furthermore included in the expression patterns shown in figure 25 and 26.

It needs to be mentioned that the ensemble of comparison matrices of stage (ii), at seven days post lesion, had to be split into two groups. Thus 16 comparison matrices derived from four pairs of hybridization experiments represent stage (ii) specific results, while 4 comparison matrices, derived from two other pairs of hybridization experiments had characteristics of stage (i) and were therefore conceived to represent a (i)/(ii)-intermediate stage.

Employed values of the result-lists are now explained:

#genes	the number of listed genes	**XLev**	arbitrary absolute expression level 1=weak, 2=moderate, 3=strong
RVal	reproduction value, the number of netto reproductions; =|POS-NEG|	**Coord**	coordinate on Clontech Atlas rat 1.2 cDNA arrays (Cat.# 7854-1)
POS	number of comparison matrices within an ensemble of stage specific comparison matrices, where the respective gene was significantly upregulated	**NEG**	number of comparison matrices within an ensemble of stage specific comparison matrices, where the respective gene was significantly downregulated
avREG	average regulation factor of a gene; positive/negative values indicate avREG/-avREG-fold induction/repression of the gene at the respective postlesional stage compared to the control	**genes**	gene names
		GB#	gene bank accession number, as provided by the array manufacturer
+3SD cutoff	genes, which are in the result lists must have an RVal > +3SDcutoff; this reproducibility threshold is calculated as avRVal+3*SD(avRVal)	**avRVal**	average of the RVals of all genes within an ensemble of stage specific comparison matrices
avRVal +3SD	average of the RVals of genes in a list	**avRVal-XLev1**	average of the RVals of listed genes with an arbitrary expression level (XLev)=1
%max RVal	Percentage of the respective value, x, on the number of comparison matrices used for the list; 100*x/number of comparison matrices		

Table 4. Identified genes at stage (i), which were highly reproducible (+3SD-list). See text for details.

Results (+3SD-list) stage (i) -acute lesion, 1d PL-

A

+3SDcutoff	%maxRVal
14,67	40,75

B

avRVal		SD	%SD	%maxRVal
2,97	+/-	3,90	131	8,26

C

avRVal+3SD			
18,24	+/-	2,79	15

D

avRVal-level 1			
19,50	+/-	3,89	20

E

#genes
29

XLev	RVal	POS	NEG	Coord.	av REG	SD av REG	genes	GB#
1	17	19	2	A11g	3,3	3,9	DCC; netrin receptor	U68725
1	15	16	1	B07h	10,7	15,5	monocarboxylate transporter MCT1	D63834
3	15	17	2	C02i	3,3	2,5	aldolase C	X06984
1	17	0	17	C09c	-3,8	1,6	mitochondrial carnitine O-palmitoyltransferase II precursor (CPT2)	J05470
2	19	2	21	D10l	-12,1	15,7	glutamate receptor, ionotropic, kainate 5	M83561
2	19	0	19	E05n	-3,0	0,6	cocaine/amphetamine-induced rat transcript, CART	U10071
1	23	1	24	E06m	-18,9	26,1	prostaglandin F2 receptor, alpha isoform, regulatory protein	U26595
1	25	0	25	E06n	-3,1	0,7	protein arginine N-methyltransferase 1	U60882
2	15	0	15	E07l	-4,1	2,3	c-Jun N-terminal kinase 1 (JNK1); (SAPK-γ)	L27129
2	24	0	24	E07m	-4,0	1,7	c-Jun N-terminal kinase 2 (JNK2); (SAPK-α)	L27112
2	20	0	20	E08m	-3,1	0,9	focal adhesion protein-tyrosine kinase (FAK)	AF020777
3	20	0	20	E08n	-3,6	1,6	protein kinase C epsilon type (PKC-ε)	M18331
3	16	0	16	E11m	-3,0	0,7	protein phosphatase 2A-β regulatory su B; beta-PR55	D38260
3	15	0	15	E11n	-3,3	1,2	nuclear tyrosine phosphatase; PRL-1; affects cell growth	L27843
3	18	0	18	E12l	-2,8	0,7	phosphatase 2A, catalytic subunit, isotype α	X16043
2	18	1	19	E12n	-3,7	2,3	Ral A; GTP-binding protein	L19698
2	16	0	16	E13j	-3,3	0,9	GTP/GDP-binding protein β su 5 (GNB5); transducin β su 5	AF001953
3	16	0	16	E13l	-2,7	0,7	GTP/GDP-binding protein G(O) alpha subunit (GNAO; GNA0)	M17526
3	19	1	20	E13m	-3,6	2,4	GTP/GDP-binding protein G(I) a 1 su (GNAI1); inhibiting	M17527
2	17	1	18	E13n	-8,1	7,2	Ras-related GTPase, ARF-like 5	X78604
3	18	1	19	F03m	-7,5	8,8	neuronal calcium sensor 1 (NCS-1))	L27421
1	20	1	21	F08l	-5,1	4,7	endothelin converting enzyme	D29683
2	15	0	15	F09k	-2,8	0,6	proteasome component C2	M29859
2	18	0	18	F09n	-3,9	0,9	proteasome subunit RC6-1	D30804
2	16	1	17	F13d	-4,5	3,9	G protein coupled receptor, putative, GPR10	S77867
2	16	1	17	F13n	-3,0	1,8	cofilin	X62908
3	21	2	23	G27	-6,1	5,7	glyceraldehyde 3-phosphate dehydrogenase (GAPDH)	M17701
3	22	0	22	G29	-5,2	3,5	tubulin α-1 (TUBA1)	V01227
3	19	0	19	G43	-4,5	1,6	cytoplasmic β-actin (ACTB)	V01217

Statistical characteristics of the result-list for identified genes at one day post lesion

The overall average netto reproduction value (avRVal) for stage (i), the degenration onset at 1d PL, was 2.97 with a standard deviation of 3.90 (, corresponding to 131% of its avRVal), meaning that on average a gene was found to be significantly regulated in netto 2.97 out of 36 comparison matrices. The corresponding +3SDcutoff was calculated to 14.67.

Therefore, only those significant genes were considered to be highly reproducible, which had an RVal of at least 14,67. The maximum RVal among the identified genes was 25 for E06n (protein arginine N-methyltransferase 1). The average RVal of the identified 29 genes (avRVal+3SD) was 18.24 +/- 2.78 (15%), meaning that the expression of the listed genes was with 15% significantly less fluctuating than of all genes together with 131%.

Comparing the smaller of the POS or NEG values (minority value) with the corresponding larger values, revealed that only 4 out of 29 genes had a minority value of 2, in only 9 out of 29 it was 1 and in the remaining 16 cases 0, indicating again that the fluctuation of these highly reproducible genes was very low, considering that for the maximal RVal of 25 and the +3SDcutoff of 14.67 a maximal minority value of 5 would have been possible.

The low level of fluctuation confirms that the idenfied genes were not randomly selected. Only 3 genes were found to be upregulated, while 26 were downregulated, as compared to the post lesion stage matched controls (sham operation). The maximal induction with the lowest percentual error was 3.3 +/- 2.5 for C02i (aldolase C) and the corresponding repression was -3.0 +/- 0.6 for E05n (CART).

Standard deviations of the average regulation values (avREG) sometimes appeared to be large, like e. g. for B07h (monocarboxylate transporter MCT1), what was related to minority values being 1 or 2. High SDavREG values do not relate to low expression levels (XLev), as is demonstrated by comparing the average netto reproduction value of genes with XLev=1 (avRVal-level1=19.5), their maximal RVal (25) and minimal RVal (15) with the corresponding values of the complete list (avRVal=18.24, maximal RVal=25, minimal RVal=15), indicating that both subgroups have similar distributions.

Table 5. Identified genes at stage (i)/(ii), which were highly reproducible (+3SD-list). See text for details.

Results (+3SD-list) stage (i)/(ii) -intermediate, 7d PL-

A

+3SDcutoff	%maxRVal
3,01	75,17

B

avRVal		SD	%SD	%maxRVal
0,53	+/-	0,83	156	13,23

C

avRVal+3SD			
4,00	+/-	0,00	0

D

avRVal-XLev 1			
4,00	+/-	0,00	0

E

#genes
12

XLev	RVal	POS	NEG	Coord.	av REG	SD av REG	genes	GB#
1	4	4	0	A14i	3,4	0,8	glutahione S-transferase subunit 13	S83436
2	4	0	4	E02j	-6,9	4,5	Glioma-derived vascular endothelial cell growth factor	M32167
3	4	0	4	E09n	-8,4	6,1	protein kinase II, alpha subunit, calcium/calmodulin dependent	J02942
3	4	0	4	E10m	-3,4	0,7	PAK-alpha Ser/Thr kinase; p21-Cdc42/Rac1 activated kinase	U23443
3	4	0	4	E13n	-4,9	2,7	Ras-related GTPase, ARF-like 5	X78604
1	4	0	4	F01j	-5,5	3,6	phospholipase C delta 1 (PLC delta-1); PLC-III	M20637
2	4	0	4	F09k	-2,9	0,6	proteasome component C2	M29859
2	4	0	4	F09n	-3,4	1,4	proteasome subunit RC6-1	D30804
3	4	0	4	G27	-6,3	2,9	glyceraldehyde 3-phosphate dehydrogenase (GAPDH)	M17701
3	4	0	4	G29	-4,2	1,1	tubulin alpha-1 (TUBA1)	V01227
1	4	0	4	G31	-8,3	3,6	ornithine decarboxylase (ODC)	J04791
3	4	0	4	G43	-2,9	0,7	cytoplasmic beta-actin (ACTB)	V01217

Table 6. Identified genes at stage (ii), which were highly reproducible (+3SD-list). See text for details.

Results (+3SD-list) stage (ii) -axonal outgrowth, 7d PL-

A

+3SDcutoff	%maxRVal
6,61	41,34

B

avRVal		SD	%SD	%maxRVal
1,34	+/-	1,76	131	8,40

C

avRVal+3SD			
7,74	+/-	0,81	10

D

avRVal-level 1			
7,50	+/-	0,53	7

E

#genes
19

XLev	RVal	POS	NEG	Coord.	av REG	SD av REG	genes	GB#
1	8	0	8	A04l	-8,8	7,0	Non-processed neurexin III-α	L14851
1	7	8	1	A05n	4,0	2,9	New England Deaconess transcription factor; Cut/Cux/CDP family	U09229
2	9	9	0	A13m	4,0	2,4	heat shock 70-kDa protein (HSP70)	Z27118
1	8	8	0	B03b	3,7	1,6	5-hydroxytryptamine (serotonin) receptor 3; 5HT3	U59672
1	8	8	0	B05g	6,8	5,3	voltage-dependent L-type calcium channel alpha 1C subunit	M59786
2	7	7	0	B11n	3,3	0,9	fatty acid transport protein	M97381
2	8	0	8	B14l	-6,9	5,0	synaptotagmin III (SYT3)	D28512
2	9	9	0	C01i	4,3	1,5	Huntingtin associated 1B	U38370
2	9	9	0	C03n	5,2	1,6	mitochondrial hydroxymethylglutaryl-CoA lyase precursor	Y10054
1	7	7	0	C06k	4,9	1,9	aldehyde dehydrogenase 3, microsomal	M73714
2	7	8	1	D10e	2,5	2,0	gamma-aminobutyric acid (GABA-A) receptor, β 3 subunit	X15468
1	7	0	7	D13k	-3,0	0,7	nociceptin precursor; orphanin FQ; PPNOC	X97375
2	8	0	8	E06c	-4,8	1,6	neurexophilin I	L27867
3	9	9	0	E06e	22,8	34,2	gastric inhibitory polypeptide precursor (GIP)	L08831
2	7	7	0	E09h	4,4	2,1	calcium/calmodulin-dependent protein kinase type II delta subunit	L13408
1	8	0	8	F02l	-3,9	1,5	cAMP-dependent 3',5'-cyclic phosphodiesterase; hormone-sensitive	Z22867
2	7	7	0	F09e	4,3	2,1	cathepsin H	M36320
2	7	0	7	F09m	-3,7	1,5	proteasome component C8	M58593
1	7	7	0	F13g	6,4	4,8	Ear-2; rCOUPg; v-erbA related proto-oncogene	AF003926

Statistical characteristics of the result-lists for identified genes at seven days post lesion

Similar results, like those described for stage (i) were also obtained for the other experimental conditions. The intermediate stage (i)/(ii) represented by 4 comparison matrices of the 7d PL experiments (designated 7d PL (4) ensemble) had a maximal possible RVal of 4. The overall average RVal of 0.53 +/- 0.83 (156%) and the resulting +3SDcutoff of 3.01, left only those genes in the list, which had an RVal of 4, what was the maximum possible.

Out of 12 identified genes, only 1 gene was upregulated, while 11 were downregulated. A14i (glutathione S-transferase subunit 13) was induced by 3.4 +/- 0.8, while the corresponding largest repression with the lowest percentual error was 3.4 +/- 0.7 for E10m (p21-Cdc 42/Rac1 activated kinase). Again the distribution of the 3 genes with XLev=1 did not deviate from the rest of the genes.

The axonal outgrowth stage (ii) at 7d PL was represented by 16 comparison matrices (7d PL (16) ensemble). The overall average netto reproducibility (avRVal) was 1.34 +/- 1.76 (131%), with a +3SDcutoff of 6.61. Thus 19 genes were selected of which 4 genes had the maximal RVal of 9. This was already indicative for a much narrower range of the RVal-value distribution between 7 and 9, as compared to stage (i) results. The average RVal of the identified genes (avRVal+3SD) was 7.74 +/- 0.81.

Again, the minority value reached its maximum of 1 only for 2 out of 19 genes and the percentual standard deviation of 10% of the avRVal+3SD-value compared to 131% for all genes (avRVal), was indicative for a low level of fluctuation within the gene list.

At stage (ii) 13 genes were found upregulated, while 6 were downregulated. The maximal induction with the lowest percentual error was 3.3 +/- 0.9 for B11n (fatty acid transport protein), with the respective largest repression of -3.0 +/- 0.7 for D13k (nociceptin precursor). The high standard deviation for E06e (GIP) was in this case related to some exceptionally high regulation values in some individual comparison matrices. Again the average RVal of low expressed genes (avRVal-level 1) was comparable to the overall avRVal (7.5 and 7.74 respectively), supporting similar reproducibility of genes with low absolute expression level.

Table 7. Identified genes at stage (iii), which were highly reproducible (+3SD-list). See text for details.

Results (+3SD-list) stage (iii) -axonal growth arrest, 3w PL-

A	+3SDcutoff			%maxRVal
	14,16			39,34

B	avRVal		SD	%SD	%maxRVal
	2,80	+/-	3,79	135	7,78

E	#genes
	17

C	avRVal+3SD			
	19,35	+/-	3,79	20

D	avRVal-level 1			
	21,00	+/-	6,00	29

XLev	RVal	POS	NEG	Coord.	av REG	SD av REG	genes	GB#
2	16	18	2	A08b	3,8	4,5	PHB; prohibitin; blocks DNA synthesis in normal fibroblasts	M61219
2	15	18	3	B08a	7,1	10,4	beta-alanine-sensitive neuronal GABA transporter	M95738
3	19	19	0	B14c	12,8	15,4	epidermal fatty acid-binding protein (E-FABP)	U13253
1	15	15	0	C09b	9,3	9,3	glutamate-cysteine ligase catalytic subunit (GLCLC)	J05181
2	17	19	2	C10h	4,8	4,4	gamma-aminobutyric acid (GABA) transaminase	U29701
2	24	24	0	C11d	5,4	3,9	60S ribosomal protein L44; L36A	M19635
1	21	0	21	D03m	-3,6	2,4	alpha-1a adrenergic receptor; RA42	L31771
2	17	0	17	D08n	-68,5	106,9	N-methyl-D-aspartate receptor (NMDAR1)	X63255
3	19	0	19	D09n	-3,0	0,8	gamma-aminobutyric acid receptor alpha 1 subunit precursor	L08490
2	20	0	20	E12n	-3,3	1,1	Ral A; GTP-binding protein	L19698
3	16	0	16	E13m	-2,7	0,6	guanine nucleotide-binding protein G(I) a1 su (GNAI1); inhibiting	M17527
2	17	0	17	E14h	-3,7	0,9	Rab-11A; Ras p21-like small GTP-binding protein; 24KG; YL8	M75153
2	17	2	19	F06h	-3,3	2,5	nitric oxide synthase 1	X59949
3	25	0	25	G27	-2,8	0,5	glyceraldehyde 3-phosphate dehydrogenase (GAPDH)	M17701
3	19	1	20	G29	-3,4	1,9	tubulin alpha-1 (TUBA1)	V01227
1	27	0	27	G31	-3,6	1,3	ornithine decarboxylase (ODC)	J04791
3	25	0	25	G43	-3,0	0,9	cytoplasmic beta-actin (ACTB)	V01217

Statistical characteristics of the result-list for identified genes at three weeks post lesion

Stage (iii) results, with again 36 comparison matrices (3w PL (36) ensemble), had an average overall netto reproduction value of 2.80 +/- 3.79 (135%), resulting in a high confidence reproducibility cut-off of 14.16. The average netto reproducibility for the listed genes (avRVal+3SD) was 19.35 +/- 3.79, with the standard deviation corresponding to 20% of the average value (135% overall). Thus, in similarity to the stage (i) and (ii) results the fluctuations among the identified genes were low.

The gene with the highest induction and lowest percentual error was C11d (60S ribosomal protein L44) with a regulation value and comparatively high error of 5.4 +/- 3.9, while the respective strongest repression was -2.8 +/- 0.5 for G27 (GAPDH). High standard deviations relate to exceptionally high regulation values in some of the individual comparison matrices or minority values being 2 or 3. The expression level of all 17 genes at this postlesional stage was at least moderate (XLev>=2).

In conclusion, 29 highly reproducible genes were identified to be differentially expressed at postlesional stage (i) -degeneration onset at 1d PL-, 12 at stage (i)/(ii), an apparently intermediate stage at 7d PL, 19 at stage (ii) -axonal outgrowth at 7d PL- and 17 at stage (iii) -axonal growth arrest at 3w PL. All expression levels of these identified genes were above a signal threshold of 5% of the average signal intensities. Furthermore all genes were differentially expressed by at least a factor =2 between the target conditions (F), being the postlesional stages (i) - (iii), and the control conditions (K), being the post lesion time matched sham operated controls.

4.5.3 Assembly of all identified genes into comprehensive expression patterns, reveal common genetic features

As far as it was known or could be inferred by the gene names, the genes of tables 4-7 and those from appendices A-C were sorted into 14 functional groups. These functional groups were basically defined by the frequent appearance of genes, which were known or assumed to be involved in the same or similar functional context in the cell or because they were associated with a family of proteins that is described by the name of the functional group.
The defined functional groups are:

A	receptors	G	plasmamembrane oxyreductase complex of synaptic vesicles (Bulliard et al., 1997; Quinn et al., 1999)
A2	channels/ion transporters	H	transcription factors/oncogenes
B	trimeric G protein associated	I	mitochondrial associated
C	small GTPases associated	J	calcium homeostasis associated
D	proteasome associated	K	lipid metabolism
E	cytoskeleton associated	L	ATPases
F	components of signalling pathways	M	functionally not categorized

It needs to be mentioned, that clustering by annotation and not by regulation pattern alone relys on the knowledge available to date, furthermore, functional groups are not standardized. However, as the employed DNA arrays contained only known genes with often profound information available from publications, this was assumed to be a reasonable approach to identify crucial groups and patterns of genes that accompany axotomy induced changes of the neuronal transcriptom.

Common features of the three studied postlesional stages,

(i) 1d PL - degeneration onset, where axons transiently remain at the lesion site, until they later retract and degenerate for a short distance in the most proximal stump,

(ii) 7d PL - axonal outgrowth, where axons approach the lesion site, and

(iii) 3w PL - axonal growth arrest, where axons have reached the lesion site and remain there without further outgrowth,

could provide biologically interesting and valuable information. These common genetic features could also correlate with the morphological responses, like outgrowth or growth arrest. Therefore the gene-lists of tables 4-7 are intended to be presented in a way that is more intuitive for the recognition of common genetic and ultimately functional features. A suggestion of such an intuitive expression pattern is now outlined.

After initial patterning of the above listed genes (tables 4-7), it was found that they were reasonably complemented by including genes of the +2SD-lists (see Appendices A-C for gene-lists). The genes of the +2SD-lists were included into the following two patterns and can be recognized, as they do not possess an XLev assignment and are written in italics.

The **short pattern** (Fig. 25) contains only those genes of the +3SD- and +2SD-lists, which were identified to be differentially expressed in **at least two of the three** above recapitulated postlesion **stages (i) - (iii)**. They fall into 12 out of 14 functional group-categories.

The complete pattern (Fig. 26) contains all genes of the +3SD- and +2SD-lists, which were sorted into one of the 14 above listed functional groups. The top to bottom arrangement was the same as in the previous short pattern. Genes within one category, which were regulated together into one direction, were kept together, followed by those, which were regulated into the other direction.

Short Pattern	stage (i)				stage (i)/(ii)			
	1d PL (36)				7d PL (4)			
Group	XLev	Coord.	avREG	GENE	XLev	Coord.	avREG	GENE
G				*				(*)
PMO	3	G27	-6,1	GAPDH	3	G27	-6,3	GAPDH
	3	C02i	3,3	aldolase C				
A				*				
receptors	1	A11g	3,3	DCC				
D				*				(*)
proteasome	2	F09k	-2,8	proteasome C2	2	F09k	-2,9	proteasome C2
		F09m	*-5,5*	proteasome C8				
	2	F09n	-3,9	proteasome su RC6-1	2	F09n	-3,4	proteasome su RC6-1
I				*				
mitochondrial		*C12e*	*-19,5*	MEF-G				
L								
ATPases								
C								
small GTPase								
				*				(*)
	2	E12n	-3,7	Ral A				
	2	E13n	-8,1	Ras-rel. GTPase	3	E13n	-4,9	Ras-rel. GTPase
A2				*				
channels/		*D08n*	*-1,3*	*NMDAR1*				
ion transporter		*D12n*	*-34,6*	*Glu-rec, metab. 4*				
B				*				
trimeric G protein	3	E13m	-3,6	G(i)α				
E				*				(*)
cytoskeleton	2	F13n	-3,0	cofilin				
	3	G29	-5,2	tubulin α1	3	G29	-4,2	tubulin α1
	3	G43	-4,5	cypl. β-actin	3	G43	-2,9	cypl. β-actin
F				*				
signalling	2	E08m	-3,1	FAK				
	3	E11n	-3,3	nu. Y-phosphat. PRL-1				
	3	E12l	-2,8	phosphatase 2A-cat. su				
		E01m	*-3,3*	*NT3*				
K				*				
lipid metabolism		*B14g*	*9,7*	*NSL-TP*				
M				*				(*)
not determined		*A14k*	*3,6*	*phosphol. GST peroxid.*				
	2	E05n	-3,0	CART				
	1	E06n	-3,1	prot. Arg-N-meth. transf.				
		F13k	*-5,9*	*plectin*				
		G31	*-8,1*	*ODC*	1	G31	-8,3	ODC
				*				
		B07d	*2,6*	*L-Pro-transporter*				

Figure 25 (continued overleaf). Short pattern of overlapping genes. 28 genes wer identified to be reproducibly altered in their expression by a factor =2 in at least two of the three poslesional stages (i) - (iii). Furthermore the genes of the intermediate stage (i)/(ii) were integrated between stage (i) and (ii). This intermediary state shares pattern features of stage (i), but none with stage (ii). The functional groups are arranged from top to bottom, first displaying the only gene (GAPDH), which was identified at all three stages, followed by those genes, which were identified at stages (i) and (ii), then those identified at stages (ii) and (iii) and finally the large list of 18 genes, which were identified at stages (i) and (iii), exclusively (except for B07d, which has just been left within its group. This order is indicated by asterisks (*) over the respective columns. See text for boxed genes.

stage (ii) 7d PL (16)				stage (iii) 3w PL (36)			
XLev	Coord.	avREG	GENE	XLev	Coord.	avREG	GENE
			*				*
	G27	*8,4*	GAPDH	3	G27	-2,8	GAPDH
	C02i	*4,3*	aldolase C				
			*				
	A11g	*4,2*	*DCC*				
			*				
2	F09m	-2,7	proteasome C8				
			*				
	C12e	*-1,8*	*MEF-G*				
			*				*
	B10i	*3,3*	*ATPase Na+/K+*		*B10i*	*7,5*	*ATPase Na+/K+*
			*				*
	E14h	*-3,1*	*Rab-11A*	2	E14h	-3,7	Rab-11A
							*
				2	E12n	-3,3	Ral A
					E13n	*-2,8*	*Ras-rel. GTPase*
							*
					D08n	-68,5	NMDAR1
					D12n	*-4,0*	*Glu-rec, metab. 4*
							*
				3	E13m	-2,7	G(i)α
							*
					F13n	*-2,5*	*cofilin*
				3	G29	-3,4	tubulin α1
				3	G43	-3,0	cypl. β-actin
							*
					E08m	*-3,1*	*FAK*
					E11n	*-2,1*	*nu. Y-phosphat. PRL-1*
					E12l	*-2,0*	*phosphatase 2A-cat. su*
					E01m	*-3,3*	*NT3*
							*
					B14g	*2,7*	*NSL-TP*
							*
					A14k	*-3,5*	*phosphol. GST peroxid.*
					E05n	*-2,3*	*CART*
					E06n	*-2,5*	*prot. Arg-N-meth. transf.*
					F13k	*-2,8*	*plectin*
				1	G31	-3,6	ODC
			*				
	B07d	*2,4*	*L-Pro transporter*				

stage (i) 1d PL (36 matrices)			stage (ii) 7d PL (16 matrices)			stage (iii) 3w PL (36 matrices)		
Coord.	GENE	avREG	Coord.	GENE	avREG	Coord.	GENE	avREG
PMO			**PMO**			**PMO**		
G27	GAPDH	-6,1	*G27*	GAPDH	*8,4*	G27	GAPDH	-2,8
C08f	aldehyde-dehydrog.2	*2,8*	C06k	aldehyde-dehydrog.3	4,9			
C02i	aldolase C	3,3	*C02i*	aldolase C	*4,3*			
receptors			**receptors**			**receptors**		
A11g	DCC	3,3	*A11g*	*DCC*	*4,2*			
			B03b	5HT3 rec.	3,7	*C14e*	*Trk-B*	*3,0*
			D01j	*IL-4 rec.*	*6,3*	*D06g*	*opioid rec. orphan rec.*	*3,0*
			D01k	*IL-1 R-1*	*3,9*			
			D04f	*5HT2 rec.*	*2,8*			
E06m	prostaglandin F2 rec.	-18,9	*A04a*	*TNF-R1*	*-2,6*			
D05m	*5HT5A*	*-4,1*	*A04c*	*IL-6 rec. ligand bind. chain*	*-2,8*			
F11l	*Trk-E, discoidin rec.*	*-3,5*	*D07i*	*galanin rec. 1*	*-3,1*			
proteasome			**proteasome**			**proteasome**		
F09k	proteasome C2	-2,8						
F09m	proteasome C8	*-5,5*	F09m	proteasome C8	-2,7			
F09n	proteasome su RC6-1	-3,9						
F09l	proteasome C3	*-4,5*	*F10g*	26S protease reg. SU 7	*3,5*			
mitochondrial			**mitochondrial**			**mitochondrial**		
C12e	MEF-G	*-19,5*	*C12e*	*MEF-G*	*-1,8*			
C09c	CPT II	-3,8	C03n	HMG-CoA lyase	5,2			
			C03d	*CYCT*	*2,3*			
			C03k	*CYC axidase SU VII a*	*4,6*			
			C04d	*ATP synthase, H+, a SU*	*5,7*			
			C07e	*CYP2C7*	*3,0*			
			C07k	*CYP2J3*	*2,5*			
ATPases			**ATPases**			**ATPases**		
			B10i	*ATPase Na+/K+*	*3,3*	*B10i*	*ATPase Na+/K+*	*7,5*
			B10g	*ATPase H+/K+ a 2a SU*	*5,4*	*B10d*	*ATPase b 2 Na+/K+ trans.*	*3,6*
			C03g	*ATPase, SU F*	*-53,6*			
small GTPase			**small GTPase**			**small GTPase**		
			E14h	*Rab-11A*	*-3,1*	E14h	Rab-11A	-3,7
E12n	Ral A	-3,7				E12n	Ral A	-3,3
E13n	Ras-rel. GTPase	-8,1				*E13n*	*Ras-rel. GTPase*	*-2,8*
E14j	*rab15*	*-2,8*						
E14k	*rab 14*	*-2,3*						
E14l	*rab 16*	*-4,5*						
F05m	ARF3	*-2,9*	*F06b*	*ARF 6*	*2,7*	*A13a*	*p120 GAP*	*3,1*
C01n	*rab GDI*	*5,6*				*F01e*	*Ral GDSB*	*3,2*
C02a	*Rab GDI a*	*2,2*				*F01g*	*RIN 1*	*5,8*
channels/ ion transporters			**channels/ ion transporters**			**channels/ ion transporters**		
D08n	*NMDAR1*	*-1,3*				D08n	NMDAR1	-68,5
D12n	*Glu-rec, metab. 4*	*-34,6*				*D12n*	*Glu-rec, metab. 4*	*-4,0*
D10l	Glu-rec, kainate 5	-12,1	*B05l*	*K+ channel drk1*	*-2,7*	D03m	α-1a adrenergic rec.	-3,6
			B06i	*K+ channel KV3.1*	*-2,7*	D09n	GABA-A rec. α1 su	-3,0
			B07n	*Glu-transport.*	*-2,5*	B08a	GABA-transp. 3	7,1
			B08h	*Na+/H+ exch. prot. 4*	*-2,3*	C10h	GABA-transaminase	4,8
						B06c	*K+-ch. RB-IRK2*	*6,1*
			B05g	CACNA1	6,8	*B09c*	*Na+/dicarb cotransp*	*7,2*
			D10e	GABA-A rec. β3 su	2,5	*B12d*	*org. anion transp.*	*3,5*
trim. G protein			**trim. G protein**			**trim. G protein**		
E13m	G(i)α	-3,6				E13m	G(i)α	-2,7
E13j	GNB5	-3,3	*E13k*	*G(i/s/o) g 7SU*	*-5,3*	*D01e*	*LCR-1, G prot. coup.*	*-4,2*
E13l	G(o)α	-2,7	*E13c*	*G(i/s/t) b SU1*	*3,1*			
F13d	G-coupl. rec.	-4,5	*F13b*	*put. G-coup. rec.*	*2,3*			

Figure 26 (part II continued overleaf). Complete pattern of identified genes. This long pattern contains all of the 174 different genes identified, which could be sorted into the 14 arbitrarily defined funtional groups. The pattern is arranged like the short pattern, showing genes belonging to the same postlesional stage in columns and functional groups in rows. Genes highlighted in yellow were identified in at least two post lesion stages. The displayed values correspond to those in the result lists (tabels 4-7). Upregulated genes are printed in red, while downregulated appear in blue. Genes written in italics were derived from the +2SDresult-lists in the appendices A-C. See text for further description.

stage (i)		pt.II	stage (ii)		pt.II	stage (iii)		pt.II
1d PL (36 matrices)			**7d PL (16 matrices)**			**3w PL (36 matrices)**		
Coord.	GENE	avREG	Coord.	GENE	avREG	Coord.	GENE	avREG
	cytoskeleton			**cytoskeleton**			**cytoskeleton**	
F13n	cofilin	-3,0				*F13n*	*cofilin*	*-2,5*
G29	tubulin α1	-5,2				G29	tubulin α1	-3,4
G43	cypl. β-actin	-4,5				G43	cypl. β-actin	-3,0
			B14l	synaptotagmin III	-6,9			
			C01a	*syntaxin 5*	*-2,6*			
			A04l	Neurexin III α	-8,8			
			E06c	Neurexophilin 1	-4,8	*E06g*	*F-Spondin*	*-7,2*
			A02n	BIG-1	*-2,5*			
			B12k	MBP S	*-2,9*			
			C01i	Huntingtin associated 1B	4,3	*A13e*	*merlin*	*3,5*
			F08i	MT3-MMP	*3,4*			
	signalling			**signalling**			**signalling**	
E08m	FAK	-3,1				*E08m*	*FAK*	*-3,1*
E11n	nu. Y-phosphat. PRL-1	-3,3				*E11n*	*nu. Y-phosphat. PRL-1*	*-2,1*
E12l	phosphatase 2A-cat. su	-2,8				*E12l*	*phosphatase 2A-cat. su*	*-2,0*
E01m	*NT3*	*-3,3*				*E01m*	*NT3*	*-3,3*
E07l	JNK1	-4,1	D13k	nociceptin precursor	-3,0	F06h	NOS1	-3,3
E07m	JNK2	-4,0	F02l	cAMP dep. phosphodiest.	-3,9	*E11e*	*CDK 4*	*-4,4*
E08n	PKC ε	-3,6	*C12h*	*BAD*	*-15,6*	*E11k*	*SH-PTP2*	*-7,8*
E11m	phosphatase 2A-reg. su	-3,0	*E10h*	*SGK*	*-2,7*	*F05j*	*PDGF-ass. prot.*	*-2,7*
E05m	*IGFBP-5*	*-3,5*	*F01k*	*FRAP/RAFT 1*	*-3,3*			
E10n	PCTAIRE2 kinase	*-5,6*	A13m	HSP 70	4,0	*A12d*	CSNK2β	*21,3*
F03l	*CN*	*-1,9*	E06e	GIP	22,8	*E08g*	MAPKK1	*2,6*
			E09h	CAMK-II Δ	4,4	*E10c*	Ctk/bratk	*6,7*
			D14a	*gastrin-rel. pept.*	*2,7*			
			E03f	*somatostatin*	*5,3*			
			E04b	*thyroid stim. horm. b*	*2,8*			
			F01h	*PLC g -1; PLC-II*	*4,7*			
			F03a	*adenyl cyclase 4*	*2,5*			
			F06g	*PLAP*	*2,5*			
	lipid metabolism			**lipid metabolism**			**lipid metabolism**	
B14g	*NSL-TP*	*9,7*				*B14g*	*NSL-TP*	*2,7*
			B11n	fatty ac. transp. prot.	3,3			
			B14e	*H-FABP*	*5,1*	B14c	*E-FABP*	12,8
			C10g	*11- b -HO-ster. dehydr. 2*	*6,2*	*C07a*	*3 b -HSD*	*3,9*
	not determined			**not determined**			**not determined**	
A14k	*phosphol. GST peroxid.*	*3,6*				*A14k*	*phosphol. GST peroxid.*	*-3,5*
E05n	CART	-3,0				*E05n*	*CART*	*-2,3*
E06n	prot. Arg-N-meth. transf.	-3,1				*E06n*	*prot. Arg-N-meth. transf.*	*-2,5*
F13k	*plectin*	*-5,9*				*F13k*	*plectin*	*-2,8*
G31	*ODC*	*-8,1*				G31	ODC	-3,6
			C09d	*GLCLR*	*4,5*	C09b	GLCLC	9,3
	*			*				
B07d	*L-Pro-transporter*	*2,6*	*B07d*	*L-Pro transporter*	*2,4*			
	transcription factors/ oncogenes			**transcription factors/ oncogenes**			**transcription factors/ oncogenes**	
A06g	*ID1*	*3,8*	A05n	CDP/Cux/Cut	4,0	*A05d*	*FRA-2*	*6,9*
			F13g	Ear-2	6,4	*A10l*	*c-ets-1*	*3,3*
A05e	*Jun-B*	*-5,0*	*A10g*	c-fos	*124,4*	*A10n*	*Rb; pp105*	*4,4*
	calcium			**calcium**			**calcium**	
F03m	NCS-1	-7,5						
F03j	*calbindin d28*	*-8,1*						
F03n	*NVP*	*-3,5*						
			F04b	*NVP-3*	*2,6*			
	left: 7			**left: 6**			**left: 11**	
	upregulated:	9			41			23
	downregulated:	45			24			27

The most important features of the presented patterns should now be pointed out, and additional features and possible neurobiological implications will be discussed.

- Stages (i), (ii) and (iii) were found to have their unique expression patterns.
- Stage (ii)-pattern was more different from stages (i) and (iii), which in turn have about 10% of all identified genes in common (18 out of 174).
- The intermediate stage (i)/(ii) could be positioned between stage (i) and (ii), although it shares common genes only with stage (i). But some of the boxed fields (Fig. 25 and 26) indicate that the regulation value (avREG) of these intermediate stage genes could, indeed be recognized as being on an intermediate level between stage (i) and (ii).
- Omitting those few genes, not categorized into one of the 14 groups, stage (i) contains more downregulated (45) than upregulated (9) genes, stage (ii) more upregulated (41), than downregulated (24) and stage (iii) about an equal number of upregulated (23) and downregulated (27) genes.
- Three functional groups, which were known or very likely to contain functionally tightly associated genes were especially prominent:

  group D - the proteasome associated genes, appeared to be functionally relevant at stage (i) and to a lesser degree at stage (ii), but not (iii). All listed proteasome component genes were downregulated.

  group C - the small GTPases associated genes, were differentially expressed at all three stages. At stages (i) and (iii) more genes of this group were identified, than at stage (ii). Again most of the transcripts were downregulated. The possible functional implications for those being upregulated will be discussed.

  group B - the trimeric G protein associated genes, were identified at comparatively high numbers at stages (i) and (ii). At stages (i) and (iii) the expression of all of the genes of this group became downregulated, while at stage (ii) 3 of 4 identified genes were upregulated.

4.5.4. Verifications of the employed analysis methodology

Despite producing highly consistent expression patterns that were just described, the analysis procedure needed to be verified by additional means. In a first verification, the sham operation derived control arrays at each stage were compared with each other, applying all of the above mentioned analysis parameters.

It was found that random fluctuations in these comparisons were higher and the resulting list of genes thus less confidential. Most importantly the identified genes were not identified in the stage specific analysis described above, with the exception of two genes at stage (iii), as will be mentioned below.

The second verification applied the procedure on a completely different experimental dataset. This dataset has been analysed independently by another analysis procedure before and three genes were identified to be reproducibly regulated. Thus, at least these genes should also have been identified with the procedure employed for data analysis in this thesis.

Analysis of control hybridization derived expression data (K vs K)

The expression data of the sham operation derived control arrays (K) for stage (i) (1d PL) and (iii) (3w PL) were compared separately. For each stage, all 6 (K) raw expression data were compared in 15 comparison matrices. Only 15 matrices needed to be compared, because one of the (K)-raw expression data always served as a target and the otherone as a control. Thus only half the number of 6x6 matrices were analysed minus six matrices, which would have contained matrices where each (K)-dataset would have been compared to itself.

According to the above outlined procedure, all genes, which had a RVal > +3SDcutoff were included in the respective +3SD-lists (Appendices D and E). For the 1d KvsK (15) ensemble of comparison matrices, the overall average RVal (avRVal) was 12.42% of the maximal possible RVal of 15. Furthermore the calculated +3SDcutoff was 62.86% of the maximal possible RVal.

Both values were higher than the respective values for the stage specific matrices (4.5.2), with the avRVal there being at about 8% and the +3SDcutoff at about 40% of the respective maximal possible RVal. This feature was less pronounced for the 3w KvsK (15) ensemble, where the average RVal was 8.26% and the +3SDcutoff was 45.6% of the maximal possible RVal of 15.

The increase of these values in the control analysis was indicative for a higher level of random fluctuations of these datasets compared with the stage specific results, as it was

expected. Therefore comparison of the sham operation derived control data (K) did not lead to high reproducibility.

The identified genes should furthermore not appear in the stage specific results. This was indeed the fact for the 1d KvsK (15) ensemble, where none of the identified genes appeared neither in the +2SD (Appendix A compared to Appendix D)- nor +3SD-lists (table 4 against Appendix D) for stage (i) results.

The RVals of the 1d KvsK (15) ensemble derived genes in the 1d PL (36) ensemble (Appendix D, column RVal-stage(i)) were on average 4.24, with the maximum being at 10, what was just below the calculated +2SDcutoff of the 1d PL (36) ensemble. Thus this lower cut-off was confirmed to include only significant results.

Likewise the RVals of the 3w KvsK (15) ensemble derived genes in the 3w PL (36) ensemble (Appendix E, column RVal-stage(iii)) were on average 4.54, but with two maximal values of 14 and 16 being just inside the +2SD-list of stage (iii). They were not excluded from the +2SD-list of the 3w PL (36) ensemble, because the respective 3w PL (36)-RVals of these two genes were exceptionally high, while the average RVal within the 3w KvsK (15) list was 4.54, being almost equally low as the respective value for the 1d KvsK (15) ensemble of 4.23.

Analysis of a foreign dataset with known results

The second verification of the applied procedure was performed with a foreign experimental dataset, derived from cell culture experiments, consisting also of 6 pairs of independent experiments. Differentially expressed genes of this dataset were identified independently with other Excel-matrices, than those used here and by another member of the laboratory.

In this particular analysis, three genes were identified to be reproducibly regulated. Furthermore, differential expression of these three genes was confirmed by quantitative PCR (Patrick Küry, personal communication).

By using the procedure and criteria applied in this thesis, 21 highly reproducible genes were identified to be differentially expressed, including the three genes which were independently identified before. The higher number of identified genes is due to the higher sensitivity of the here employed methodology. Again the calculated +3SDcutoff was at about 40%, thus being similar to those for the stage specific results of the experimental dataset treated in this thesis. The RVals of the identified genes within the +3SD-list were 31, 28 and 17. Thus the latter was close to the +3SDcutoff of 14.93. These data will not be included within this thesis, as they are still under investigation in a different project.

4.5.5 Distribution of genes, which were identified with cDNA arrays, revealed by in situ hybridization

In the here described experimental approach, subicular tissue was first isolated with a scalpel and then total RNA was extracted as a starting material for cDNA array hybridization experiments. This setup was basically necessary for two reasons.
First of all, there were no methods available for the isolation of projecting subicular neurons. Secondly, DNA array hybridization experiments required a sufficiently high amount of starting material, as 5 µg of total RNA per hybridization were needed. Despite these constraints in the experimental setup, the primary intention was to detect axotomy-induced responses in the lesioned neurons.
Thus the distribution of identified genes needed to be confirmed to be either neuronal or glial or both. Although some information about the distribution of identified genes was available in the literature, additional information about the postlesional distribution was needed.
Therefore, a small selection of identified genes was characterized by in situ hybridization and compared to the distribution in the unlesioned subiculum. This offered the possibility to determine the cell type, which preferentially expressed a gene. Moreover, could in situ hybridization intensities be related to the expression level on cDNA arrays.
Five of the six genes selected belonged to group F, components of signalling pathways, and one belonged to group E, cytoskeleton associated. Gastric inhibitory polypeptide (GIP), c-Jun N-terminal kinases 1 and 2 (JNK 1/2), focal adhesion kinase (FAK), cofilin and serum/glucocorticoid regulated serine/threonine proteine kinase (SGK) were selected, as representatives for a number of putatively important genes after fornix axotomy.

Expression of gastric inhibitory polypeptide (GIP)

Gastric inhibitory polypeptide or glucose-dependent insulinotropic polypeptide is a small secreted peptide (precursor: 144 amino acids; mature peptide: 42 amino acids) of the VIP-secretin-glucagon superfamily. It is evolutionary highly conserved (Tseng et al., 1993) and was initially described in the gastrointestinal system, where it is known to amplify the effect of insulin in a glucose dependent manner (Yip and Wolfe, 2000).

Its G protein-coupled receptor is distributed in several brain regions, like cerebral cortex, hippocampus and olfactory bulb (Usdin et al., 1993). High affinity and specific binding sites for GIP were also detected in rat subiculum (Kaplan and Vigna, 1994). Activation of the receptor stimulates cAMP production and increases intracellular calcium accumulation (Usdin et al., 1993). Furthermore it potentiates the effect of insulin on incorporation of fatty acids into triglycerids (Beck, 1989; Yip and Wolfe, 2000). Moreover, GIP significantly stimulates glucocorticoid secretion in rats in a cAMP/protein kinase A dependent manner (Mazzocchi et al., 1999).

Despite that the peptide is known for a long time, its distribution within the brain appears to be disputed, as some groups could not detect it in the brain (Usdin et al., 1993; Beck, 1989), while others detected both, mRNA (Tseng et al., 1993) and protein (Tatemoto and Mutt, 1980) in the brain. This disagreement on the distribution of GIP within the brain especially required confirmation by collecting own data.

GIP was identified to be induced (avREG=22.8) at stage (ii), 7d PL. The strong array hybridization signal and high induction made it possible to identify the induction even by visual inspection of array hybridization images (Fig. 27 F and K). Specific in situ hybridization signals were found throughout the adult brain. Distribution exclusively over grey matter areas, like the cortex and some areas of the hippocampal formation (Fig. 27 A and B) were suggestive for a preferential neuronal localization. Especially within the hippocampal region, hybridization signals were found to be high over areas enriched in principal neurons (Fig. 27 B). This was also true for the subicular complex, where labeling corresponded to the known distribution of projecting neurons (Fig. 27 B, D and E). Comparison of the dorsal subiculum in the fornix transected hemisphere, with the contralateral unlesioned identical structure confirmed the putative neuronal distribution. Labeling pattern and hybridization intensity appeared to be unaltered in axotomized or unlesioned subiculum (Fig. 27 D and E). Furthermore the moderate in situ hybridization signal could be related to a strong signal on cDNA arrays (Fig. 27 F and K).

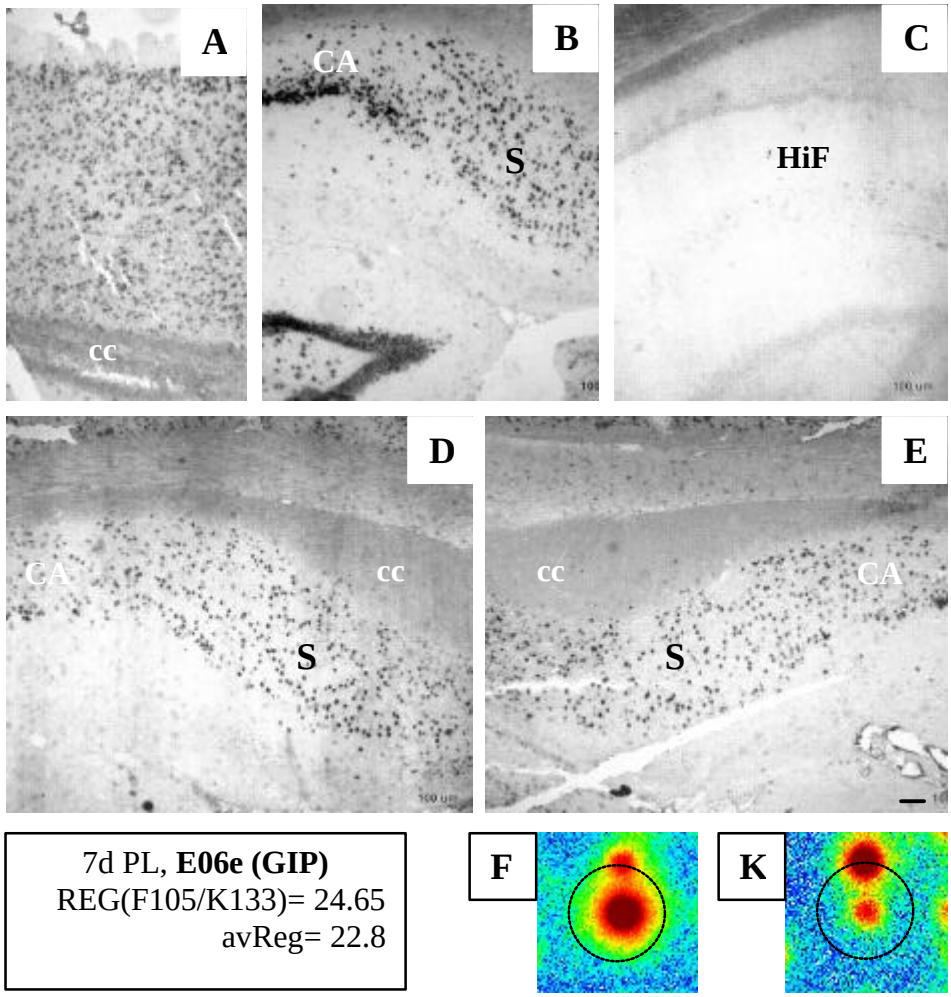

Figure 27. In situ and cDNA array expression data of GIP. Non radioactive in situ hybridization of an antisense cRNA probe specific for rat GIP (A, B, D, E) and its sense control (C). Hybridization to adult rat cortex (A), subiculum (B, D, E) and hippocampus (C) is shown. Hybridization of the axotomized (D) and unlesioned (E) subiculum (n=2) in the coronal plane reveals approximately identical hybridization patterns and intensities. Hybridized array spots of GIP (circled) are shown in (F) and (K), with hybridization intensities being colour-coded in analogy to the electromagnetic spectrum, from low (blue) to high (red) intensity. The target (F) and control (K) hybridizations display the representative pair of hybridized arrays (F105/K133), as annotated in the box to their left. The average regulation value (avReg) of GIP is also in the box for comparison. cc, corpus callosum; CA1, CA1 region of the hippocampus; HiF, hippocampal formation; S, subiculum. Scale bar 100 μm.

Expression of c-Jun N-terminal kinases 1 and 2

Multiple mitogen-activated protein kinase (MAPK) pathways are known within mammalian cells (Chang and Karin, 2001), which are basically composed of three enzymes, which become sequentially phosphorylated, thereby activating each other. c-Jun N-terminal kinases (JNKs), also called stress-activated protein kinases (SAPKs) belong to the terminally activated MAPKs, which are stimulated by both stressful signals, like heat shock or ultraviolet irradiation, but also physiological stimuli, like G protein-coupled receptors. The outcome of the JNK pathway stimulation was described to lead to opposite responses, like apoptosis (Yang et al., 1997) or rescue from apoptosis (Nishina et al., 1997), proliferation (Mitsui et al., 1997) and differentiation (Yao et al., 1997).

Specific phosphorylation of c-Jun on Ser-63 and Ser-73 may play a role in some of these responses. Both, c-Jun and JNKs were described to be involved in neurite outgrowth (Herdegen et al., 1997; Herdegen et al., 1998). Distribution of both JNK 1 and JNK 2 in rat brain is known and was already described (Carboni et al., 1998). To confirm these data and evaluate the effect of axotomy on distribution and expression of these genes, in situ hybridizations were performed.

JNK 1 and JNK 2 were identified to be repressed at stage (i) at 1d PL (avREG=-4.1 and -4.0, respectively). The employed cRNA-probe could not differentiate between JNK 1 or 2 transcripts. Therefore the in situ hybridization pattern reflects the overlay of the distribution of JNK 1 and 2 mRNAs. A weak to moderate in situ hybridization signal was found to be specifically distributed throughout the adult rat brain, again with preferential distribution over grey matter areas (Fig. 28 A, B, D, E). The unlesioned dorsal subiculum was only weakly to moderately labeled (Fig. 28 B). Again both, labeling intensity and distribution were similar in the axotomized and unlesioned subiculum (Fig. 28 D and E) and corresponded to a distribution within principal neurons. The weak to moderate in situ hybridization signal could be related to a moderate array hybridization signal, what was in line with the relations found for GIP. These data were again suggestive for the differential expression on cDNA arrays (Fig. 28 F and K), being attributable to neuronal expression of the gene.

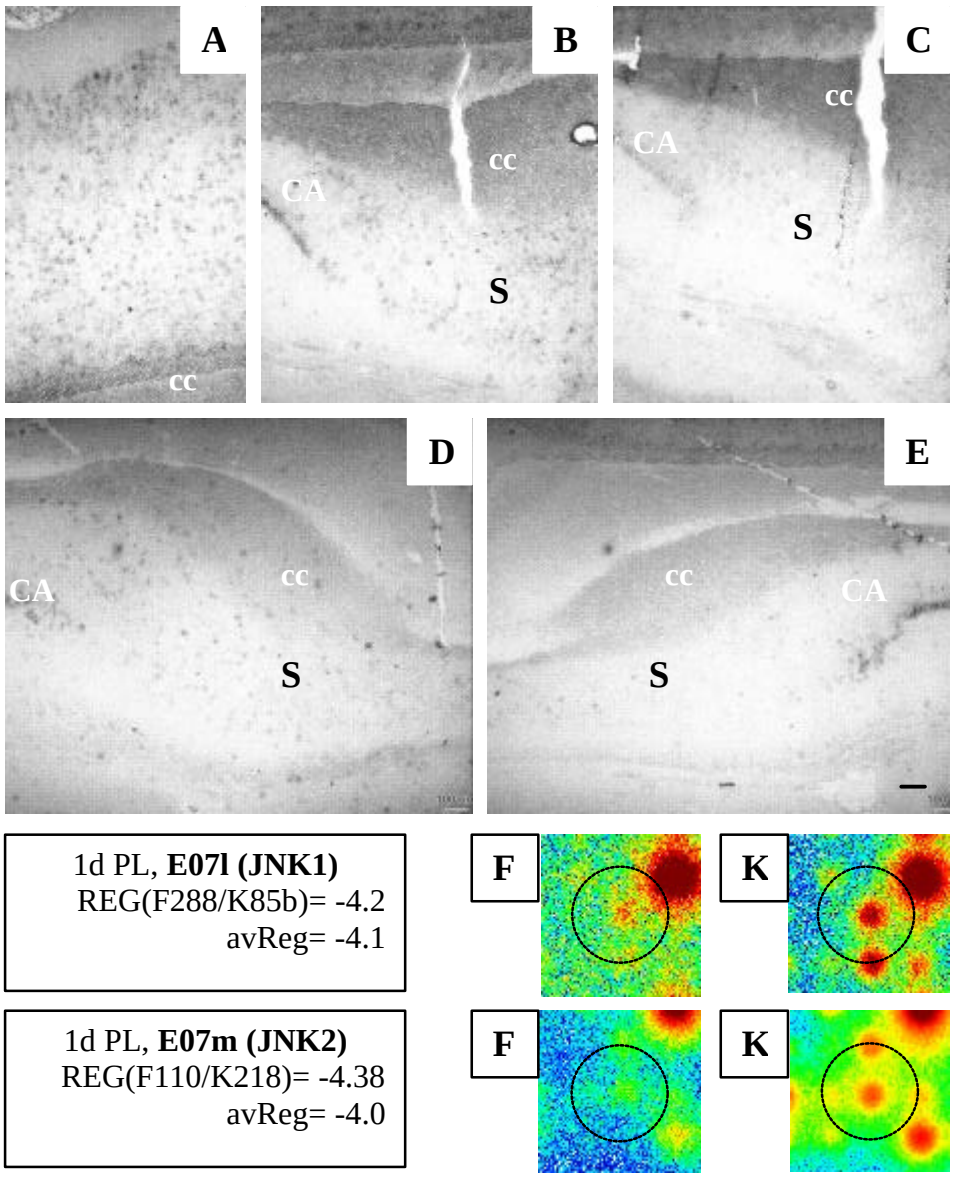

Figure 28. In situ and cDNA array expression data of JNK 1 and 2. Non radioactive in situ hybridization of an antisense cRNA probe specific for rat JNK 1 and 2 (A, B, D, E) and its sense control (C). Hybridization to adult rat cortex (A) and subiculum (B, C, D, E) is shown. Hybridization of the axotomized (D) and unlesioned (E) subiculum (n=2) in the coronal plane reveals approximately identical hybridization pattern and intensities. Hybridized array spots of JNK 1 and 2 (circled) are shown in (F) and (K), with hybridization intensities being colour-coded in analogy to the electromagnetic spectrum, from low (blue) to high (red) intensity. The target (F) and control (K) hybridizations display representative pairs of hybridized arrays (F288/K85b) and (F110/K218), as annotated in the box to their left. The average regulation values (avReg) of JNK 1 and 2 are also in the box for comparison. cc, corpus callosum; CA1, CA1 region of the hippocampus; S, subiculum. Scale bar 100 μm.

Expression of focal adhesion kinase (FAK)

Focal adhesion kinase (FAK) is a non-receptor, cytoplasmic tyrosine kinase, which becomes autophosphorylated upon activation. Integrins and seven transmembrane receptors appear to be involved in FAK activation, which then leads to recruitment of various signalling proteins, like Src family tyrosine kinases (Schlaepfer et al., 1998; Lacoste et al., 1998; Girault et al., 1999). It could therefore be recognized to be essentially an adaptor protein. A splice variant derived protein (FAK+), with additional three amino acids (Pro-Trp-Arg) in its aminoterminus, was shown to be enriched in neuronal perikarya and growth cones during development, while it was confined to the cell bodies of older neurons (Menegon et al., 1999). FAK was downregulated at stages (i) and (iii) (avREG=-3.1 and -3.1, respectively). Both, neurons and to a lesser extent glia appeared to be weakly labeled by in situ hybridization (Fig. 29 A, B, D and E). Distribution and hybridization of the unlesioned and axotomized dorsal subiculum was identical (Fig. 29 D and E). Labeling intensities of neurons varied within the cortex, with stronger labeling of layer V and VI (Fig. 29 A), while the hippocampus and subiculum were considerably less intensively labeled (Fig. 29 B, D and E). In similarity to JNK 1/2 hybridization relations, a weak in situ hybridization pattern corresponded to a moderate array hybridization signal.

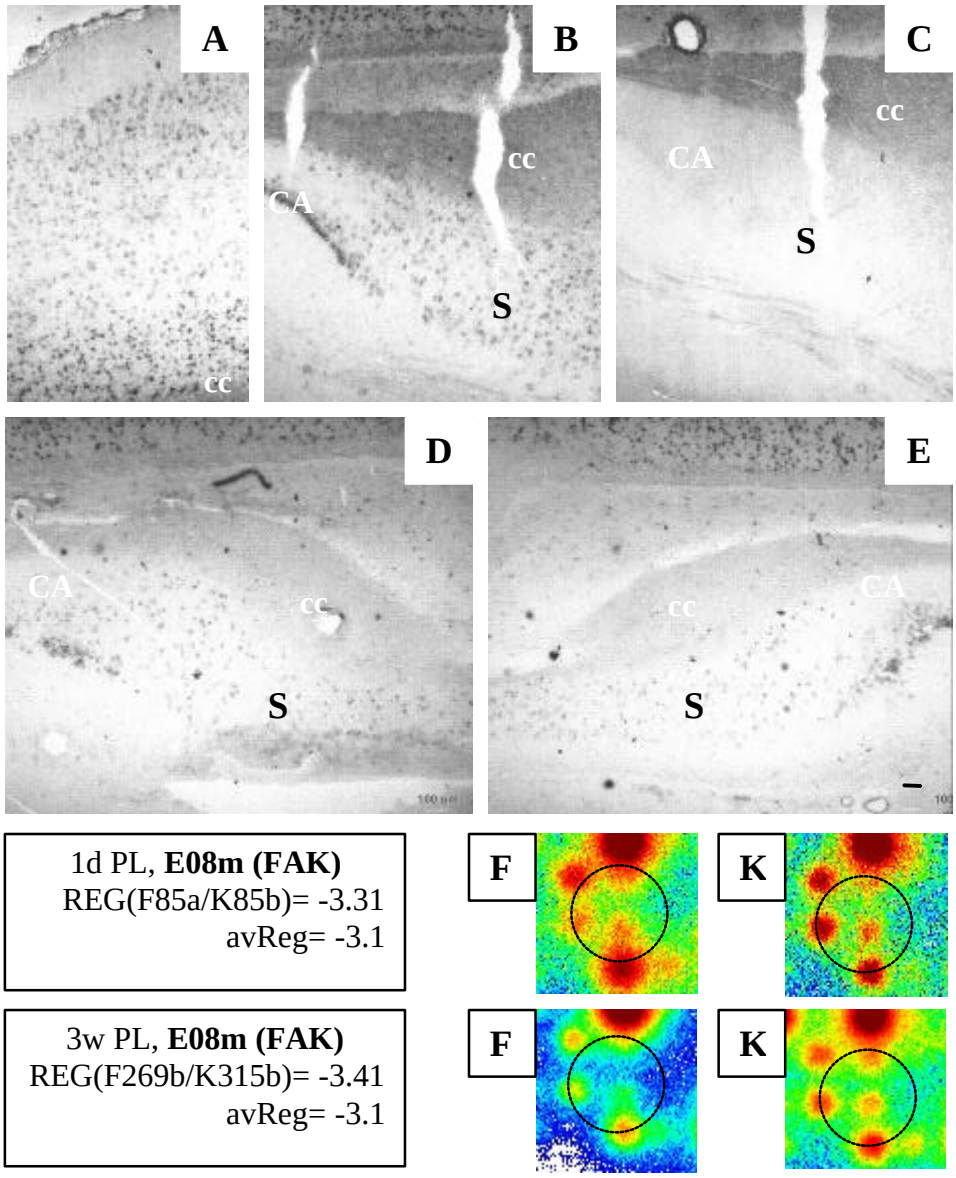

Figure 29. In situ and cDNA array expression data of FAK. Non radioactive in situ hybridization of an antisense cRNA probe specific for rat FAK (A, B, D, E) and its sense control (C). Hybridization to adult rat cortex (A), subiculum (B, C, D, E) is shown. Hybridization of the axotomized (D) and unlesioned (E) subiculum at 1d PL (n=2) in the coronal plane reveals approximately equal hybridization patterns and intensities. Hybridized array spots of FAK (circled) are shown in (F) and (K), with hybridization intensities being colour-coded in analogy to the electromagnetic spectrum, from low (blue) to high (red) intensity. The target (F) and control (K) hybridizations display representative pairs of hybridized arrays for 1d PL (F85a/K85b) and 3w PL (F269b/K315b), as annotated in the box to their left. The average regulation values (avReg) of FAK are also in the box for comparison. cc, corpus callosum; CA1, CA1 region of the hippocampus; S, subiculum. Scale bar 100 µm.

Expression of cofilin

Cofilin and the structurally and functionally related ADF both contribute to actin network disassembly and cooperatively bind to older ADP-actin filaments (Wear et al., 2000). Their actin depolymerizing activity is suppressed through phosphorylation by LIM kinases, which are in turn controlled by consecutive activation of Rho like GTPases and p21-activated protein kinase (PAK) (Kuhn et al., 2000; Pollard et al., 2001). Overexpression of ADF significantly enhanced neurite outgrowth, but also decreased filopodia numbers (Meberg and Bamburg, 2000).

Cofilin was found to be downregulated at stages (i) and (iii) (avREG=-3.0 and -2.5, respectively), like the aforementioned FAK. As was true for many other genes identified, this almost identical level of downregulation during two non-axon outgrowth stages needs to be noted. Neurons were labeled very strong by in situ hybridization, but white matter areas were also labeled to a lesser extent (Fig. 30 B, D and E). Dorsal subicular grey matter of the unlesioned and axotomized hemispheres displayed identical hybridization patterns for all cell types (predominantly principal neurons, as could be inferred by their distribution) (Fig. 30 D and E). The very strong in situ hybridization intensity corresponded to one of the strongest hybridization signals on cDNA arrays (Fig. 30 F and K). Again, intensities of in situ and cDNA array hybridization signals match very well, as compared to the other genes studie by in situ hybridization.

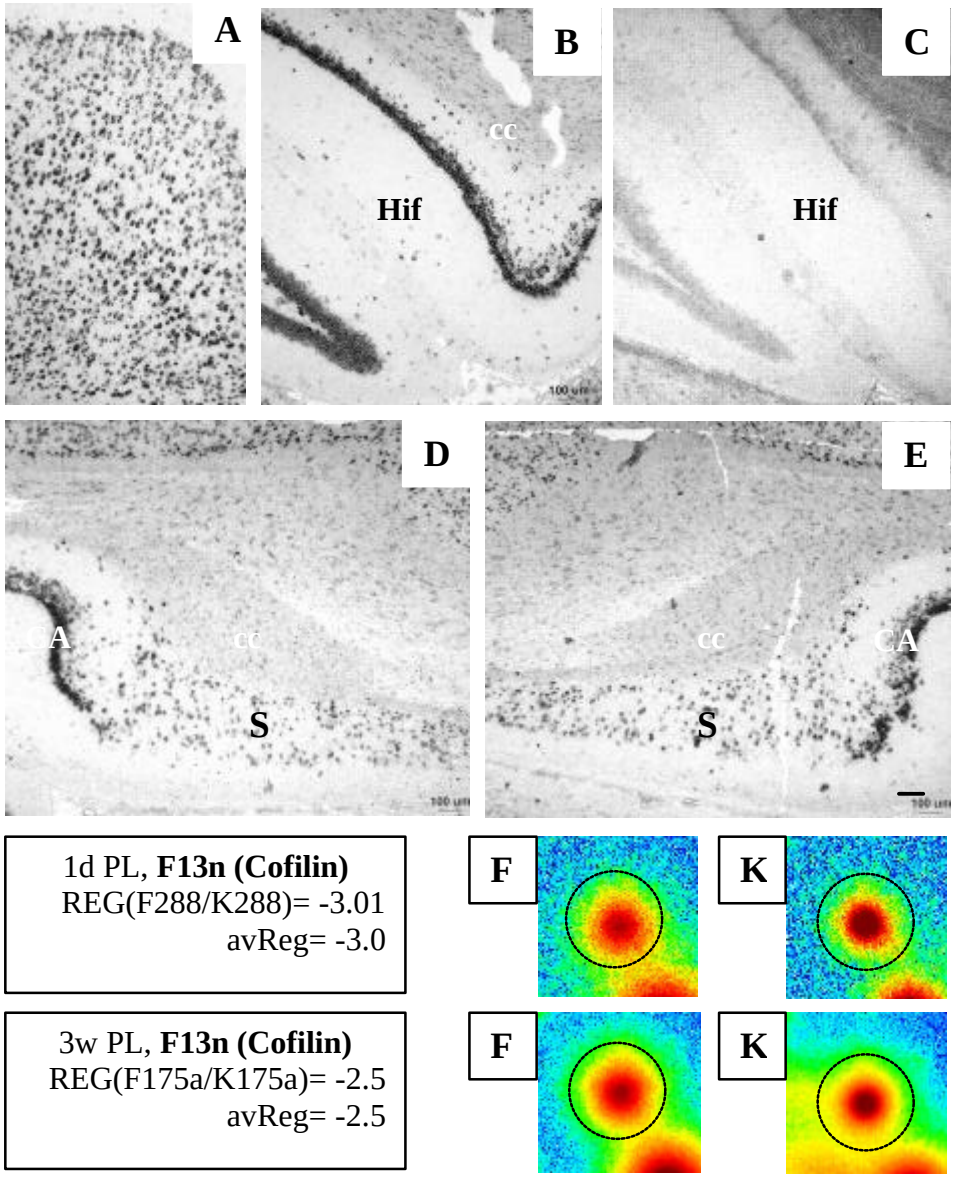

Figure 30. In situ and cDNA array expression data of cofilin. Non radioactive in situ hybridization of an antisense cRNA probe specific for rat cofilin (A, B, D, E) and its sense control (C). Hybridization to adult rat cortex (A), hippocampus (B, C) and subiculum (D, E) is shown. Hybridization of the axotomized (D) and unlesioned (E) subiculum at 3w PL (n=1) in the coronal plane reveals approximately equal hybridization patterns and intensities. Hybridized array spots of FAK (circled) are shown in (F) and (K), with hybridization intensities being colour-coded in analogy to the electromagnetic spectrum, from low (blue) to high (red) intensity. The target (F) and control (K) hybridizations display the representative pairs of hybridized arrays for 1d PL (F288/K288) and 3w PL (F175a/K175a), as annotated in the box to their left. The average regulation values (avReg) of cofilin are also in the box for comparison. cc, corpus callosum; CA1, CA1 region of the hippocampus; HiF, hippocampal formation; S, subiculum. Scale bar 100 µm.

Expression of serum- and glucocorticoid-inducible kinase (SGK)

Serum- and glucocorticoid-inducible kinase (SGK) is known as a glucocorticoid-inducible gene with high homology of its catalytic domain with rac protein kinase, protein kinase C family, ribosomal S6 kinase and cAMP-dependent protein kinase (Webster et al., 1993).

SGK was shown to be rapidly transcriptionally upregulated by glucocorticoids in fibroblasts (Maiyar et al., 1997) and p53 (Maiyar et al., 1996) in mammary epithelial cell lines, but with p53 blocking glucocorticoid stimulated binding of glucocorticoid receptors to its sgk-promotor element and vice versa (Maiyar et al., 1997). Perinuclear or cytoplasmic localization of the hypophosphorylated SGK protein in G1 is shifted to nuclear localization of the protein upon glucocorticoid stimulation, which induces hyperphosphorylation (Buse et al., 1999). Expression levels are furthermore influenced by inflammatory mediators, such as granulocyte-macrophage colony stimulating factor (GM-CSF), lipopolysaccharide or tumor necrosis factor α (Cowling and Birnboim, 2000).

SGK activity was found to be regulated by insulin-like growth factor 1 (IGF-1) or hydrogenperoxide induced phosphorylation on Thr-256 and Ser-422 in human embryo kidney (HEK) 293 cells. Stimulation with these agents mediates activation of 3-phosphoinosite-dependent protein kinases-1 and -2 (PDK1 and PDK2). Phosphorylation on Ser-422 by PDK2 is furthermore phosphatidylinositol-3,4,5-triphosphate (PI3)-dependent, while phosphorylation on Thr-256 by PDK1 is not PI3-dependent (Kobayashi and Cohen, 1999; Park et al., 1999).

SGK induction by aldosterone leads to an increased epithelial sodium channel (ENaC) activity (Chen et al., 1999), probably by increasing the number of ENaCs in Xenopus oocyte plasma membrane (Alvarez de la Rosa et al., 1999).

Three days after cortical lesion SGK mRNA was found upregulated and was maintained upregulated for at least fourteen days. It was found to be localized to the deep cortical layers and the corpus callosum. Its similar distribution with myelin proteolipid protein (PLP) mRNA was suggestive for oligodendrocytic expression. But postnatally, also neurons of layer I and II of the cortex and of some thalamic nuclei were found to express SGK mRNA, while no such expression was found in fetal or adult brain (Imaizumi et al., 1994).

After unilateral axotomy of the postcommissural fornix, SGK was identified to be downregulated by a factor of 2.7 (avREG=-2.7) at stage (ii). Distribution in the adult rat brain could be assessed with two different cRNA probes (Fig. 31 A, B, C and D, E, F, respectively). These probes revealed preferential distribution in white matter areas and no or much lesser expression in neurons (Fig. 31 A, B, D, E). This was the only example among the selected

genes, which showed preferential localization presumably to glial cells by in situ hybridization. This is remarkable, as regulation of those genes with preferential localization to glia could therefore also be detected by cDNA array hybridization experiments. Again, moderate expression over white matter areas, as detected by in situ hybridization, corresponded to a moderate hybridzation signal on DNA arrays (Fig. 31 F, K).

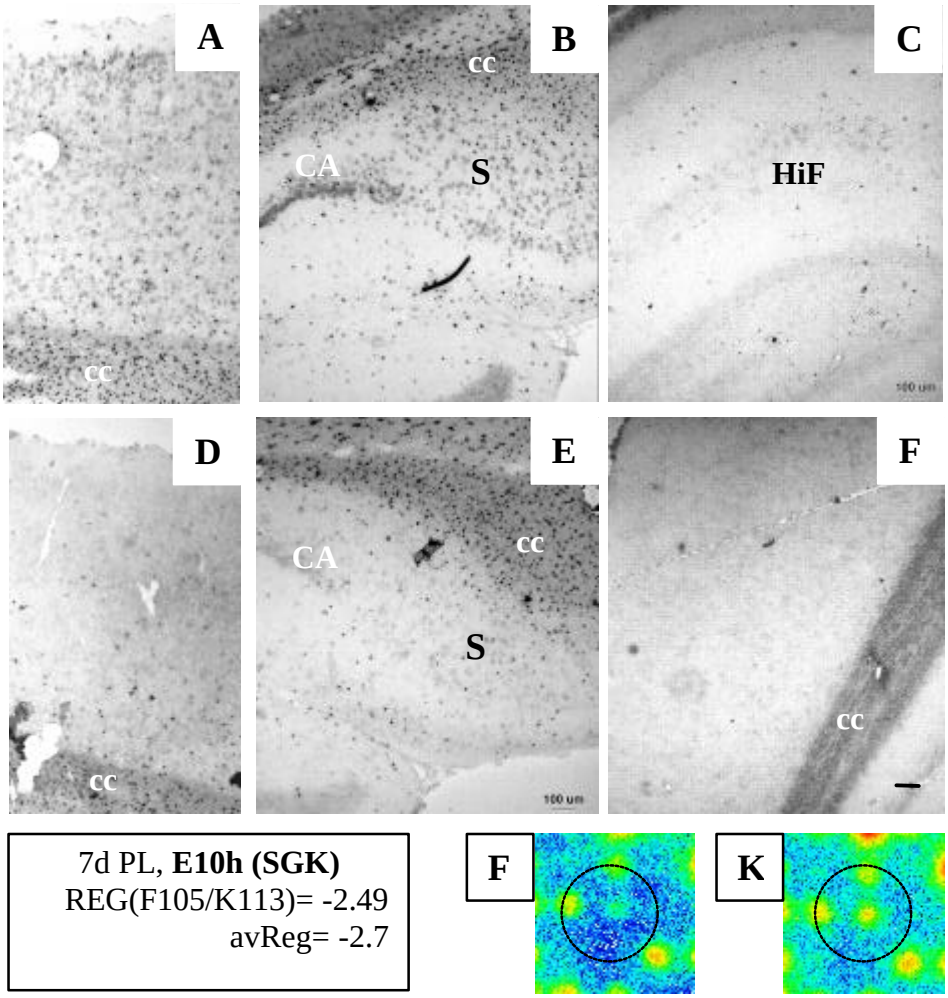

Figure 31. In situ and cDNA array expression data of SGK. Non radioactive in situ hybridization of two similar antisense cRNA probes specific for rat SGK (A, B and D, E) and their sense controls (C, F). Hybridization to adult rat cortex (A, D, F), hippocampus (C) and subiculum (B, E) is shown. Hybridized array spots of SGK (circled) are shown in (F) and (K), with hybridization intensities being colour-coded in analogy to the electromagnetic spectrum, from low (blue) to high (red) intensity. The target (F) and control (K) hybridizations display a representative pair of hybridized arrays (F105/K113), as annotated in the box to their left. The average regulation values (avReg) of SGK is also in the box for comparison. cc, corpus callosum; CA1, CA1 region of the hippocampus; HiF, hippocampal formation; S, subiculum. Scale bar 100 µm.

Conclusion of cDNA array analysis

This chapter demonstrated that differentially expressed genes can be identified with cDNA arrays by analysing a cellularly heterogenous brain tissue preparation, if a sufficiently high number of experiments is used.

Gene expression changes, which must reflect the axotomy induced response within the subicular tissue were identified with high confidence. Generated patterns were specific, highly consistent and revealed distinct expression patterns for one day, seven days and three weeks post lesion. The expression pattern at seven days post lesion appeared to be significantly different from the patterns at one day and three weeks post lesion. The cellular distribution of six of the identified genes was analysed by in situ hybridization and revealed that most of them were expressed by neurons, but some also by glia, what could be expected by the experimental setup.

Many genes were identified, which were previously not associated with the axotomy induced response or axonal outgrowth.

5. DISCUSSION

In this thesis, the expression pattern of 1191 different rat genes was studied after postcommissural fornix axotomy. The axotomy induced molecular responses must originate at the lesion site and it can be postulated that they are retrogradely propageted to the neuronal somata. As the exact nature of such retrograde signals is still unknown, in part A the expression pattern of a few typical regeneration and degeneration associated genes was investigated at the lesion site upon axotomy. Distinct morphological and molecular changes were found, which might accompany retrograde propagation of signals to the subiculum, where the projecting neurons are localized. The response of the subiculum was analysed with cDNA arrays, which contained 1185 genes. The applied analysis procedure lead to the identification of genes, which were differentially expressed after fornix transection. The generated expression patterns revealed the participation of many different cellular components and pathways upon axotomy.

5.1 The molecular response after fornix axotomy is initiated at the lesion site

After axotomy of the postcommissural fornix, the proximal stump was shown to remain at the lesion site at one day post lesion, with increased neurofilament, GAP-43 and L1 immunolabeling within a ribbon like structure at a distance of about 400 µm proximal to the lesion site. Furthermore, bulbous structures, with increased neurofilament and/or GAP-43 immunoreactivity could be recognized within the proximal stump. In vitro observations on laser transected embryonic septal neurons revealed similar bulbous structures, but on a different spatial and temporal scale (Xie and Barrett, 1991). After in vitro axotomy, round, beadlike swellings of the axons were rapidly observed within minutes, but persisted only for about ten minutes, at a distance of less than 50 µm from the lesion site (Xie and Barrett, 1991). Similar results with Aplysia neurons demonstrated significant changes of the axonal cytoskeleton on the ultrastructural level at about 80 µm from the lesion site within 5 minutes (Ziv and Spira, 1997). These cytoarchitectonical alterations included disruption of microtubules and neurofilaments, as well as formation of electron-dense filamentous material. These alterations within the cytoskeleton in vitro may correspond to the bulbous morphological changes observed in the in vivo model of the transected fornix. Differences on

the spatial and temporal scale could arise from the more complex molecular and cellular environment encountered in vivo.

A different temporal course of events after axotomy in vivo is supported by a delay of about five hours in the peripheral nervous system, until new axon sprouts emerge (Tomatsuri et al., 1993). Studies on isolated peripheral axons suggested that the responsible molecular machinery for growth cone induction was independent of the neuronal cell body (Kato and Ide, 1994). Observations in vitro revealed a strict dependence of the observed changes on a transient calcium rise up to several hundred micromolar within the transected axon, which was necessary and sufficient to trigger membrane resealing and growth cone formation (Ziv and Spira, 1997; Xie and Barrett, 1991). Calcium concentrations might be more tightly controlled in vivo, than in vitro, thus contriubuting to a different spatial and temporal profile.

The influence of calcium is supported by observations on delayed degeneration and regeneration in Ola(Wld)-mice (Chen and Bisby, 1993), which display neurofilament degradation of the facial nerve, only if calcium levels are increased, as compared to normal mice (Glass et al., 1994). This apparently different responsiveness of degenerating axons towards calcium could be attributed to an altered calpain activation in different experimental systems.

Activation of the calcium induced protease calpain appeared to be necessary for reinduction of a new growth cone (Gitler and Spira, 1998; Xie and Barrett, 1991), but could also be the reason for aberrant phophorylation activity, leading to aggregates of cytoskeletal components (Ahlijanian et al., 2000). Hyperphosphorylation of cytoskeletal components, like the tau and neurofilament proteins, could be generated by excessive activity of cdk5, which was shown to be prolonged activated and mislocalized, if its neuron specific activator p35 was cleaved to p25. On the other hand, could cleavage of p35 to p25 be reduced by specific calpain inhibitors (Lee et al., 2000a), suggesting that unphysiological calpain activation by high calcium transients could, on the one hand, initiate a cascade of restorative events, leading to reinduction of a growth cone, but, on the other hand, could also induce a cytotoxic cascade, with hyperphosphorylation of cytoskelatal components.

Altogether, these calcium triggered events could provide an explanation for the bulbous structures observerd within transected postcommissural fornix.

Apart from direct effects on the cytoskeleton, altered calcium levels could also have an effect on reduced macrophage invasion into the distal stump. This cellular response was also observed in mutant Ola(Wld)-mice (Brown et al., 1991), suggesting that the complex environment in vivo is influenced not only by its molecular, but also cellular constituents.

Interestingly, the apparent diminished calcium responsiveness in neurofilament degradation (Glass et al., 1994) and retarded macrophage invasion, are both in agreement with a delayed degeneration and regeneration in Ola(Wld)-mice (Brown et al., 1991).

The observed GAP-43 positive spherical or bulbous structures, which appeared as free vesicles in the confocal images, could be explained by aberrantly enhanced vesicle fusion or exocytosis. GAP-43 phosphorylation by protein kinase C (PKC) was shown to potentiate the magnesium-adenosinetriphosphate-dependent priming step of vesicle fusion in adrenal chromaffin cells (Misonou et al., 1998). And calmodulin, which could block GAP-43 phosphorylation is likely to be saturated with calcium after axotomy induced calcium rises, what in turn would abolish binding of GAP-43 to calmodulin (Alexander et al., 1987; Chapman et al., 1991). This would leave GAP-43 unprotected for PKC phosphorylation and vesicle fusion. In line with these results, GAP-43 was shown to bind to the synaptic core complex, including syntaxin, 25 kDa synaptosome-associated protein (SNAP-25) and vesicle-associated membrane protein (VAMP) at 100 µM (Haruta et al., 1997), what was shown to be reached, even at a distance of over 100 µm from the lesion site (Ziv and Spira, 1997). Whether this was truely the case after axotomy in vivo could be revealed by performing additional immunohistochemical labelings at the lesion site.

The appearance of GAP-43 positive bulbous structures within the axons was also reported after traumatic injury to rat spinal cord (Li et al., 1995a) or after diffuse axonal injury by brain trauma in cats (Christman et al., 1997) at post lesion times between one and seven days. The temporal profile of the latter response resembles the one found for the appearance of neurofilament and GAP-43 positve bulbous structures after fornix axotomy. Alternatively, the altered axon morphology could be partially attributable to a decreased slow axonal transport, which was observed after optic nerve crush (McKerracher et al., 1990).

The observed proximal degeneration distance of about 600 µm at five days post lesion was less than the about 1000 µm, which were previously reported within this lesion model (Wunderlich et al., 1994). This difference might arrise from the employed techniques. While in this study only neurofilament immunohistochemistry was employed to determine the advance of the proximal stump, wheat germ agglutinin coupled to horseradish-peroxidase was anterogradely transported to trace the proximal fornix stump in the previous work (Wunderlich et al., 1994). On the other hand, similar degeneration distances were reported at three days or seven days post axotomy in other previous studies on this lesion model (Stichel and Mueller, 1994; Stichel et al., 1995a).

Increased L1 and clusterin immunoreactivity in the immediate proximal, but also in the distal stump were indicative for axonal degeneration within these areas especially at five and seven days post lesion. Although increased L1 labeling is generally not associated with degenerative events, alternative events could explain the increased L1 immunoreactivity.

During myelination of axons five to six weeks postnatally, L1 became less detectable over white matter tracts in rat (Stallcup et al., 1985), what is in agreement of L1 being localized to the axoplasm and between axolemma and compact myelin, but not in compact myelin itself (Joosten, 1991). Therefore, L1-epitopes appeared to be masked by myelination. During demyelination of the proximal stump in this lesion model, both myelin basic protein and NI-35/250, a myelin constituent that was recognized by the IN-1 antibody and is now termed NOGO (Chen et al., 2000; GrandPre et al., 2000; Prinjha et al., 2000), dissappeared at least at seven or three days post lesion, respectively (Stichel et al., 1995a). Just around these post lesion times an increased L1 immunoreactivity, both in the proximal and distal fornix stump, could be observed in this study, corresponding to the putative unmasking of L1-epitopes.

The ongoing degenerative events of the proximal stump were also evident by the increase in clusterin immunoreactivity. This complement inhibitor is known to accumulate in degenerating neurons of CA1 hippocampal area after status epilepticus (Dragunow et al., 1995) or to be deposited in the neuropil of the deafferented striatum after decortication (Cheng et al., 1994). These deposits and additional strong labeling of degenerating fornix fibres at five days post lesion were also seen within this lesion paradigm.

Increased labeling of fornix fibres, both in the degenerating proximal and distal stumps could reflect clusterin deposition near aggregated amyloid beta-peptide, which could have been generated from the anterogradely transported APP in the axons (Koo et al., 1990; Moya et al., 1994; Amaratunga and Fine, 1995). This is supported by the finding that clusterin is associated with amyloid beta-peptide (Oda et al., 1995). But of course, deposition of amyloid beta-peptide, colocalized to clusterin in degenerating fornix fibres remains to be shown.

Most cells displaying increased clusterin immunoreactivity at the post lesion times studied were likely to be astrocytes. This was also reported for the cellular response in the dorsal horn after sciatic nerve transection (Liu et al., 1995). But also larger cells with neuron-like size and morphology were seen to be clusterin positive. This would be in agreement with secretion of clusterin in astrocytes (Pasinetti et al., 1994) and accumulation in neurons that were destined to die by apoptosis, as it was suggested for dying neurons in the hippocampus after ischaemic insult (Walton et al., 1996).

The increased expression of clusterin over the degenerating distal stump especially at two weeks post axotomy strikingly parallels the induction of clusterin in oligodendrocytes during Wallerian degeneration of the dorsal funiculus after lumbar dorsal rhizotomy (Liu et al., 1998), suggesting that all neural cell types display increased labeling with clusterin after axotomy. Persistent expression of clusterin in cells in the perilesional area of the fornix at four weeks post lesion could be indicative for ongoing activation within these cells, probably associated with permanent amyloid beta-peptide deposition.

Increased activation of cells over the degenerating white matter of the distal stump at seven days post lesion is also supported by the increased expression of Sox 10, an oligodendrocytic marker in the CNS (Kuhlbrodt et al., 1998; Zhou et al., 2000), which may also play a role in other glial cells of the brain (Touraine et al., 2000). But the upregulation of an oligodendrocytic marker gene during axon degeneration and myelin disintegration, has not been reported previously.

The uniform and almost unaltered expression of rMDC15 in the unlesioned and lesioned fornix is in marked contrast to the initial increase until two days post lesion as described for the distal stump of the crushed or transected sciatic nerve. Here, rMDC15 expression dropped below control levels (Bosse et al., 2000). However, rMDC15 was found to be localized largely to Schwann cells in the PNS, while in the CNS expression was found in neurons (Bosse et al., 2000). The latter finding is confirmed by the subicular expression pattern described here. Therefore, rMDC15 may serve a function in the CNS that is different from the PNS.

Taken together, the regenerative and degenerative events within the proximal and distal fornix stumps suggested a series of complex molecular and cellular changes. The degenerative events within the proximal and distal stump appeared to be very similar, suggesting that the spontaneously outgrowing proximal fornix stump should also be able to elongate within the distal tract. However, like in many other CNS lesion paradigms the lesion site must consitute an impediment for the outgrowing axons, which were found to rest within their former tract at the lesion site, with no sprouting around it being detectable. This elongation within its proper pathway is remarkable, as it suggests that guidance cues and the guidance machinery must be functional in the surrounding tissue and within the outgrowing fornix axons, respectively. How and to what extent subicular neurons might respond after axotomy will be discussed in the last chapter.

5.2 DPY treatment is not sufficient for fornix regeneration

Treatment of the lesion site with collagen IV formation inhibiting DPY was previously reported to be sufficient for axonal regeneration of the postcommissural fornix (Stichel et al., 1999b). It was reported that even at six days post lesion axons traversed the lesion site into the distal stump (figure 6 in Stichel et al., 1999b). Similar results were obtained using Schwann cell suspension grafts in the same lesion model, where fornix axons were found distal from the lesion site by 18 days post lesion.

Therefore, the employed survival times of between two and four weeks after transection and treatment were considered to be sufficient to observe regenerating axonal fibres by pan-axonal marker (PAM; neurofilament) immunohistochemistry of the fornix stumps.

But despite the high number of 88 analysed animals no regeneration was found. The communicated proportion of at least 50% of regenerating animals after immediat DPY treatment, should in this case have lead to about 44 regenerating animals. But no regenerating animals could be identified. This corresponds to the negative data described by Lausberg, 2000 (Lausberg, 2000).

In search of reasons for the failure of regeneration, some original data that were left of the previous work by Stichel et al. (Stichel et al., 1999b) were reanalysed. It soon became obvious that the size of the lesion was insufficient in those cases, where regeneration was believed to have occurred. The incompleteness of the transections cannot be recognized in the figures of the respective publications, but only if the size of the complete proximal stump and the known trajectory of the fornix were compared to the lesion size and position at lower magnification, where all these components could be recognized. Incomplete transection in the previous work is furthermore suggested by the trajectory of "regenerating" fornix fibres across the lesion site (e.g. figure 6 G in Stichel et al., 1999b). A characteristic upwards kink was interpreted as a result of the upward movement of the Scouten wire knife, which could be partially true. But there was never such a kink seen within the proximal stump, which first retracted from the lesion site, then sprouted and finally stopped at the lesion site within its (straight) former pathway.

Therefore, the data presented in this thesis suggest that DPY treatment is insufficient for axonal regeneration of the postcommissural fornix.

5.3 Detection of the subicular response upon fornix transection

Within this thesis, the adult rat subiculum was found to respond with profound changes in gene expression following axotomy. The multipoint or time-course comparison of the induced transcriptional responses revealed the dynamic expression of 174 different genes at three postlesional stages. Correlating the differential expression of analysed genes with characterized axon elongation stages, make it possible for the first time to gain unprecedented insight into critical cellular functions in the course of axonal regeneration in vivo.
Therfore, cDNA array derived results will be preferentially discussed, while histologically characterized genes will be included where appropriate. First the methodological aspects of this approach will be discussed, followed by discussion of probable functions of some of the identified genes. Finally, retrograde signalling pathways will be discussed, which could be involved in the molecular responses observed after CNS axotomy.

5.3.1 Approach and methodological issues

The selected cDNA arrays provide an overview over transcriptional changes after axotomy

The intention of the employed approach was, to identify the dynamic pattern of differentially expressed genes. The most important constraint within this approach was the limited amount of isolated brain tissue as starting material.
Several molecular biological techniques exist, which try to identify differentially expressed genes. Especially reverse transcription representational difference analysis (RT-RDA) or differential display (DD) could have been useful in this approach, considering that these techniques both require a minimum of starting material of about 10-100 ng polyA RNA. But they both lack sufficient reproducibility, afford sequencing of selected clones and provide no direct means for quantification of expressed genes (Carulli et al., 1998). However, both techniques have been more or less successfully applied.
For example, the RT-RDA was used for the generation of a selection of clones, which were then analysed with DNA microarrays (Geschwind et al., 2001). On the other hand, differential display was applied for the analysis of axotomy induced responses within lesioned neurons in several cases. But, whenever results were reported, they focused on the expression of a single gene only, like on isopentenyl diphospate (IPP) isomerase, which was identified among five other genes to be upregulated in the neonatal rat cortex, but also after nerve transection

(Morihara et al., 1999); ceruloplasmin, which was also identified after fornix transection and was found being upregulated after optic nerve crush (Levin and Geszvain, 1998); cytoskeletal motor proteins were identified after axotomy in hypoglossal motor neurons (Su et al., 1997); cyclin G, was upregulated within axotomized hypoglossal motor neurons (Morita et al., 1996); a neuronal glutamate transporter, rat EAAC1, which was also identified after fornix transection, was increased in hypoglossal motor neurons (Kiryu et al., 1995).

This small collection of reports on differentially expressed genes already demonstrates, that despite using the same lesion paradigm of the axotomized hypoglossal nerve, three different genes were found to be differentially expressed, indicating the low level of reproducibility and the incompleteness of the generated results.

In similar paradigms serum/glucocorticoid regulated kinase (SGK), which was also identified in this thesis, was found to be upregulated after cortical injury, very likely within oligodendrocytes, but was nevertheless associated with axonal regenerations after brain injury (Imaizumi et al., 1994). Furthermore, the proteasome component proteasome C2, which was also identified in this analysis, was found to be downregulated in the contralateral hemisphere after a circumscribed unilateral infarct (Keyvani et al., 2000).

Nevertheless, it is reassuring of the approach performed here, that some genes, which were identified in this analysis, were also identified within other related lesion paradigms.

Alternative techniques, like expressed-sequence-tag (EST) cloning identified about thirty axotomy induced genes in the hypoglossal motor neurons, thus being more successful than the DD-approaches, but again without quantitative data or dynamic information and with a high demand of starting material (Tanabe et al., 1999). The only technique providing semiquantifyable data is serial analysis of gene expression (SAGE), which would have required both, a high amount of tissue and high sequencing effort (Carulli et al., 1998). However, this would have been unfavourable with the limited amount of starting material available in this approach and the intention to generate functional information.

Therefore, the application of cDNA arrays was the most suitable approach. The intention to generate stand alone expression data, which would provide functional insight into axotomy induced responses, was further supported by employing commercially available cDNA arrays with annotated genes. The number of 1185 genes, which were analysed by cDNA array hybridization pattern comparison, appears small in relation to the number of genes on high-density microarrays, which can often analyse 10,000 genes and more (Lockhart and Winzeler, 2000). But high-density arrays often carry large numbers of ESTs or genes with as yet unknown functions. Scientists who use such microarrays often intend to annotate a

presumptive new function to such genes, simply by the fact that they corregulate with functionally characterized genes (often termed as guilt-by association-principle) (DeRisi et al., 1997). But this kind of approach was not intended here, as it demands specialized bioinformatics support. Therefore, analysing more than one thousand rat cDNAs in one approach is satisfactorily, considering that latest estimates of the number of genes within an eucaryotic genome range between 30,000-90,000 for the mouse or human genome (Venter et al., 2001; Nadeau et al., 2001).

Another limitation, concerning the conclusions that can be drawn from the reported results, was that the expression patterns reflected the response within the isolated tissue and not the projecting neurons alone. Isolation of the projecting neurons alone would only have been possible by laser capture microdissection (LCM), a method that was already successfully employed to investigate the different mRNA contents within large- and small-sized neurons of the dorsal root ganglia (Luo et al., 1999). This sophisticated technique was shown to provide about 1000 cells per hybridization, which was still not sufficient as starting material. Therefore, preamplification of the isolated RNA was performed in order to produce sufficient amounts of nucleic acid for reproducible hybridization experiments. However, preamplification can never be done, such that every mRNA within the sample is linearly amplified within even a low number of PCR cycles. This was the personal experience gathered with real-time PCR and is supported by the comments of more experienced groups (Lockhart and Winzeler, 2000), which rather suggest linear amplification based on cDNA synthesis and a template-directed in vitro transcription reaction (Guatelli et al., 1990; Eberwine et al., 1992). But neither technique was required in this approach, as two isolated subiculi provided enough starting material for one cDNA array hybridization experiment, thus demanding a total number of 72 animals for the present investigation.

An alternative approach in vitro, which would also aim at the observation of the neuronal response, would have been fraught with a similar cellular heterogeneity, as the employed in vivo approach. Using primary neurons or transfected neuronal cell lines would both result in impure cell populations. On the one hand, the astrocytic cell layer for primary neurons and on the other hand, non-transfected cells would contriubute to the cellular heterogeneity. Furthermore, no in vitro paradigm would have been suitable to reflect the complexity encountered in vivo upon axotomy. Moreover, heterogenous cancer tissue samples, which likely have a comparable degree of heterogeneity, were already shown to produce valuable data (Ross et al., 2000; Alon et al., 1999; Perou et al., 1999).

In situ hybridizations of six of the identified genes, as described in the results section, have revealed that both neurons and glia contribute to the observed expression patterns. But taking into account that neurons were the cell type primarily affected by axotomy, glial responses can only be secondary and might, therefore, only be seen at seven days and three weeks post lesion. However, confirming the localization of all of the identified genes would demand almost two hundred in situ hybridizations.

Here the advantage of having analysed only known genes comes into play, because there often is a large body of information available in the literature about each gene. Many identified genes, which could be sorted into one of the prominent functional groups were already known to be involved in cellular reactions during axonal outgrowth. Whether an identified gene is more likely to be involved in neuronal or glial reactions and which functional consequences are associated with such an expression, will be disscussed further below (5.2.2). But in the following chapter the applied parameters will be discussed.

The applied analysis parameters and procedure lead to the identification of genes, which were differentially expressed after fornix transection

The variety of DNA array platforms is reflected in different approaches for data analysis. Only recently guidelines were defined on the analysis parameters, which have to be added to expression data for publication or storage in databases. Several parameters, like signal threshold and normalization value are intrinsic to each hybridization or the respective experimental system and cannot be standardized. Within the analysis procedure applied here, no compact software solution could be used, performing all steps from signal analysis to the finally presented expression patterns. Instead, a combination of an image analysis software and Microsoft Excel based analysis matrices was employed. This was advantageous, because often encountered problems, like signal intensity threshold and regulation threshold setting, but especially the choice of a normalization value, could be solved independently of any software inherent parameters. But on the other hand, many statistical calculations and graphical representations could not be realized within this basic approach. However, the employed parameters worked very well and the final identification of differentially expressed genes, which were sufficiently reproducible, was successfully solved.

Initial results with global background areas revealed some genes, which could not be confirmed to be differentially expressed, but instead only a strong signal adjacent to the respective hybridized cDNA-spot was regulated. This signal intensity spill over was due to the employed phosphorus-32 for cDNA synthesis and needed to be eliminated by the image

analysis software. Therefore, individual background areas were assigned in a circular ring, placed at an empirically defined distance around the hybridized spots. Similar procedures, which used localized background areas were also reported elsewhere (Luo et al., 1999; DeRisi et al., 1997).

Furthermore, signals with comparatively low hybridization intensity needed to be excluded, as they were more prone to be affected by random fluctuations. Like it was just mentioned, this stringency was realized on the one hand by using local background subtraction. On the other hand, an intensity threshold was defined at five percent of the average hybridization intensity of hybridized signals, which had a positive signal intensity, even after background subtraction. The intensity threshold of five percent of the average hybridization intensity, corresponded very well with the initially employed mean global backgrounds plus three times their standard deviations. A similar threshold calculation was also reported for custom made arrays (White et al., 1999).

As it was true for background subtraction and signal intensity threshold definition, no standards on signal intensity normalization exist. The applied normalization with the average signal intensity of all positive signals (after background subtraction), provided a very stable normalization value. This stability became visible especially in the reproducibility spectrum of the stage (ii) analysis (Fig. 24).

The approach, which employed the average signal intensity for normalization was significantly more sensitive than the one, which employed the GAPDH-signal for normalization.This was demonstrated by the significantly lower +3SDcutoff-value. In general, normalization with the average hybridization intensity can best be used, if a sufficiently high number of signals is averaged to reduce the influence of random fluctuations, and if the different conditions, which are intended to be compared show similar hybridization patterns. Both requirements were realized in the approach discussed here, supporting the correctness of the normalization with the average signal intensity values.

In order to identify differentially expressed genes, the sensitivity for differential expression ratio detection has to be known. Microarrays were shown to detect changes as subtle as a factor of 1.3 to 2 (Lockhart and Winzeler, 2000). Therefore, the employed regulation threshold of a factor of 2 was considered to be sufficient to eliminate random fluctuations. So called split-sample comparisons, where the starting material (RNA) is split into two identical fractions, which are then independently labeled with two different fluorophors and hybridized to the same microarray, could not be performed, as the applied approach utilized radioactive hybridization on two different arrays. In fact, random noise, biological variation and

occasional array-specific physical defects were reported to be critical for reliable array data analysis. But associated problems, especially false positive results, could successfully be eliminated by selecting only genes, wich were consistently identified in independent replicates (Lockhart and Winzeler, 2000).

Therefore, high reproducibility was the most important criterion for the identification of differentially expressed genes, as they were reported in this thesis. The employed netto reproducibility or reproduction value (RVal) of each gene takes random fluctuations by variably isolated tissue, variations in the biochemical steps and variations in the physical array support into account. This was further realized by performing the high number of six experiments at each stage and comparing each target (F) array dataset with each control (K) array dataset. As a result, 36 comparison matrices could be analysed, in order to identify differentially expressed genes. The employed netto reproducibility reflects that random fluctuations by any of the above mentioned variables lead to a low netto reproducibility, while highly reproducible genes had high values. The defined lowest cut-off, which was calculated as the average reproduction value plus two times its standard deviation, was shown to eliminate genes with highest random reproduction values in comparisons of control (K) array datsets. Furthermore, this analysis procedure was successfully used in the analysis of a foreign experimental dataset, which was formerly verified by independent techniques.

Therefore, the employed analysis methodology fullfilled all basic requirements for reliable cDNA array experiment analysis and produced sets of differentially expressed genes, which reflect the subicular response towards axotomy.

The patterning approach and generation of functional information

In order to generate patterns, which would allow extraction of biologically important functional information, the identified genes were manually arranged in stage correlated expression patterns. Manual examination and arrangement of expression data generally depends on published data and manual data processing, what bears the risk to gather information in a subjective manner. Alternatively, computer algorithms could be used to arrange analysed genes. Bioinformatic support is especially required if larger datasets derived, e. g., from DNA arrays with some 10,000 of genes, need to be analysed (Zhang, 1999). The bioinformatic's possibilities to use database linked analysis tools have a huge potential wherever DNA sequences and expression data need to be linked. For example, the comparison of upstream activation sequences (UASs) of coregulated genes could provide valuable insight into genome organization and genetic networks within an organism. So far,

there are no standardized algorithms for the identification of coregulated genes, but some were shown to efficiently cluster together genes of known and similar functions, thereby also allowing the assignment of putative functions to hitherto unknown genes, simply by the fact that they are coregulated with known genes (Eisen et al., 1998). However, one of the main intentions of these algorithms is to arrange expression data in a way that enables scientists to extract biologically relevant functional information either by suitable visualization of data or intricate database networking.

Therefore, the manual approach taken here, with only 1185 genes analysed and 174 different genes finally identified, was recognized to be sufficient to generate functional information and develop new hypotheses, as will be discussed further below. Moreover, the number of genes analysed in this thesis corresponds to about one to five percent of expected genes in the rodent genome and is, therefore, likely to provide some insight into the response of the complete transcriptom. The significance of the results is further supported by the fact, that about ten percent of all analysed genes were found to be differentially expressed, which is in good agreement with the ten to fifteen percent reported in other controlled experiments with samples derived from complex tissues, but with some 10,000 of genes being analysed (Lockhart and Winzeler, 2000).

Therefore, the interpretation of the generated expression patterns could finally demonstrate their usefullness. Three different sets of differentially expressed genes were identified at stages (i), (ii), and (iii). This was not surprising, as they were correlated with three different morphological events at the respective post lesion times. The generated data support the concept of retrograde signalling after axotomy, possibly with a special relevance of signalling upon axonal contact with the lesion site, as it was postulated (Zagrebelsky et al., 1998). Moreover, the response of glial cells upon axotomy, as demonstrated by the localization of the gene SGK at least preferentially to glial cells by in situ hybridization, suggested that multiple levels of a retrograde response exist, with affected neurons possibly signalling to the surrounding glial cells. So far, axotomy induced glial reactions have been reported to be associated with neuronal degeneration after facial nerve axotomy in mice (Raivich et al., 1998). Whether SGK-levels were influenced by glucocorticoids, secreted by the axotomized neurons, and how far this glial response is associated with axonal regeneration is unknown. Interestingly, SGK induction in oligodendrocytes within three days after cortical lesion, was associated with axonal regenerations (Imaizumi et al., 1994). Further evidences for possible retrograde signalling pathways within the axotomized neurons will be discussed below (5.2.3).

The arrangement of the genes revealed overlapping gene expression, i.e. identical genes that were identified to be differentially expressed at more than one stage. Thus 28 genes were arranged into a short pattern (Fig. 25), revealing that gene expression is dynamic after axotomy, with some of the genes being coexpressed during degeneration onset (i) and axonal outgrowth (ii), others during axonal outgrowth (ii) and axonal growth arrest(iii). But most remarkably, during degeneration onset (i) and axonal growth arrest (iii) 18 genes were shared, corresponding to about ten percent of all identified genes.

These overlaps between the stages suggest a transition between different transcriptional states within the tissue (or cells). This was supported by the fact that two experiments at 7days post lesion had genetic features of degeneration onset (i) results. Moreover, three out of seven identified genes at this intermediary (i)/(ii) termed stage, had regulation values just between those of stages (i) and (ii). This is supportive for the dynamic and interconnected nature of the expression patterns. But this also implicated that stage (ii) expression pattern is not always stably reached at 7days post lesion.

The finding that during degeneration onset (i) and axonal growth arrest (iii) identical genes often had very similar regulation values, was indicative for these genes sharing a common function at these two non-axon-outgrowth stages. This property of stages (i) and (iii) was in contrast to stage (ii), which is exemplified by the expression pattern of GAPDH. It was the only gene, which became downregulated at stages (i) and (iii), while it was upregulated at stage (ii). Stage (ii) furthermore contained the highest proportion of upregulated genes, with one of them, GIP, actually showing one of the highest overall inductions.

The following discussion of the known functions of identified genes will emphasize large groups of genes and their interactions within the group and other identified stage specific genes. Thus, important signalling pathways, wich are emphasized or reduced after axotomy might be identified.

5.3.2 Important functions and interplay of identified genes

As it is not possible to discuss each of the 174 identified differentially expressed genes one by one, the intention here is to exploit the patterning approach and to verify, whether shared genes of stages (i) and (iii) are molecular indicators of a non-elogation mode, as this is the most obvious shared morphological feature of these two stages. On the other hand, it will be discussed, whether stage (ii) represents an elongation or regeneration mode.

Downregulation of GAPDH during axon stalling

The only gene, which was found to be differentially expressed at all three postlesional stages (i)-(iii), was glyceraldehyde-3-phosphate dehydrogenase (GAPDH). It is remarkable that this gene was downregulated at stages (i) and (iii), but upregulated at stage (ii), what parallels the observed morphological responses of non-axon-outgrowth at stages (i) and (iii), but axon-outgrowth at stage (ii). This individual expression pattern was suggestive for an overall "stop- go-stop"-pattern of identified genes at stages (i)-(iii).

GAPDH has long been recognized to exhibit only its well established glycolytic function in the cell and for the fundamentality of this reaction within all higher eukaryotes was considered to remain at a constant level within each cell. But recent data provide additional functions, which are ascribed to this gene. GAPDH was shown to be involved in apoptosis, neurodegenerative disease, cancer and viral pathogenesis (reviewed in Sirover, 1999). Like in this study, identification of GAPDH (coordinate on Clontech Atlas rat 1.2 Array, G27) in a non-glycolytic context always came as a surprise in studies describing its novel functions. Two biochemical properties and the involvement in apoptosis and neurodegenerative diseases appear to be especially remarkable within the context studied here and will now be discussed.

A membrane bound GAPDH isoform with membrane fusing (fusogenic) activity was discovered to have different biochemical properties from another isoform, which displayed classical dehydrogenase activity (Glaser and Gross, 1995). The membrane fusing activity was also reported for naturally occurring membranes (Han et al., 1998). The necessity for the regulation of membrane fusion events appears reasonable to be considered during axon outgrowth, but also within the intact axons. Therefore, downregulation of GAPDH at stages (i) and (iii), corresponding to a less then normal GAPDH fusogenic activity and upregulation at stage (ii), corresponding to an increased demand for fusogenic activity during axon outgrowth, were in good agreement with this new GAPDH activity.

Furthermore, different activities of GAPDH appeared to rely also on its oligomerization state. As a tetramer, GAPDH was shown to have specific tubulin polymerizing activity (Huitorel and Pantaloni, 1985), but also classical dehydrogenase activity (Durrieu et al., 1987). It is remarkable that ATP facilitated dissociation of the tetrameric GAPDH to the monomeric protein (Oguchi et al., 1973; Bartholmes and Jaenicke, 1978), as these properties in combination could provide a way for coupling cell growth (tubulin polymerization) and increased energy demand (glycolytic activity) by the universal energy metabolite ATP.

Therefore, coregulation of GAPDH and tubulin at stages (i) and (iii) were in agreement with their putative combined function. Downregulation of these components would result in less tubulin polymerizing activity, than in the intact fornix, possibly contributing to the observed stalling of axons at the lesion site at one day post lesion and outgrowth cessation at three weeks post lesion.

On the other hand, upregulation of GAPDH at stage (ii) could also have detrimental effects for the cell, like it was discovered for cerebral granular cells, which undergo apoptosis at approximately 17 days in vitro, with concomitant GAPDH upregulation (Sunaga et al., 1995; Ishitani and Chuang, 1996). Induction of apoptosis also lead to nuclear translocation of GAPDH (Sawa et al., 1997; Saunders et al., 1997). Therefore, a shift in the GAPDH expression and/or other cofactors could be involved in the regulation of opposing cell fates, like cell growth and apoptosis.

The specific interaction of GAPDH with neurodegenerative disease associated proteins, like β-amyloid precursor protein, huntingtin or ataxin (Schulze et al., 1993; Burke et al., 1996; Koshy et al., 1996) provides further evidence for the multiple roles of this protein and the significance of GAPDH regulation after axotomy. Again at least two identified genes could be associated with involvement of GAPDH in apoptosis and neurodegeneration. The proapoptotic gene BAD (C12h) (del Peso et al., 1997; Hsu et al., 1997) was markedly downregulated at stage (ii), while the gene huntingtin-associated 1B (C01i) (Li et al., 1995b; Block-Galarza et al., 1997) was found upregulated.

Huntingtin-associated 1B upregulation could have consequences for Huntington pathogenesis, because the two genes, GAPDH and Huntingtin associated 1B both display affinities for Huntingtin (Li et al., 1995b; Burke et al., 1996) and are coregulated upon axotomy. Furthermore, GAPDH induction is finteresting as it was identified to be associated with trans-plasma-membrane oxyreductases (PMO) isolated from bovine and rat brains together with TOAD64, also known as CRMP-2, aldolase C and enolase-γ (Bulliard et al., 1997). It is conspicious to find the PMO activity in a synaptic and recycling vesicle-derived tight protein

complex, which containd two proteins, which were also identified in this project, namely GAPDH and aldolase C. While GAPDH was downregulated at stages (i) and (iii), and upregulated at (ii), aldolase C was identified to be upregulated at stage (i) and (ii), but not at stage (iii). Furthermore, a molecule related to CRMP-2, CRMP-4, was studied in this thesis. While CRMP-2 was identified to be upregulated after sciatic nerve crush (Minturn et al., 1995), no induction of CRMP-4 transcript could be detected by in situ hybridization within the axotomized or unlesioned subiculum.

The functional implications of the protein complex of GAPDH, TOAD64, aldolase C and enolase-γ is still unknown, but a function of PMOs as a sensor for extracellular oxidative stress of the cell was suggested(Bulliard et al., 1997). Whether another dehydrogenase, aldehyde dehydrogenase 2 (C08f), which co-upregulates with the glycolitic enzyme aldolase C is also involved within the GAPDH containing or similar complexes, would be interesting to know. These initial findings associated with the altered GAPDH expression after axotomy, already illustrate the complex molecular networks and functions, which have to be considered.

As it was already pointed out, coregulated genes at stage (i) and (iii) were especially suspicious to be functionally related to the non-axon-outgrowth morphology at these stages. It was furthermore interesting to know, whether some of these genes were known to be involved in some of the new GAPDH functions, like vesicle dynamics, cytoskeletal changes, apoptosis or other functions.

Small GTPases and their signalling pathways

The gene RalA (E12n), which belongs to the Ras-branch of the Ras-superfamily (Reuther and Der, 2000), was identified to be downregulated at stages (i) and (iii), like GAPDH.

Activation of RalA depends either on Ras-dependent activation of its guanosine nucleotide exchange factors (GEF) (Wolthuis and Bos, 1999), RalGDS, Rgl and Rlf, or on calcium (Hofer et al., 1998; Wang and Roufogalis, 1999). The Ral-GEF, Ral GDSB (F01e) was found upregulated at stage (iii), contrasting to the RalA downregulation. Downregulation of RalA could be interpreted as decreasing its activity, while Ral-GEF upregulation could lead to enhanced RalA activation, by replacing GTP for GDP.

Activation of Ral-GEF by Ras or overexpression of the Ral-GEF, Rgr, lead to a reduction of neurite outgrowth in NGF stimulated PC12 cells and a delay of cell cycle arrest (Goi et al., 1999). Furthermore, Ral-GEFs were shown to activate the c-fos promotor (Okazaki et al., 1997; Murai et al., 1997). Another function of RalA could be the regulation of endocytosis

(Nakashima et al., 1999). Functional involvement in vesicle turnover was supported by the identification of the GTPases Rab 15 (E14j), Rab 14 (E14k), Rab 16 (E14l), which were downregulated at stage (i), while Rab-specific GDP dissociation inhibitors Rab GDI β (C01n) and Rab GDI α (C02a) were identified to be upregulated. Rab proteins are implicated in targeted vesicle transport (Schimmoller et al., 1998; Chavrier and Goud, 1999), with multiple members of the family being arrayed at distict domains within the cell (Simons and Zerial, 1993). Their GTPase activity is believed to be induced at their target membranes (Lupashin and Waters, 1997; Cao and Barlowe, 2000).

Therefore, downregulation of Rabs and upregulation of Rab GDIs cooperate in suppressing Rab activity, possibly reducing vesicle fusion events in the cells at stage (i). Again, this is in agreement with the observed non-axon-outgrowth mode, and could explain why axons appeared to have retracted at five days post lesion.

Participation of this class of proteins in retraction is supported by the similar pattern seen at stage (iii). As it was already mentioned, regulation of RalA and Ral GDSB appear to be contradictory. Downregulation of another ARF-like GTPase (E13n) at stage (i) and (iii), but also induction of a GTPase activating protein p120 GAP (A13a) and Rin 1 (F01g) could explain different morphological outcomes of stages (i) and (iii). The Ras-related Rin was found to be exclusively expressed in neurons and is known to display calmodulin binding (Lee et al., 1996).

Although the interactions and functions of the small GTPases cannot readily be explained, they are remarkable. Previous work on the involvement of small GTPases has almost exclusively focused on the function of Rho, Rac, Cdc42 and their remodelling activity on the cytoskeleton (Hall, 1998; Mackay et al., 1995). Unfortunately, these genes could not be studied here, as they were not represented on the cDNA arrays. But identification of genes of trimeric G proteins and G protein coupled receptors (GPCRs), prostaglandin receptor, focal adhesion kinase (FAK), c-Jun N-terminal kinases (JNKs) could provide indirect evidence for the important role of these small GTPases also within this in vivo lesion paradigm.

The small GTPases Cdc42 and Rac1 were shown to induce filopodia and subsequently lamellipodia in fibroblasts, but also if injected into neuroblastoma cells (Nobes and Hall, 1995; Kozma et al., 1997), while lysophosphatidic acid (LPA)-activated RhoA produced neurite retraction or growth cone collapse (Kozma et al., 1997; Tigyi et al., 1996; Jalink et al., 1994). This activation of RhoA was shown to involve tyrosine phosphorylation (Kozma et al., 1997; Kranenburg et al., 1999; Katoh et al., 1998b) and could be blocked by the *Clostridium*

botulinum exoenzyme C3, which ADP-ribosylates RhoA, thereby blocking LPA induced collapse (Jalink et al., 1994).

GAP-43 and trimeric G proteins

GAP-43 is recognized to be an intrinsic indicator for increased axonal regeneration (Caroni, 1997), because it was found to be upregulated upon axotomy in regenerating nerve cells, like zebrafish RGCs (Bormann et al., 1998) or in the rat RGCs, if they were provided with a stimulating peripheral nerve graft (Schaden et al., 1994). Nevertheless, a strict correlation of axotomy induced GAP-43 upregulation could not be found, as different lesion paradigms produced different transcriptional responses of GAP-43 and other cytoskeletal genes (Bisby and Tetzlaff, 1992).

This became especially apparent in lesion paradigms of dorsal root ganglia, which induced GAP-43 levels upon lesion of their peripheral branch, but not (or only diminished) if they were axotomized in their (most proximal) central branch (Chong et al., 1994). Lesion of the entorhinal cortex of adult rats, which constitutively expresses GAP-43, lead to even more subtle changes including an increase in axonal transport to the sprouting contralateral hemisphere without an overall induction of GAP-43 (Lin et al., 1992). These data could provide an explanation for the lack of GAP-43 induction after distal axotomy of subicular neurons that was found in this study. This parallels the apparently constant moderate expression of L1 after fornix transection, which was also reported in this thesis. A moderate steady state expression of L1 was also found in sensory and motor neurons after sciatic nerve transection (Zhang et al., 2000).

Evidence for the involvement of heterotrimeric G proteins and their receptors in this collapse response has also been provided. Especially Go and Gi were isolated from growth cone membranes (Edmonds et al., 1990). Amplification of Go activation by unpalmitoylated GAP-43 peptides increased the growth cone collapse that would be induced by myelin, brain membranes or serotonin. However, growth cone collapse was blocked if cystein residues in the peptides were exchanged especially for tyrosine and methionine (Igarashi et al., 1995).

Again it is remarkable to find trimeric Gi and Go protein components downregulated at stage (i) in concert with a downregulated serotonin receptor (5HT5A, D05m), which could render growth cones less responsive to inhibitory molecules, such as serotonin. On the other hand, two serotonin receptors were upregulated at stage (ii) (5HT3, B03b and 5HT2, D04f), possibly leading to an increased sensitization of neurons towards inhibitory cues during axonal outgrowth.

With respect to Gi proteins it could be demonstrated that inactivation by ADP-ribosylation of their alpha subunit and concomitant trapping in the GDP-bound state protects growth cones from collapse (Igarashi et al., 1993), supporting the notion that downregulation of the Giα component (E13m) at stage (i) and (iii) renders growth cones less sensitive towards repulsive molecules. This is further supported by data showing that constitutively active Gα12, Gα13 and Gαq, but not Gαi2 subunits lead to neurite retraction via a RhoA dependent pathway (Katoh et al., 1998b; Kranenburg et al., 1999). This neurite inhibitory action of trimeric G proteins could also be associated with a reduced exocytosis rate, which was found after Go activation in chromaffin cells (Gasman et al., 1998).

Most of these neurite retraction responses were shown to be mediated by RhoA, which was also shown to mediate ephrin-A5-associated inhibitory activity (Wahl et al., 2000). But neurite outgrowth inhibition does not necessarily depend solely on RhoA activation. The collapsin-1/SemaphorinIII induced collapse of chicken dorsal root ganglia (DRG), was found to depend on Rac1 (Jin and Strittmatter, 1997). But interestingly, C3 transferase again augmented neurite outgrowth on both myelin and collapsin-1, suggesting Rac1-dependent activation of RhoA.

The importance of the results shown in this thesis could additionally be supported by the identification of the downregulation of the prostaglandin F2 receptor (E06m). Expression of the prostaglandin E receptor EP3B in PC12 cells was shown to lead to neurite retraction (Katoh et al., 1996) via RhoA-dependent activation of p160 RhoA-binding kinase ROKα (Katoh et al., 1998a). It is likely that downregulation of the prostaglandin receptor also contributes to a decrease in neurite retraction, in addition to the regulation patterns of the trimeric G protein genes at stage (i).

Signalling and cytoskeletal proteins

Putative implication of Rho dependent pathways could also be supported by the downregulation of focal adhesion kinase (FAK, E08m), which is known to be RhoA dependently phosphorylated upon LPA stimulation in neuroblastoma cells (Linseman et al., 2000). Immediate interaction of FAK and Rho is likely to happen within vinculin-enriched point contacts, which can be found all over on rat DRG growth cone membrane surfaces, as these proteins were found to colocalize at these cell-extracellular matrix contacts (Renaudin et al., 1999). Activation of FAK by phosphorylation leads to recruitment of Src family tyrosine kinases (Schlaepfer and Hunter, 1998; Lacoste et al., 1998; Girault et al., 1999), suggesting that FAK may act as an adaptor protein. Increased tyrosine phosphorylation of FAK and

paxillin was also found during neuronal differentiation, as cell spreading and neurite outgrowth was initiated (Leventhal and Feldman, 1996). Predepolarization of cerebellar granule cells with high potassium chloride in the absence of extracellular calcium followed by calcium influx through L-type voltage-dependent calcium channels lead to increased tyrosine phosphorylation of FAK like in early stages of development (Evans and Pocock, 1999).

Downregulation of FAK at stages (i) and (iii) could, therefore, be correlated with stages of neuronal development where no neurite outgrowth can be seen, while an increased expression of the L-type calcium channel, CACNA1 (B05g), at stage (ii) could participate in increased tyrosine phosphorylation of FAK.

Changes in the neuronal axon elongation propensity were found to be reflected in the regulation of cytoskeletal genes after axotomy. The transcription of the actin depolymerizing protein cofilin (F13n) was identified to be downregulated, again at the two non-axon-outgrowth stages (i) and (iii).

Cofilins actin depolymerizing activity is reduced by phosphorylation (Arber et al., 1998) upon LPA stimulation of neuroblastoma cells. LPA induced growth cone collapse was already mentioned to activate RhoA, and indeed it could be demonstrated that activated RhoA stimulates Rho-associated kinase (ROCK), which phosphorylates and activates LIM kinase. LIM kinase then inactivates cofilin by phosphorylation (Maekawa et al., 1999), suggesting that activated, unphosphorylated cofilin should enhance neurite outgrowth. This was demonstrated by an increased neurite length of primary rat neurons, which were transfected with a *Xenopus* ADF/cofilin mutant, which could not be phosphorylated (Meberg and Bamburg, 2000). But it needs to be noted that this mutant increased the neurite length to a lesser extent than the wild type *Xenopus* ADF/cofilin, which was present as a partially phosphorylated pool. Apart from an outgrowth inhibiting increase in RhoA-dependent phosphorylation of cofilin, outgrowth stimulating dephosphorylation could be identified in PC12 cells (Meberg et al., 1998). Stimulation by increased calcium or cAMP were shown to dephosphorylate cofilin via activation of phosphatase 2B (PP2B) and PP1, respectively. After fornix axotomy, the two genes encoding for subunits of the abundant phosphatase 2A (E12l and E11m) were identified to be downregulated at stages (i) and (iii) again supporting the overall outcome of reduced neurite extension.

The effect of cofilin on cytoskeletal reorganization could be supported by the change of cytoskeletal gene expression itself. Both tubulin-α1 and cytoplasmic β-actin were identified to be downregulated at stages (i) and (iii). While gene expression of cytoskeletal proteins actin and tubulin were generally found to be upregulated after peripheral nerve injury (Bisby

and Tetzlaff, 1992), central neurons displayed a differnt pattern of gene expression. If not provided with a regeneration permissive peripheral nerve graft, transcripts of different tubulin isotypes were downregulated after axotomy of the optic nerve in adult rats (Fournier et al., 1997), whereas only an initial transient increase in tubulin mRNA levels was seen without treatment (McKerracher et al., 1993a). Mouse transcallosal cortical neurons were comparably refractory to axotomy induced tubulin expression, even if the lesion was very close to the cell body (Elliott et al., 1999). This is in contrast to proximal axotomy and a consecutive appropriate cell body response with induction of regeneration associated genes, like tubulin and GAP-43 in regenerating rubrospinal neurons (Fernandes et al., 1999). Interestingly, corticospinal neurons displayed a downregulation of tubulin-Mα1 in layer V neurons of the sensorimotor cortex two days after lateral spinal cord hemilesion, resembling the expression pattern identified after fornix transection (Mikucki and Oblinger, 1991). This is important to note, as many therapeutic interventions aim at restoring spinal cord lesions. It would be interesting to know, whether similar tubulin expression patterns observed after spinal cord injury and after postcommissural fornix transection are the only identical gene expression characteristics of these CNS axotomy paradigms or whether the subicular response that was found here could also serve as a model for axotomized cortical neurons.

Guidance and second messengers

In addition to the elongation or retraction of axons, which might be reflected within the above mentioned gene regulations, correct guidance of the axons has to be assured. The guidance molecule deleted in colorectal cancer (DCC, A11g), which is involved in mediating the attractive response towards netrin-1 (Stein et al., 2001), was identified to be upregulated at stages (i) and (ii). As the fornix tract elongated within its former pathway, this could be indicative for a guided outgrowth up to the lesion site.

In situ hybridization and immunohistochemical studies have shown that the DCC gene is expressed within the rat hippocampus (Volenec et al., 1997) and increased in specific axon populations, also in those originating in the hippocampus during developmental outgrowth phases in the mouse (Shu et al., 2000). Upregulation after fornix transection contrasts to the lesion induced-response within rat RGCs, which downregulated DCC and other netrin-1 receptors by two days after lesion to the optic nerve, regardless whether regeneration was supported by a peripheral nerve graft or not (Ellezam et al., 2001; Petrausch et al., 2000).

But also other genes which were identified after postcommissural fornix transection might be involved in directed outgrowth of axons. The matrix metalloprotease MT3-MMP (MMP-16,

F08i) was found to be upregulated at stage (ii). Metalloproteases may serve multiple functions within the CNS but the collagen and gelatin degradation potential of MT3-MMP (Yong et al., 1998) is especially interesting, as collagen IV was shown to be expressed in a basement membrane at the fornix lesion site (Stichel et al., 1999b). Furthermore, a related molecule, MMP-2 was demonstrated to degrade neurite inhibiting chondroitinsulphate proteoglycans (CSPGs) thus increasing neurite outgrowth of DRG neurons in vitro on MMP-2 pretreated peripheral nerves (Zuo et al., 1998). Data from genetic experiments in Drosophila provided further evidence for the requirement of metalloproteases for correct axon pathfinding, as mutations in the kuz gene, which encodes a disintegrin metalloprotease lead to severe pathfinding defects (Fambrough et al., 1996). The disintegrin rMDC15, which was studied by in situ hybridization did not show any axotomy induced changes in its expression level. It was constitutively expressed at moderate levels in the subiculum.

An additional group of genes deserves some attention. It was mentioned in the introduction that calcium transients and calcium levels within growth cones are critical for axon guidance. Therefore, the finding that it calcium binding proteins are differentially expressed at stages (i) and (ii) is very interesting. While the EF-hand calcium binding proteins neuronal calcium sensor 1 (NCS-1, F03m), neural visinin-like calcium binding protein (NVP, F03j) and calbindin d28 (F03n) were downregulated at stage (i), the neural visinin-like calcium binding protein 3 (NVP-3, F04b) was identified to be induced at stage (ii). A decreased calcium buffering capacity at stage (i) and, on the other hand, an increased buffering capacity at stage (ii) could have important functional implications for neurite outgrowth. This is supported by the distribution of the myristoylated protein NVP-3, which was reported to bind to the membrane in a calcium dependent way and was found to be localized to dendrites and nerve terminals (Hamashima et al., 2001).

Another second messenger, cAMP, was mentioned in the introduction to modulate the growth cone response towards attractive or repulsive cues. It is generally assumed that an increased cAMP level promotes axonal elongation, therefore, it was very interesting to find the gastric inhibitory polypeptide (GIP, E06e) upregulated at stage (ii).

Stimulation of the G protein coupled GIP receptor induces cAMP production and intracellular calcium accumulation (Usdin et al., 1993). The significance of this discovery is supported by the expression data collected in this thesis, as it could be shown that GIP was expressed by subicular neurons. Additional reports on the presence of high affinity binding sites for the peptide within the subiculum (Kaplan and Vigna, 1994) and the distribution of the G protein coupled receptor within the hippocampus (Usdin et al., 1993), suggest a possible autocrine or

paracrine stimulation of subicular neurons. This stimulation might be a prerequisite for the observed axonal elongation at stage (ii).

Another important effect of GIP in cooperation with insulin is the potentiated incorporation of fatty acids into triglycerids (Beck, 1989; Yip and Wolfe, 2000) as the increased membrane growth during elongation of the axons demands more lipids. This increased requirement for fatty acids was further supported by the upregulation of genes encoding the fatty acid transport protein (B11n), fatty acid binding protein (H-FABP, B14e) and possibly 11-β-hydroxysteroid dehydrogenase 2 (C10g).

In conclusion, the gene expression patterns identified in this thesis reveal molecular components, which could be associated with vesicle transport, cytoskeletal changes and other fundamental reorganization of the cellular physiology and are, therefore, likely to contribute to changes in the observed axon outgrowth states.

The interpretation was generally not only based on one gene, but a set of genes, which could determine the respective cell morphological outcome. This is important to note for another reason. Intrinsic regeneration potentials of neurons were previously derived from the expression profile of very few genes, such as GAP-43 and c-Jun. The results presented here are based on the substantial set of 1185 annotated genes, which correspond to 1-5% of the anticipated number of all genes in the rat genome. Therefore, the identified 174 differentially expressed genes likely do not represent all responsive genes. A rough calculation of the total number of regulated genes following fornix axotomy, would result in approximately 2,000-10,000 responsive genes.

Therefore, identification of key regulatory events and mechanisms will be of primary interest in future. In the next chapter, possible upstream regulatory events will be discussed, based on the data generated in this study.

5.3.3 Perspectives on possible upstream signalling events

As it was mentioned before, the observed transcriptional changes following transection of the postcommissural fornix are initiated by the axotomy, which was about 8 mm distal to the neuronal somata. Therefore, the signalling pathways, which initiate these changes have to act retrogradely along the unsevered proximal axon stump up to the neuronal perikarya in the subiculum. At present the molecular nature of these signals, how fast and how they act on the neuron is not clear. But it is likely that transcription factors and axonal constituents have to interact in one or the other way.

The JAK/STAT signalling pathway could be a candidate for such a retrograde response. After facial nerve axotomy, several JAK and STAT genes were induced, while only STAT3 protein levels were found to have increased specifically in this regeneration competent PNS lesion model (Schwaiger et al., 2000). Increased tyrosine phosphorylation and nuclear translocation of STAT3 transcription factor was detected as early as three hours after axotomy, representing a very early response. The transcriptional response induced by STAT3 was associated with the induction of genes, which could be necessary for an immunological response in the area of the lesioned neurons. But no direct link to an enhanced regeneration competence was demonstrated. On the other hand, two signalling pathways, which are known to directly affect axonal outgrowth and plastic responses in the developing and adult brain could be involved in the lesion model of the transected postcommissural fornix.

The Wnt signalling pathway is involved in cell differentiation and cell fate determination during development. The high number of 24 members of this family and a likewise large number of more than ten cognate receptors in mammals make it quite difficult to dissect the individual functions (Patapoutian and Reichardt, 2000; Boutros et al., 1998). But recently the Wnt-7a molecule was shown to mimick the axon modulatory activity of cerebellar granule cell conditioned medium, which was associated with an increased axon diameter and axonal branching (Burden, 2000), but also with a contact dependent stop of mossy fiber axons on cerebellar granule cells (Baird et al., 1992; Zhang and Mason, 1998). Furthermore, the former activities could be blocked with a soluble, dominant interfering form of Frizzled (Fz) (Hall et al., 2000).

The Wnt signalling pathway is not yet completely understood, but appears to have at least two branches, the Wingless (Wg), via β-catenin and the planar polarity pathway via JNK (Boutros et al., 1998). Both pathways employ Fz receptors and Dishevelled (Dsh), but only the former is known to be associated with ligands of the Wg-family. The classical wingless pathway via

the G protein coupled Fz receptor, calcium changes and protein kinase C (Peifer, 1999) leads to reduced phosphorylation of β-catenin upon binding of Wg/Wnt ligands. This leads to translocation of β-catenin into the nucleus and subsequent initiation of transcription in cooperation with the HMG-box protein TCF (reviewed in Seidensticker and Behrens, 2000).
Binding of Wnt ligands leads to an activation of Dsh and subsequent reduced phosphorylation activity of GSK3β. But without Wnt stimulation, β-catenin is constitutively phosphorylated by GSK3β within a complex that contains Dsh, the scaffolding protein axin, the protooncogene APC and protein phosphatase 2A (PP2A) (Seidensticker and Behrens, 2000). The substrate of the latter in this complex is still not known, but evidence for dephosphorylation of GSK3β from in vitro data exist, which would lead to an activated GSK3β and subsequent reduced levels of β-catenin (Virshup, 2000). Other reports described axin as a substrate for PP2A, which could have a reduced affinity for β-catenin in its dephosphorylated form, leading to an increase in β-catenin levels (Willert et al., 1999). It is important to note, that sequestering of β-catenin to the transmembrane cadherin proteins was sufficient to reduce Wnt associated signalling (Fagotto et al., 1996; Simcha et al., 1998; Sadot et al., 1998), implicating that increased cadherin dependent cell-cell contact formation could regulate the Wnt pathway.
Several identified genes at stage (i) but also (ii) and (iii) could be indicative for the involvement of the Wnt pathway. The measured downregulation of JNK1/2 at stage (i) could reduce the activity of the planar polarity pathway and reduction of proteasome components may contribute to an increased β-catenin level, with subsequent enhanced β-catenin dependent transcriptional activity.
The downregulation of PP2A at stage (i) and (iii) cannot be interpreted due to the contradictory information present in the literature. But downregulation of PP2A might also have antiapoptotic effects, as dephoshorylation of Bcl-2 by PP2A enhances cell death (Deng et al., 1998). Interestingly, increased levels of β-catenin were shown to elevate p53 levels, thus also protecting against apoptosis (Damalas et al., 1999). In conclusion this would correspond to a hypothetical selective activation of the antiapoptotic Wnt/Wg pathway, including the activation of the putative Wnt dependent "stop"-signal, while the planar polarity pathway activity might be reduced at stages (i) and (iii). The likeliness of an involvement of Wnt-signalling in subicular neurons is suggested, as the absence of Wnt-3a perturbed proper hippocampal formation, including a reduction of the rostral subiculum during development (Lee et al., 2000c).

Wnt targets are often transcription factors whose target genes are not well known (Nusse, 1999). Two chick homologues of the gene CDP/Cux/Cut (A05n), which was found to be upregulated at stage (ii), were associated with apical ectodermal ridge (AER) positioning during limb development (Tavares et al., 2000). Likewise, the Drosophila homologue Cut is induced by nuclear Notch (Micchelli et al., 1997; Neumann and Cohen, 1996) and promotes the expression of wingless (wg), while inhibiting serrate and delta expression in the wing margin (de Celis and Bray, 1997; Neumann and Cohen, 1996).

The chick homologue cux1 was found to be induced around ridge-like ectodermal structures, which were induced upon ectopic expression of active β-catenin (Tavares et al., 2000). Therefore, cux1 expression was assumed to be induced by factors produced by active β-catenin expressing cells in the ridges. Thus the expression of the transcription factor CDP/Cux/Cut is indicative for the involvement of Notch and Wnt signalling pathways after fornix axotomy.

This is further supported, as a CCAAT box binding factor NF-Y/CBF, similar to the Notch target CBF1, was found to induce the human thymidine promotor in serum stimulated cells, while CDP/Cut was shown to bind the promotor primarily in quiescent cells, thereby inhibiting transcriptional activity (Kim et al., 1997). This interplay of the Notch and Wnt pathways is supported by the identification of a novel member of the β-catenin/Armadillo family, which interacts with presenelin 1 (PS1) (Zhou et al., 1997), which is also known to be necessary for Notch signalling (Selkoe, 2000). It could recently be shown that Alzeimer disease (AD) associated mutated PS1 inhibits Wnt-3-dependent accumulation of β-catenin, supporting the importance of the Wnt pathway for AD, which was postulated to depend largely on a loss of Wnt signalling (De Ferrari and Inestrosa, 2000).

But also the Notch pathway alone could be associated with modulating neurite outgrowth in several ways. Mouse cerebral cortex neurons displayed a density dependent activation of Notch. Low density cultures had a low level of Notch activity, while high density cultures, with dense neuritic networks showed a high level of Notch activity. Nuclear Notch localization could be associated with neurite outgrowth cessation and even neurite retraction (Sestan et al., 1999). In the latter model, stimulation with the Notch activating ligands Delta1 and Jagged1 had an effect dimilar to high density cultures, while the intracellular modulators of Notch signalling Numb (Nmb), Numb-like (Nbl) and Deltex (Dx) could rescue the neurite outgrowth inhibition or retraction in high density cultures or after Notch pathway activation by Notch1/2 intracellular domains. Very similar observations were made on hippocampal neurons, which displayed reduced neurite outgrowth and retraction upon Notch1 or Notch

intracellular domain (ICD) transfection, which could also be rescued by Nmb cotransfection (Berezovska et al., 1999). An additional effect was observed in N2a neuroblastoma cells, which also produced shorter neurites upon Notch ICD expression or trans activation by contact of quail cells expressing Delta1. This phenotype could be rescued by expression of dominant-negative Notch1 or dominant-negative Delta1 in N2a cells. Remarkably, Delta1 overexpression alone in N2a cells could enhance neurite extension, suggesting a modulatory activity of cis expressed Notch ligands on Notch activation (Franklin et al., 1999). Similar effects on dendrites in the developing cortex were suggested, as activation and nuclear translocation of Notch1 inhibited dendritic growth, but promoted dendritic branching (Redmond et al., 2000).

This second wave of Notch activity during later embryonic stages contrasts to early cell determination events, where Notch-ligand expressing cells adopt the neuronal phenotype, while Notch expressing cells switch to the glial phenotype (Gaiano et al., 2000; Morrison et al., 2000).

Notch activation by trans binding of one of its ligands of the Delta/Serrate/Lag-2 (DSL) family leads to PS1-dependent intracellular release of Notch ICD, which translocates to the nucleus and very likely associates with members of DNA-binding proteins of the CSL (CBF1/Su(H)/Lag-1) family to induce transcription of E(spl)/HES (Enhancer of split/Hairy and E(spl)) genes (Weinmaster, 2000). Hes genes are basic helix-loop-helix (bHLH) factors, which could in combination with members of the groucho-family negatively regulate the activity of the bHLH proteins of the achaete/scute complex and of daughterless, which induce cell differentiation (Campuzano and Modolell, 1992). Furthermore, the activity of this group of genes is counteracted by helix-loop-helix proteins of the Id family, which act as dominant negative heterodimeric binding partners (Benezra, r 90 cell).

Therefore, upregulation of Id1 (A06g) at stage (i), but not Id2 or Id3, which were also represented on the arrays, is important to be noted. These Id genes are generally conceived to be inhibitors of differentiation, adding a second differentiation inhibiting transcription factor to the list of identified genes, as CDP/Cux/Cut could also represent such a negative regulator.

Id genes were shown to be induced by TNFα application to developing postnatal rats (Tzeng et al., 1999), suggesting involvement of the TNF-pathway in response to fornix axotomy.

In addition, the bone morphogenetic proteins (BMPs) could be involved in the initial response, as BMP2/4 increased the expression level of Jun-B in mouse embryonic stem cells (Hollnagel et al., 1999). Jun-B (A05e) was found to be repressed at stage (i). Interestingly, Id genes, such as Id3, Id1 and Id2, were also found to be responsive to BMPs in the screen for

BMP target genes (Hollnagel et al., 1999). Moreover, Id1, Id2, Id3 and Id4 were recognized to be rapidly degraded by the ubiquitin-proteasome pathway, if they were not complexed with a bHLH protein (Bounpheng et al., 1999).

Future experiments will help to understand, whether the proposed pathways are indeed involved in response to axotomy.

6. LITERATURE

Ahlijanian MK, Barrezueta NX, Williams RD, Jakowski A, Kowsz KP, McCarthy S, Coskran T, Carlo A, Seymour PA, Burkhardt JE, Nelson RB, McNeish JD (2000) Hyperphosphorylated tau and neurofilament and cytoskeletal disruptions in mice overexpressing human p25, an activator of cdk5. Proc Natl Acad Sci U S A 97:2910-2915.

Alexander KA, Cimler BM, Meier KE, Storm DR (1987) Regulation of calmodulin binding to P-57. A neurospecific calmodulin binding protein. J Biol Chem 262:6108-6113.

Allen GV, Hopkins DA (1989) Mamillary body in the rat: topography and synaptology of projections from the subicular complex, prefrontal cortex, and midbrain tegmentum. J Comp Neurol 286:311-336.

Alon U, Barkai N, Notterman DA, Gish K, Ybarra S, Mack D, Levine AJ (1999) Broad patterns of gene expression revealed by clustering analysis of tumor and normal colon tissues probed by oligonucleotide arrays. Proc Natl Acad Sci U S A 96:6745-6750.

Alvarez de la Rosa D, Zhang P, Naray-Fejes-Toth A, Fejes-Toth G, Canessa CM (1999) The serum and glucocorticoid kinase sgk increases the abundance of epithelial sodium channels in the plasma membrane of Xenopus oocytes. J Biol Chem 274:37834-37839.

Amaral DG, Witter MP (1995) Ch. 21 - Hippocampal Formation. In: The Rat Nervous System, 2nd Edition (Paxinos G, ed). San Diego, New York, Boston ...: Academic Press.

Amaratunga A, Fine RE (1995) Generation of amyloidogenic C-terminal fragments during rapid axonal transport in vivo of beta-amyloid precursor protein in the optic nerve. J Biol Chem 270:17268-17272.

Arber S, Barbayannis FA, Hanser H, Schneider C, Stanyon CA, Bernard O, Caroni P (1998) Regulation of actin dynamics through phosphorylation of cofilin by LIM-kinase. Nature 393:805-809.

Aubert I, Ridet JL, Schachner M, Rougon G, Gage FH (1998) Expression of L1 and PSA during sprouting and regeneration in the adult hippocampal formation. J Comp Neurol 399:1-19.

Bagnard D, Lohrum M, Uziel D, Puschel AW, Bolz J (1998) Semaphorins act as attractive and repulsive guidance signals during the development of cortical projections. Development 125:5043-5053.

Bagnard D, Thomasset N, Lohrum M, Puschel AW, Bolz J (2000) Spatial distributions of guidance molecules regulate chemorepulsion and chemoattraction of growth cones. J Neurosci 20:1030-1035.

Baird DH, Hatten ME, Mason CA (1992) Cerebellar target neurons provide a stop signal for afferent neurite extension in vitro. J Neurosci 12:619-634.

Bandtlow CE, Loschinger J (1997) Developmental changes in neuronal responsiveness to the CNS myelin-associated neurite growth inhibitor NI-35/250. Eur J Neurosci 9:2743-2752.

Bartholmes P, Jaenicke R (1978) Reassociation and reactivation of yeast glyceraldehyde-3-phosphate dehydrogenase after dissociation in the presence of ATP. Eur J Biochem 87:563-567.

Beck B (1989) Gastric inhibitory polypeptide: a gut hormone with anabolic functions. J Mol Endocrinol 2:169-174.

Becker T, Wullimann MF, Becker CG, Bernhardt RR, Schachner M (1997) Axonal regrowth after spinal cord transection in adult zebrafish. J Comp Neurol 377:577-595.

Becker T, Bernhardt RR, Reinhard E, Wullimann MF, Tongiorgi E, Schachner M (1998) Readiness of zebrafish brain neurons to regenerate a spinal axon correlates with differential expression of specific cell recognition molecules. J-Neurosci 18:5789-5803.

Behar O, Mizuno K, Neumann S, Woolf CJ (2000) Putting the spinal cord together again. Neuron 26:291-293.

Benfey M, Aguayo AJ (1982) Extensive elongation of axons from rat brain into peripheral nerve grafts. Nature 296:150-152.

Benowitz LI, Routtenberg A (1997) GAP-43: an intrinsic determinant of neuronal development and plasticity. Trends-Neurosci 20:84-91.

Benowitz LI, Apostolides PJ, Perrone-Bizzozero N, Finklestein SP, Zwiers H (1988) Anatomical distribution of the growth-associated protein GAP-43/B-50 in the adult rat brain. The Journal of Neuroscience 8:339-352.

Berezovska O, McLean P, Knowles R, Frosh M, Lu FM, Lux SE, Hyman BT (1999) Notch1 inhibits neurite outgrowth in postmitotic primary neurons. Neuroscience 93:433-439.

Berridge MJ (1998) Neuronal calcium signaling. Neuron 21:13-26.

Berridge MJ, Lipp P, Bootman MD (2000) The versatility and universality of calcium signalling. Nat Rev Mol Cell Biol 1:11-21.

Bisby MA, Tetzlaff W (1992) Changes in cytoskeletal protein synthesis following axon injury and during axon regeneration. Mol-Neurobiol 6:107-123.

Björklund A, Hökfelt T, eds (1987) Handbook of chemical neuroanatomy. Amsterdam, New York Oxford: Elsevier.

Block-Galarza J, Chase KO, Sapp E, Vaughn KT, Vallee RB, DiFiglia M, Aronin N (1997) Fast transport and retrograde movement of huntingtin and HAP 1 in axons. Neuroreport 8:2247-2251.

Borgens RB, Blight AR, McGinnis ME (1987) Behavioral recovery induced by applied electric fields after spinal cord hemisection in guinea pig. Science 238:366-369.

Borgens RB, Toombs JP, Breur G, Widmer WR, Waters D, Harbath AM, March P, Adams LG (1999) An imposed oscillating electrical field improves the recovery of function in neurologically complete paraplegic dogs. J Neurotrauma 16:639-657.

Bormann P, Zumsteg VM, Roth LW, Reinhard E (1998) Target contact regulates GAP-43 and alpha-tubulin mRNA levels in regenerating retinal ganglion cells. J Neurosci Res 52:405-419.

Bosse F, Petzold G, Greiner Petter R, Pippirs U, Gillen C, Muller HW (2000) Cellular localization of the disintegrin CRII-7/rMDC15 mRNA in rat PNS and CNS and regulated expression in postnatal development and after nerve injury. Glia 32:313-327.

Bounpheng MA, Dimas JJ, Dodds SG, Christy BA (1999) Degradation of Id proteins by the ubiquitin-proteasome pathway. Faseb J 13:2257-2264.

Boutros M, Paricio N, Strutt DI, Mlodzik M (1998) Dishevelled activates JNK and discriminates between JNK pathways in planar polarity and wingless signaling. Cell 94:109-118.

Brown MC, Perry VH, Lunn ER, Gordon S, Heumann R (1991) Macrophage dependence of peripheral sensory nerve regeneration: possible involvement of nerve growth factor. Neuron 6:359-370.

Bruckner K, Pablo Labrador J, Scheiffele P, Herb A, Seeburg PH, Klein R (1999) EphrinB ligands recruit GRIP family PDZ adaptor proteins into raft membrane microdomains. Neuron 22:511-524.

Brummendorf T, Kenwrick S, Rathjen FG (1998) Neural cell recognition molecule L1: from cell biology to human hereditary brain malformations. Curr-Opin-Neurobiol 8:87-97.

Brustle O, McKay RD (1996) Neuronal progenitors as tools for cell replacement in the nervous system. Curr Opin Neurobiol 6:688-695.

Bulliard C, Zurbriggen R, Tornare J, Faty M, Dastoor Z, Dreyer JL (1997) Purification of a dichlorophenol-indophenol oxidoreductase from rat and bovine synaptic membranes: tight complex association of a glyceraldehyde-3-phosphate dehydrogenase isoform, TOAD64, enolase-gamma and aldolase C. Biochem J 324:555-563.

Burden Gulley SM, Pendergast M, Lemmon V (1997) The role of cell adhesion molecule L1 in axonal extension, growth cone motility, and signal transduction. Cell-Tissue-Res 290:415-422.

Burden SJ (2000) Wnts as retrograde signals for axon and growth cone differentiation [comment]. Cell 100:495-497.

Burke JR, Enghild JJ, Martin ME, Jou YS, Myers RM, Roses AD, Vance JM, Strittmatter WJ (1996) Huntingtin and DRPLA proteins selectively interact with the enzyme GAPDH. Nat Med 2:347-350.

Buse P, Tran SH, Luther E, Phu PT, Aponte GW, Firestone GL (1999) Cell cycle and hormonal control of nuclear-cytoplasmic localization of the serum- and glucocorticoid-inducible protein kinase, Sgk, in mammary tumor cells. A novel convergence point of anti-proliferative and proliferative cell signaling pathways. J Biol Chem 274:7253-7263.

Campenot RB (1994) NGF and the local control of nerve terminal growth. J Neurobiol 25:599-611.

Campuzano S, Modolell J (1992) Patterning of the Drosophila nervous system: the achaete-scute gene complex. Trends Genet 8:202-208.

Canteras NS, Swanson LW (1992) Projections of the ventral subiculum to the amygdala, septum, and hypothalamus: a PHAL anterograde tract-tracing study in the rat. J Comp Neurol 324:180-194.

Cao X, Barlowe C (2000) Asymmetric requirements for a Rab GTPase and SNARE proteins in fusion of COPII vesicles with acceptor membranes. J Cell Biol 149:55-66.

Carboni L, Carletti R, Tacconi S, Corti C, Ferraguti F (1998) Differential expression of SAPK isoforms in the rat brain. An in situ hybridisation study in the adult rat brain and during post-natal development. Brain Res Mol Brain Res 60:57-68.

Caroni P (1997) Intrinsic neuronal determinants that promote axonal sprouting and elongation. BioEssays 19:767-775.

Caroni P, Schwab ME (1989) Codistribution of neurite growth inhibitors and oligodendrocytes in rat CNS: appearance follows nerve fiber growth and precedes myelination. Dev Biol 136:287-295.

Carulli JP, Artinger M, Swain PM, Root CD, Chee L, Tulig C, Guerin J, Osborne M, Stein G, Lian J, Lomedico PT (1998) High throughput analysis of differential gene expression. J Cell Biochem Suppl 31:286-296.

Chang L, Karin M (2001) Mammalian MAP kinase signalling cascades. Nature 410:37-40.

Chapman ER, Au D, Alexander KA, Nicolson TA, Storm DR (1991) Characterization of the calmodulin binding domain of neuromodulin. Functional significance of serine 41 and phenylalanine 42. J Biol Chem 266:207-213.

Chavrier P, Goud B (1999) The role of ARF and Rab GTPases in membrane transport. Curr Opin Cell Biol 11:466-475.

Chen A, Xu XM, Kleitman N, Bunge MB (1996) Methylprednisolone administration improves axonal regeneration into Schwann cell grafts in transected adult rat thoracic spinal cord. Exp Neurol 138:261-276.

Chen DF, Schneider GE, Martinou JC, Tonegawa S (1997) Bcl-2 promotes regeneration of severed axons in mammalian CNS. Nature 385:434-439.

Chen MS, Huber AB, van der Haar ME, Frank M, Schnell L, Spillmann AA, Christ F, Schwab ME (2000) Nogo-A is a myelin-associated neurite outgrowth inhibitor and an antigen for monoclonal antibody IN-1. Nature 403:434-439.

Chen S, Bisby MA (1993) Impaired motor axon regeneration in the C57BL/Ola mouse. J-Comp-Neurol 333:449-454.

Chen SY, Bhargava A, Mastroberardino L, Meijer OC, Wang J, Buse P, Firestone GL, Verrey F, Pearce D (1999) Epithelial sodium channel regulated by aldosterone-induced protein sgk. Proc Natl Acad Sci U S A 96:2514-2519.

Cheng HW, Jiang T, Brown SA, Pasinetti GM, Finch CE, McNeill TH (1994) Response of striatal astrocytes to neuronal deafferentation: an immunocytochemical and ultrastructural study. Neuroscience 62:425-439.

Chong MS, Reynolds ML, Irwin N, Coggeshall RE, Emson PC, Benowitz LI, Woolf CJ (1994) GAP-43 expression in primary sensory neurons following central axotomy. J Neurosci 14:4375-4384.

Christman CW, Salvant JBJ, Walker SA, Povlishock JT (1997) Characterization of a prolonged regenerative attempt by diffusely injured axons following traumatic brain injury in adult cat: a light and electron microscopic immunocytochemical study. Acta Neuropathol 94:329-337.

Coleman WP, Benzel D, Cahill DW, Ducker T, Geisler F, Green B, Gropper MR, Goffin J, Madsen PWr, Maiman DJ, Ondra SL, Rosner M, Sasso RC, Trost GR, Zeidman S (2000) A critical appraisal of the reporting of the National Acute Spinal Cord Injury Studies (II and III) of methylprednisolone in acute spinal cord injury. J Spinal Disord 13:185-199.

Corset V, Nguyen-Ba-Charvet KT, Forcet C, Moyse E, Chedotal A, Mehlen P (2000) Netrin-1-mediated axon outgrowth and cAMP production requires interaction with adenosine A2b receptor. Nature 407:747-750.

Cowling RT, Birnboim HC (2000) Expression of serum- and glucocorticoid-regulated kinase (sgk) mRNA is up-regulated by GM-CSF and other proinflammatory mediators in human granulocytes. J Leukoc Biol 67:240-248.

Dahlin LB (1995) Prevention of macrophage invasion impairs regeneration in nerve grafts. Brain Res 679:274-280.

Damalas A, Ben-Ze'ev A, Simcha I, Shtutman M, Leal JF, Zhurinsky J, Geiger B, Oren M (1999) Excess beta-catenin promotes accumulation of transcriptionally active p53. Embo J 18:3054-3063.

Davenport RW, Thies E, Cohen ML (1999) Neuronal growth cone collapse triggers lateral extensions along trailing axons [published erratum appears in Nat Neurosci 1999 May;2(5):485]. Nat Neurosci 2:254-259.

David S, Aguayo AJ (1981) Axonal elongation into peripheral nervous system "bridges" after central nervous system injury in adult rats. Science 214:931-933.

Davies SJ, Fitch MT, Memberg SP, Hall AK, Raisman G, Silver J (1997) Regeneration of adult axons in white matter tracts of the central nervous system. Nature 390:680-683.

de Celis JF, Bray S (1997) Feed-back mechanisms affecting Notch activation at the dorsoventral boundary in the Drosophila wing. Development 124:3241-3251.

De Ferrari GV, Inestrosa NC (2000) Wnt signaling function in Alzheimer's disease. Brain Res Brain Res Rev 33:1-12.

de La Houssaye BA, Mikule K, Nikolic D, Pfenninger KH (1999) Thrombin-induced growth cone collapse: involvement of phospholipase A(2) and eicosanoid generation. J Neurosci 19:10843-10855.

Decherchi P, Gauthier P (1996) In vitro pre-degenerated nerve autografts support CNS axonal regeneration. Brain Res 726:181-188.

del Peso L, Gonzalez-Garcia M, Page C, Herrera R, Nunez G (1997) Interleukin-3-induced phosphorylation of BAD through the protein kinase Akt. Science 278:687-689.

Deng X, Ito T, Carr B, Mumby M, May WS, Jr. (1998) Reversible phosphorylation of Bcl2 following interleukin 3 or bryostatin 1 is mediated by direct interaction with protein phosphatase 2A. J Biol Chem 273:34157-34163.

DeRisi JL, Iyer VR, Brown PO (1997) Exploring the metabolic and genetic control of gene expression on a genomic scale. Science 278:680-686.

DeVivo MJ, Kartus PL, Stover SL, Fine PR (1990) Benefits of early admission to an organised spinal cord injury care system. Paraplegia 28:545-555.

Diefenbach TJ, Guthrie PB, Kater SB (2000) Stimulus history alters behavioral responses of neuronal growth cones. J Neurosci 20:1484-1494.

DiProspero NA, Meiners S, Geller HM (1997) Inflammatory cytokines interact to modulate extracellular matrix and astrocytic support of neurite outgrowth. Exp Neurol 148:628-639.

Donovan MK, Wyss JM (1983) Evidence for some collateralization between cortical and diencephalic efferent axons of the rat subicular cortex. Brain Res 259:181-192.

Dragunow M, Preston K, Dodd J, Young D, Lawlor P, Christie D (1995) Clusterin accumulates in dying neurons following status epilepticus. Brain Res Mol Brain Res 32:279-290.

Dubuisson AS, Foidart-Dessalle M, Reznik M, Grosdent JC, Stevenaert A (1997) Predegenerated nerve allografts versus fresh nerve allografts in nerve repair. Exp Neurol 148:378-387.

Durrieu C, Bernier-Valentin F, Rousset B (1987) Binding of glyceraldehyde 3-phosphate dehydrogenase to microtubules. Mol Cell Biochem 74:55-65.

Eberwine J, Yeh H, Miyashiro K, Cao Y, Nair S, Finnell R, Zettel M, Coleman P (1992) Analysis of gene expression in single live neurons. Proc Natl Acad Sci U S A 89:3010-3014.

Eckhardt F, Behar O, Calautti E, Yonezawa K, Nishimoto I, Fishman MC (1997) A novel transmembrane semaphorin can bind c-src. Mol Cell Neurosci 9:409-419.

Edmonds BT, Moomaw CR, Hsu JT, Slaughter C, Ellis L (1990) The p38 and p34 polypeptides of growth cone particle membranes are the alpha- and beta-subunits of G proteins. Brain Res Dev Brain Res 56:131-136.

Eisen MB, Spellman PT, Brown PO, Botstein D (1998) Cluster analysis and display of genome-wide expression patterns. Proc Natl Acad Sci U S A 95:14863-14868.

Ellezam B, Selles-Navarro I, Manitt C, Kennedy TE, McKerracher L (2001) Expression of netrin-1 and its receptors DCC and UNC-5H2 after axotomy and during regeneration of adult rat retinal ganglion cells. Exp Neurol 168:105-115.

Elliott EJ, Parks DA, Fishman PS (1999) alpha 1-tubulin expression in proximally axotomized mouse cortical neurons. J Neurotrauma 16:333-339.

Eriksson PS, Perfilieva E, Bjork Eriksson T, Alborn AM, Nordborg C, Peterson DA, Gage FH (1998) Neurogenesis in the adult human hippocampus [see comments]. Nat Med 4:1313-1317.

Evans GJ, Pocock JM (1999) Modulation of neurotransmitter release by dihydropyridine-sensitive calcium channels involves tyrosine phosphorylation. Eur J Neurosci 11:279-292.

Fagotto F, Funayama N, Gluck U, Gumbiner BM (1996) Binding to cadherins antagonizes the signaling activity of beta-catenin during axis formation in Xenopus. J Cell Biol 132:1105-1114.

Fambrough D, Pan D, Rubin GM, Goodman CS (1996) The cell surface metalloprotease/disintegrin Kuzbanian is required for axonal extension in Drosophila. Proc Natl Acad Sci U S A 93:13233-13238.

Fan J, Mansfield SG, Redmond T, Gordon Weeks PR, Raper JA (1993) The organization of F-actin and microtubules in growth cones exposed to a brain-derived collapsing factor. J Cell Biol 121:867-878.

Fawcett JW, Asher RA (1999) The glial scar and central nervous system repair. Brain Res Bull 49:377-391.

Fernandes KJ, Fan DP, Tsui BJ, Cassar SL, Tetzlaff W (1999) Influence of the axotomy to cell body distance in rat rubrospinal and spinal motoneurons: differential regulation of GAP-43, tubulins, and neurofilament-M. J Comp Neurol 414:495-510.

Fischer D, Pavlidis M, Thanos S (2000) Cataractogenic lens injury prevents traumatic ganglion cell death and promotes axonal regeneration both In vivo and in culture. Invest Ophthalmol Vis Sci 41:3943-3954.

Fitch MT, Silver J (1997) Activated macrophages and the blood-brain barrier: inflammation after CNS injury leads to increases in putative inhibitory molecules. Exp Neurol 148:587-603.

Fournier AE, GrandPre T, Strittmatter SM (2001) Identification of a receptor mediating Nogo-66 inhibition of axonal regeneration. Nature 409:341-346.

Fournier AE, Beer J, Arregui CO, Essagian C, Aguayo AJ, McKerracher L (1997) Brain-derived neurotrophic factor modulates GAP-43 but not T alpha1 expression in injured retinal ganglion cells of adult rats. J Neurosci Res 47:561-572.

Fournier AE, Nakamura F, Kawamoto S, Goshima Y, Kalb RG, Strittmatter SM (2000) Semaphorin3A enhances endocytosis at sites of receptor-F-actin colocalization during growth cone collapse. J Cell Biol 149:411-422.

Franken S (2000) Charakterisierung von Rezeptoren neurotropher Glykosaminoglykane im Rattenhirn. In: Biologie. Düsseldorf: Heinrich-Heine-Universität.

Franklin JL, Berechid BE, Cutting FB, Presente A, Chambers CB, Foltz DR, Ferreira A, Nye JS (1999) Autonomous and non-autonomous regulation of mammalian neurite development by Notch1 and Delta1. Curr Biol 9:1448-1457.

Frisen J, Barbacid M (1997) Genetic analysis of the role of Eph receptors in the development of the mammalian nervous system. Cell Tissue Res 290:209-215.

Fu SY, Gordon T (1997) The cellular and molecular basis of peripheral nerve regeneration. Mol Neurobiol 14:67-116.

Fujisawa H, Kitsukawa T (1998) Receptors for collapsin/semaphorins. Curr Opin Neurobiol 8:587-592.

Gaiano N, Fishell G (1998) Transplantation as a tool to study progenitors within the vertebrate nervous system. J Neurobiol 36:152-161.

Gaiano N, Nye JS, Fishell G (2000) Radial glial identity is promoted by Notch1 signaling in the murine forebrain. Neuron 26:395-404.

Galko MJ, Tessier-Lavigne M (2000a) Function of an axonal chemoattractant modulated by metalloprotease activity. Science 289:1365-1367.

Galko MJ, Tessier-Lavigne M (2000b) Biochemical characterization of netrin-synergizing activity. J Biol Chem 275:7832-7838.

Gao PP, Yue Y, Cerretti DP, Dreyfus C, Zhou R (1999) Ephrin-dependent growth and pruning of hippocampal axons. Proc Natl Acad Sci U S A 96:4073-4077.

Gasman S, Chasserot Golaz S, Hubert P, Aunis D, Bader MF (1998) Identification of a potential effector pathway for the trimeric Go protein associated with secretory granules. Go stimulates a granule-bound phosphatidylinositol 4-kinase by activating RhoA in chromaffin cells. J Biol Chem 273:16913-16920.

Geschwind DH, Ou J, Easterday MC, Dougherty JD, Jackson RL, Chen Z, Antoine H, Terskikh A, Weissman IL, Nelson SF, Kornblum HI (2001) A genetic analysis of neural progenitor differentiation. Neuron 29:325-339.

Giger RJ, Pasterkamp RJ, Heijnen S, Holtmaat AJ, Verhaagen J (1998) Anatomical distribution of the chemorepellent semaphorin III/collapsin-1 in the adult rat and human brain: predominant expression in structures of the olfactory-hippocampal pathway and the motor system. J-Neurosci-Res 52:27-42.

Girault JA, Costa A, Derkinderen P, Studler JM, Toutant M (1999) FAK and PYK2/CAKbeta in the nervous system: a link between neuronal activity, plasticity and survival? Trends Neurosci 22:257-263.

Gitler D, Spira ME (1998) Real time imaging of calcium-induced localized proteolytic activity after axotomy and its relation to growth cone formation. Neuron 20:1123-1135.

Glaser PE, Gross RW (1995) Rapid plasmenylethanolamine-selective fusion of membrane bilayers catalyzed by an isoform of glyceraldehyde-3-phosphate dehydrogenase: discrimination between glycolytic and fusogenic roles of individual isoforms. Biochemistry 34:12193-12203.

Glass JD, Schryer BL, Griffin JW (1994) Calcium-mediated degeneration of the axonal cytoskeleton in the Ola mouse. J-Neurochem 62:2472-2475.

Goi T, Rusanescu G, Urano T, Feig LA (1999) Ral-specific guanine nucleotide exchange factor activity opposes other Ras effectors in PC12 cells by inhibiting neurite outgrowth. Mol Cell Biol 19:1731-1741.

Goldberg DJ, Grabham PW (1999) Braking news: calcium in the growth cone. Neuron 22:423-425.

Gomez TM, Spitzer NC (1999) In vivo regulation of axon extension and pathfinding by growth-cone calcium transients. Nature 397:350-355.

Gomez TM, Robles E, Poo M, Spitzer NC (2001) Filopodial calcium transients promote substrate-dependent growth cone turning. Science 291:1983-1987.

Goodman CS (1996) Mechanisms and molecules that control growth cone guidance. Annu Rev Neurosci 19:341-377.

Goshima Y, Nakamura F, Strittmatter P, Strittmatter SM (1995) Collapsin-induced growth cone collapse mediated by an intracellular protein related to UNC-33. Nature 376:509-514.

GrandPre T, Nakamura F, Vartanian T, Strittmatter SM (2000) Identification of the Nogo inhibitor of axon regeneration as a Reticulon protein. Nature 403:439-444.

Green BA, Kahn T, Klose KJ (1980) A comparative study of steroid therapy in acute experimental spinal cord injury. Surg Neurol 13:91-97.

Grill R, Murai K, Blesch A, Gage FH, Tuszynski MH (1997) Cellular delivery of neurotrophin-3 promotes corticospinal axonal growth and partial functional recovery after spinal cord injury. J Neurosci 17:5560-5572.

Guatelli JC, Whitfield KM, Kwoh DY, Barringer KJ, Richman DD, Gingeras TR (1990) Isothermal, in vitro amplification of nucleic acids by a multienzyme reaction modeled after retroviral replication. Proc Natl Acad Sci U S A 87:1874-1878.

Hall A (1998) Rho GTPases and the actin cytoskeleton. Science 279:509-514.

Hall AC, Lucas FR, Salinas PC (2000) Axonal remodeling and synaptic differentiation in the cerebellum is regulated by WNT-7a signaling. Cell 100:525-535.

Hamashima H, Tamaru T, Noguchi H, Kobayashi M, Takamatsu K (2001) Immunochemical assessment of neural visinin-like calcium-binding protein 3 expression in rat brain. Neurosci Res 39:133-143.

Han X, Ramanadham S, Turk J, Gross RW (1998) Reconstitution of membrane fusion between pancreatic islet secretory granules and plasma membranes: catalysis by a protein constituent recognized by monoclonal antibodies directed against glyceraldehyde-3-phosphate dehydrogenase. Biochim Biophys Acta 1414:95-107.

Harkey HL, al-Mefty O, Marawi I, Peeler DF, Haines DE, Alexander LF (1995) Experimental chronic compressive cervical myelopathy: effects of decompression. J Neurosurg 83:336-341.

Haruta T, Takami N, Ohmura M, Misumi Y, Ikehara Y (1997) Ca2+-dependent interaction of the growth-associated protein GAP-43 with the synaptic core complex. Biochem J 325:455-463.

Hattori M, Osterfield M, Flanagan JG (2000) Regulated cleavage of a contact-mediated axon repellent. Science 289:1360-1365.

He Q, Dent EW, Meiri KF (1997) Modulation of actin filament behavior by GAP-43 (neuromodulin) is dependent on the phosphorylation status of serine 41, the protein kinase C site. J Neurosci 17:3515-3524.

Heiduschka P, Thanos S (2000) Aurintricarboxylic acid promotes survival and regeneration of axotomised retinal ganglion cells in vivo. Neuropharmacology 39:889-902.

Herdegen T, Skene P, Bahr M (1997) The c-Jun transcription factor--bipotential mediator of neuronal death, survival and regeneration. Trends Neurosci 20:227-231.

Herdegen T, Sandkuhler J, Gass P, Kiessling M, Bravo R, Zimmermann M (1993) JUN, FOS, KROX, and CREB transcription factor proteins in the rat cortex: basal expression and induction by spreading depression and epileptic seizures. J Comp Neurol 333:271-288.

Herdegen T, Claret FX, Kallunki T, Martin Villalba A, Winter C, Hunter T, Karin M (1998) Lasting N-terminal phosphorylation of c-Jun and activation of c-Jun N-terminal kinases after neuronal injury. J Neurosci 18:5124-5135.

Hofer F, Berdeaux R, Martin GS (1998) Ras-independent activation of Ral by a Ca(2+)-dependent pathway. Curr Biol 8:839-842.

Hollnagel A, Oehlmann V, Heymer J, Ruther U, Nordheim A (1999) Id genes are direct targets of bone morphogenetic protein induction in embryonic stem cells. J Biol Chem 274:19838-19845.

Holmberg J, Clarke DL, Frisen J (2000) Regulation of repulsion versus adhesion by different splice forms of an Eph receptor. Nature 408:203-206.

Holmes TC, de Lacalle S, Su X, Liu G, Rich A, Zhang S (2000) Extensive neurite outgrowth and active synapse formation on self-assembling peptide scaffolds. Proc Natl Acad Sci U S A 97:6728-6733.

Hong K, Nishiyama M, Henley J, Tessier Lavigne M, Poo M (2000) Calcium signalling in the guidance of nerve growth by netrin-1. Nature 403:93-98.

Horner PJ, Gage FH (2000) Regenerating the damaged central nervous system. Nature 407:963-970.

Hortsch M (1996) The L1 family of neural cell adhesion molecules: old proteins performing new tricks. Neuron 17:587-593.

Houweling DA, Lankhorst AJ, Gispen WH, Bar PR, Joosten EA (1998) Collagen containing neurotrophin-3 (NT-3) attracts regrowing injured corticospinal axons in the adult rat spinal cord and promotes partial functional recovery. Exp Neurol 153:49-59.

Hsu SY, Kaipia A, Zhu L, Hsueh AJ (1997) Interference of BAD (Bcl-xL/Bcl-2-associated death promoter)-induced apoptosis in mammalian cells by 14-3-3 isoforms and P11. Mol Endocrinol 11:1858-1867.

Hsueh YP, Sheng M (1998) Eph receptors, ephrins, and PDZs gather in neuronal synapses. Neuron 21:1227-1229.

Huang DW, McKerracher L, Braun PE, David S (1999) A therapeutic vaccine approach to stimulate axon regeneration in the adult mammalian spinal cord. Neuron 24:639-647.

Huitorel P, Pantaloni D (1985) Bundling of microtubules by glyceraldehyde-3-phosphate dehydrogenase and its modulation by ATP. Eur J Biochem 150:265-269.

Hurlbert RJ (2000) Methylprednisolone for acute spinal cord injury: an inappropriate standard of care J Neurosurg 93:1-7.

Ide C (1996) Peripheral nerve regeneration. Neurosci Res 25:101-121.

Igarashi M, Strittmatter SM, Vartanian T, Fishman MC (1993) Mediation by G proteins of signals that cause collapse of growth cones. Science 259:77-79.

Igarashi M, Li WW, Sudo Y, Fishman MC (1995) Ligand-induced growth cone collapse: amplification and blockade by variant GAP-43 peptides. J Neurosci 15:5660-5667.

Imaizumi K, Tsuda M, Wanaka A, Tohyama M, Takagi T (1994) Differential expression of sgk mRNA, a member of the Ser/Thr protein kinase gene family, in rat brain after CNS injury. Brain Res Mol Brain Res 26:189-196.

Ishitani R, Chuang DM (1996) Glyceraldehyde-3-phosphate dehydrogenase antisense oligodeoxynucleotides protect against cytosine arabinonucleoside-induced apoptosis in cultured cerebellar neurons. Proc Natl Acad Sci U S A 93:9937-9941.

Itoh Y, Mizoi K, Tessler A (1999) Embryonic central nervous system transplants mediate adult dorsal root regeneration into host spinal cord. Neurosurgery 45:849-856; discussion 856-848.

Ivins JK, Raper JA, Pittman RN (1991) Intracellular calcium levels do not change during contact-mediated collapse of chick DRG growth cone structure. J Neurosci 11:1597-1608.

Jakeman LB, Wei P, Guan Z, Stokes BT (1998) Brain-derived neurotrophic factor stimulates hindlimb stepping and sprouting of cholinergic fibers after spinal cord injury. Exp Neurol 154:170-184.

Jalink K, van Corven EJ, Hengeveld T, Morii N, Narumiya S, Moolenaar WH (1994) Inhibition of lysophosphatidate- and thrombin-induced neurite retraction and neuronal cell rounding by ADP ribosylation of the small GTP-binding protein Rho. J Cell Biol 126:801-810.

Jeffery DR, Absher J, Pfeiffer FE, Jackson H (2000) Cortical deficits in multiple sclerosis on the basis of subcortical lesions. Mult Scler 6:50-55.

Jin Z, Strittmatter SM (1997) Rac1 mediates collapsin-1-induced growth cone collapse. J Neurosci 17:6256-6263.

Johnson GV, Litersky JM, Jope RS (1991) Degradation of microtubule-associated protein 2 and brain spectrin by calpain: a comparative study. J Neurochem 56:1630-1638.

Joosten EA (1991) Immuno-electronmicroscopic visualization of cell adhesion molecule L1 in adult rat pyramidal tract: localization on neuronal and oligodendrocytic processes. Brain-Res 546:155-160.

Kalderon N, Fuks Z (1996) Severed corticospinal axons recover electrophysiologic control of muscle activity after x-ray therapy in lesioned adult spinal cord [published erratum appears in Proc Natl Acad Sci U S A 1996 Dec 10;93(25):14993]. Proc Natl Acad Sci U S A 93:11185-11190.

Kaplan AM, Vigna SR (1994) Gastric inhibitory polypeptide (GIP) binding sites in rat brain. Peptides 15:297-302.

Kato S, Ide C (1994) Axonal sprouting at the node of Ranvier of the peripheral nerve disconnected with the cell body. Restorat Neurol Neurosci 6:181-187.

Katoh H, Negishi M, Ichikawa A (1996) Prostaglandin E receptor EP3 subtype induces neurite retraction via small GTPase Rho. J Biol Chem 271:29780-29784.

Katoh H, Aoki J, Ichikawa A, Negishi M (1998a) p160 RhoA-binding kinase ROKalpha induces neurite retraction. J Biol Chem 273:2489-2492.

Katoh H, Aoki J, Yamaguchi Y, Kitano Y, Ichikawa A, Negishi M (1998b) Constitutively active Galpha12, Galpha13, and Galphaq induce Rho-dependent neurite retraction through different signaling pathways. J Biol Chem 273:28700-28707.

Keirstead HS, Dyer JK, Sholomenko GN, McGraw J, Delaney KR, Steeves JD (1995) Axonal regeneration and physiological activity following transection and immunological disruption of myelin within the hatchling chick spinal cord. J Neurosci 15:6963-6974.

Keyvani K, Reinecke S, Abts HF, Paulus W, Witte OW (2000) Suppression of proteasome C2 contralateral to ischemic lesions in rat brain. Brain Res 858:386-392.

Kim EC, Lau JS, Rawlings S, Lee AS (1997) Positive and negative regulation of the human thymidine kinase promoter mediated by CCAAT binding transcription factors NF-Y/CBF, dbpA, and CDP/cut. Cell Growth Differ 8:1329-1338.

Kiryu S, Morita N, Ohno K, Maeno H, Kiyama H (1995) Regulation of mRNA expression involved in Ras and PKA signal pathways during rat hypoglossal nerve regeneration. Brain Res Mol Brain Res 29:147-156.

Kobayashi T, Cohen P (1999) Activation of serum- and glucocorticoid-regulated protein kinase by agonists that activate phosphatidylinositide 3-kinase is mediated by 3-phosphoinositide-dependent protein kinase-1 (PDK1) and PDK2. Biochem J 339:319-328.

Koenig E, Kinsman S, Repasky E, Sultz L (1985) Rapid mobility of motile varicosities and inclusions containing alpha-spectrin, actin, and calmodulin in regenerating axons in vitro. J Neurosci 5:715-729.

Kohler C (1990) Subicular projections to the hypothalamus and brainstem: some novel aspects revealed in the rat by the anterograde Phaseolus vulgaris leukoagglutinin (PHA-L) tracing method. Prog Brain Res 83:59-69.

Komuro H, Rakic P (1998) Orchestration of neuronal migration by activity of ion channels, neurotransmitter receptors, and intracellular Ca2+ fluctuations. J Neurobiol 37:110-130.

Koo EH, Sisodia SS, Archer DR, Martin LJ, Weidemann A, Beyreuther K, Fischer P, Masters CL, Price DL (1990) Precursor of amyloid protein in Alzheimer disease undergoes fast anterograde axonal transport. Proc Natl Acad Sci U S A 87:1561-1565.

Koshy B, Matilla T, Burright EN, Merry DE, Fischbeck KH, Orr HT, Zoghbi HY (1996) Spinocerebellar ataxia type-1 and spinobulbar muscular atrophy gene products interact with glyceraldehyde-3-phosphate dehydrogenase. Hum Mol Genet 5:1311-1318.

Kozma R, Sarner S, Ahmed S, Lim L (1997) Rho family GTPases and neuronal growth cone remodelling: relationship between increased complexity induced by Cdc42Hs, Rac1, and acetylcholine and collapse induced by RhoA and lysophosphatidic acid. Mol Cell Biol 17:1201-1211.

Kranenburg O, Poland M, van Horck FP, Drechsel D, Hall A, Moolenaar WH (1999) Activation of RhoA by lysophosphatidic acid and Galpha12/13 subunits in neuronal cells: induction of neurite retraction. Mol Biol Cell 10:1851-1857.

Kugler S, Klocker N, Kermer P, Isenmann S, Bahr M (1999) Transduction of axotomized retinal ganglion cells by adenoviral vector administration at the optic nerve stump: an in vivo model system for the inhibition of neuronal apoptotic cell death. Gene Ther 6:1759-1767.

Kuhlbrodt K, Herbarth B, Sock E, Hermans Borgmeyer I, Wegner M (1998) Sox10, a novel transcriptional modulator in glial cells. J Neurosci 18:237-250.

Kuhn TB, Brown MD, Wilcox CL, Raper JA, Bamburg JR (1999) Myelin and collapsin-1 induce motor neuron growth cone collapse through different pathways: inhibition of collapse by opposing mutants of rac1. J Neurosci 19:1965-1975.

Kuhn TB, Meberg PJ, Brown MD, Bernstein BW, Minamide LS, Jensen JR, Okada K, Soda EA, Bamburg JR (2000) Regulating actin dynamics in neuronal growth cones by ADF/cofilin and rho family GTPases. J Neurobiol 44:126-144.

Lacoste J, Ma A, Parsons JT (1998) Assay and purification and focal adhesion kinase. Methods Enzymol 298:89-102.

Lausberg F (2000) Die Rolle von Extrazellulärmatrix assoziierten Molekülen nach Läsion des Zentralnevensystems der adulten Ratte. In: Biologie. Düsseldorf: Heinrich-Heine-Universität.

Lautermilch NJ, Spitzer NC (2000) Regulation of calcineurin by growth cone calcium waves controls neurite extension. J Neurosci 20:315-325.

Lee CH, Della NG, Chew CE, Zack DJ (1996) Rin, a neuron-specific and calmodulin-binding small G-protein, and Rit define a novel subfamily of ras proteins. J Neurosci 16:6784-6794.

Lee MS, Kwon YT, Li M, Peng J, Friedlander RM, Tsai LH (2000a) Neurotoxicity induces cleavage of p35 to p25 by calpain. Nature 405:360-364.

Lee SH, Lumelsky N, Studer L, Auerbach JM, McKay RD (2000b) Efficient generation of midbrain and hindbrain neurons from mouse embryonic stem cells. Nat Biotechnol 18:675-679.

Lee SM, Tole S, Grove E, McMahon AP (2000c) A local Wnt-3a signal is required for development of the mammalian hippocampus. Development 127:457-467.

Leighton PA, Mitchell KJ, Goodrich LV, Lu X, Pinson K, Scherz P, Skarnes WC, Tessier-Lavigne M (2001) Defining brain wiring patterns and mechanisms through gene trapping in mice. Nature 410:174-179.

Leventhal PS, Feldman EL (1996) Tyrosine phosphorylation and enhanced expression of paxillin during neuronal differentiation in vitro. J Biol Chem 271:5957-5960.

Levin LA, Geszvain KM (1998) Expression of ceruloplasmin in the retina: induction after optic nerve crush. Invest Ophthalmol Vis Sci 39:157-163.

Li GL, Farooque M, Holtz A, Olsson Y (1995a) Increased expression of growth-associated protein 43 immunoreactivity in axons following compression trauma to rat spinal cord. Acta Neuropathol 92:19-26.

Li XJ, Li SH, Sharp AH, Nucifora FC, Schilling G, Lanahan A, Worley P, Snyder SH, Ross CA (1995b) A huntingtin-associated protein enriched in brain with implications for pathology. Nature 378:398-402.

Li Y, Field PM, Raisman G (1998) Regeneration of adult rat corticospinal axons induced by transplanted olfactory ensheathing cells. J Neurosci 18:10514-10524.

Lin LH, Bock S, Carpenter K, Rose M, Norden JJ (1992) Synthesis and transport of GAP-43 in entorhinal cortex neurons and perforant pathway during lesion-induced sprouting and reactive synaptogenesis. Brain Res Mol Brain Res 14:147-153.

Linseman DA, Hofmann F, Fisher SK (2000) A role for the small molecular weight GTPases, Rho and Cdc42, in muscarinic receptor signaling to focal adhesion kinase. J Neurochem 74:2010-2020.

Lips K, Stichel CC, Muller HW (1995) Restricted appearance of tenascin and chondroitin sulphate proteoglycans after transection and sprouting of adult rat postcommissural fornix. J Neurocytol 24:449-464.

Liu L, Persson JK, Svensson M, Aldskogius H (1998) Glial cell responses, complement, and clusterin in the central nervous system following dorsal root transection. Glia 23:221-238.

Liu L, Tornqvist E, Mattsson P, Eriksson NP, Persson JK, Morgan BP, Aldskogius H, Svensson M (1995) Complement and clusterin in the spinal cord dorsal horn and gracile nucleus following sciatic nerve injury in the adult rat. Neuroscience 68:167-179.

Liu Y, Kim D, Himes BT, Chow SY, Schallert T, Murray M, Tessler A, Fischer I (1999a) Transplants of fibroblasts genetically modified to express BDNF promote regeneration of adult rat rubrospinal axons and recovery of forelimb function. J Neurosci 19:4370-4387.

Liu Y, Himes BT, Solowska J, Moul J, Chow SY, Park KI, Tessler A, Murray M, Snyder EY, Fischer I (1999b) Intraspinal delivery of neurotrophin-3 using neural stem cells genetically modified by recombinant retrovirus. Exp Neurol 158:9-26.

Lockhart DJ, Winzeler EA (2000) Genomics, gene expression and DNA arrays. Nature 405:827-836.

Logan A, Oliver JJ, Berry M (1994) Growth factors in CNS repair and regeneration. Prog Growth Factor Res 5:379-405.

Loschinger J, Bandtlow CE, Jung J, Klostermann S, Schwab ME, Bonhoeffer F, Kater SB (1997) Retinal axon growth cone responses to different environmental cues are mediated by different second-messenger systems. J Neurobiol 33:825-834.

Lu J, Ashwell KW, Waite P (2000) Advances in secondary spinal cord injury: role of apoptosis. Spine 25:1859-1866.

Luo L, Salunga RC, Guo H, Bittner A, Joy KC, Galindo JE, Xiao H, Rogers KE, Wan JS, Jackson MR, Erlander MG (1999) Gene expression profiles of laser-captured adjacent neuronal subtypes. Nat Med 5:117-122.

Lupashin VV, Waters MG (1997) t-SNARE activation through transient interaction with a rab-like guanosine triphosphatase. Science 276:1255-1258.

Mackay DJ, Nobes CD, Hall A (1995) The Rho's progress: a potential role during neuritogenesis for the Rho family of GTPases. Trends Neurosci 18:496-501.

Maekawa M, Ishizaki T, Boku S, Watanabe N, Fujita A, Iwamatsu A, Obinata T, Ohashi K, Mizuno K, Narumiya S (1999) Signaling from Rho to the actin cytoskeleton through protein kinases ROCK and LIM-kinase. Science 285:895-898.

Maiyar AC, Phu PT, Huang AJ, Firestone GL (1997) Repression of glucocorticoid receptor transactivation and DNA binding of a glucocorticoid response element within the serum/glucocorticoid-inducible protein kinase (sgk) gene promoter by the p53 tumor suppressor protein. Mol Endocrinol 11:312-329.

Maiyar AC, Huang AJ, Phu PT, Cha HH, Firestone GL (1996) p53 stimulates promoter activity of the sgk. serum/glucocorticoid-inducible serine/threonine protein kinase gene in rodent mammary epithelial cells. J Biol Chem 271:12414-12422.

Marcotte EM, Pellegrini M, Thompson MJ, Yeates TO, Eisenberg D (1999a) A combined algorithm for genome-wide prediction of protein function. Nature 402:83-86.

Marcotte EM, Pellegrini M, Ng HL, Rice DW, Yeates TO, Eisenberg D (1999b) Detecting protein function and protein-protein interactions from genome sequences. Science 285:751-753.

Mark MD, Lohrum M, Puschel AW (1997) Patterning neuronal connections by chemorepulsion: the semaphorins. Cell Tissue Res 290:299-306.

Martone ME, Holash JA, Bayardo A, Pasquale EB, Ellisman MH (1997) Immunolocalization of the receptor tyrosine kinase EphA4 in the adult rat central nervous system. Brain Res 771:238-250.

Mazzocchi G, Rebuffat P, Meneghelli V, Malendowicz LK, Tortorella C, Gottardo G, Nussdorfer GG (1999) Gastric inhibitory polypeptide stimulates glucocorticoid secretion in rats, acting through specific receptors coupled with the adenylate cyclase-dependent signaling pathway. Peptides 20:589-594.

McDonald JW, Liu XZ, Qu Y, Liu S, Mickey SK, Turetsky D, Gottlieb DI, Choi DW (1999) Transplanted embryonic stem cells survive, differentiate and promote recovery in injured rat spinal cord. Nat Med 5:1410-1412.

McKerracher L, Essagian C, Aguayo AJ (1993a) Temporal changes in beta-tubulin and neurofilament mRNA levels after transection of adult rat retinal ganglion cell axons in the optic nerve. J Neurosci 13:2617-2626.

McKerracher L, Essagian C, Aguayo AJ (1993b) Marked increase in beta-tubulin mRNA expression during regeneration of axotomized retinal ganglion cells in adult mammals. J Neurosci 13:5294-5300.

McKerracher L, Vidal Sanz M, Essagian C, Aguayo AJ (1990) Selective impairment of slow axonal transport after optic nerve injury in adult rats. J Neurosci 10:2834-2841.

Meberg PJ, Bamburg JR (2000) Increase in neurite outgrowth mediated by overexpression of actin depolymerizing factor. J Neurosci 20:2459-2469.

Meberg PJ, Ono S, Minamide LS, Takahashi M, Bamburg JR (1998) Actin depolymerizing factor and cofilin phosphorylation dynamics: response to signals that regulate neurite extension. Cell Motil Cytoskeleton 39:172-190.

Meier C, Parmantier E, Brennan A, Mirsky R, Jessen KR (1999) Developing Schwann cells acquire the ability to survive without axons by establishing an autocrine circuit involving insulin-like growth factor, neurotrophin-3, and platelet-derived growth factor-BB. J Neurosci 19:3847-3859.

Mellitzer G, Xu Q, Wilkinson DG (1999) Eph receptors and ephrins restrict cell intermingling and communication. Nature 400:77-81.

Menegon A, Burgaya F, Baudot P, Dunlap DD, Girault JA, Valtorta F (1999) FAK+ and PYK2/CAKbeta, two related tyrosine kinases highly expressed in the central nervous system: similarities and differences in the expression pattern. Eur J Neurosci 11:3777-3788.

Micchelli CA, Rulifson EJ, Blair SS (1997) The function and regulation of cut expression on the wing margin of Drosophila: Notch, Wingless and a dominant negative role for Delta and Serrate. Development 124:1485-1495.

Mikucki SA, Oblinger MM (1991) Corticospinal neurons exhibit a novel pattern of cytoskeletal gene expression after injury. J Neurosci Res 30:213-225.

Ming GL, Song HJ, Berninger B, Holt CE, Tessier Lavigne M, Poo MM (1997) cAMP-dependent growth cone guidance by netrin-1. Neuron 19:1225-1235.

Minturn JE, Fryer HJ, Geschwind DH, Hockfield S (1995) TOAD-64, a gene expressed early in neuronal differentiation in the rat, is related to unc-33, a C. elegans gene involved in axon outgrowth. J Neurosci 15:6757-6766.

Miranda JD, White LA, Marcillo AE, Willson CA, Jagid J, Whittemore SR (1999) Induction of Eph B3 after spinal cord injury. Exp Neurol 156:218-222.

Misonou H, Ohara Imaizumi M, Murakami T, Kawasaki M, Ikeda K, Wakai T, Kumakura K (1998) Protein kinase C controls the priming step of regulated exocytosis in adrenal chromaffin cells. Cell Mol Neurobiol 18:379-390.

Mitsui H, Takuwa N, Kurokawa K, Exton JH, Takuwa Y (1997) Dependence of activated Galpha12-induced G1 to S phase cell cycle progression on both Ras/mitogen-activated protein kinase and Ras/Rac1/Jun N-terminal kinase cascades in NIH3T3 fibroblasts. J Biol Chem 272:4904-4910.

Morihara T, Tanabe K, Yoneda T, Tanaka T, Kudo T, Gomi F, Kiyama H, Imaizumi K, Tohyama M, Takeda M (1999) IPP isomerase, an enzyme of mevalonate pathway, is preferentially expressed in postnatal cortical neurons and induced after nerve transection. Brain Res Mol Brain Res 67:231-238.

Morita N, Kiryu S, Kiyama H (1996) p53-independent cyclin G expression in a group of mature neurons and its enhanced expression during nerve regeneration. J Neurosci 16:5961-5966.

Morrison SJ, Perez SE, Qiao Z, Verdi JM, Hicks C, Weinmaster G, Anderson DJ (2000) Transient Notch activation initiates an irreversible switch from neurogenesis to gliogenesis by neural crest stem cells. Cell 101:499-510.

Moya KL, Confaloni AM, Allinquant B (1994) In vivo neuronal synthesis and axonal transport of Kunitz protease inhibitor (KPI)-containing forms of the amyloid precursor protein. J Neurochem 63:1971-1974.

Mueller BK (1999) Growth cone guidance: first steps towards a deeper understanding. Annu Rev Neurosci 22:351-388.

Murai H, Ikeda M, Kishida S, Ishida O, Okazaki-Kishida M, Matsuura Y, Kikuchi A (1997) Characterization of Ral GDP dissociation stimulator-like (RGL) activities to regulate c-fos promoter and the GDP/GTP exchange of Ral. J Biol Chem 272:10483-10490.

Nadeau JH, Balling R, Barsh G, Beier D, Brown SD, Bucan M, Camper S, Carlson G, Copeland N, Eppig J, Fletcher C, Frankel WN, Ganten D, Goldowitz D, Goodnow C, Guenet JL, Hicks G, de Angelis MH, Jackson I, Jacob HJ, Jenkins N, Johnson D, Justice M, Kay S, Kingsley D, Lehrach H, Magnuson T, Meisler M, Poustka A, Rinchik EM, Rossant J, Russell LB, Schimenti J, Shiroishi T, Skarnes WC, Soriano P, Stanford W, Takahashi JS, Wurst W, Zimmer A (2001) Sequence interpretation. Functional annotation of mouse genome sequences. Science 291:1251-1255.

Nakahara Y, Gage FH, Tuszynski MH (1996) Grafts of fibroblasts genetically modified to secrete NGF, BDNF, NT-3, or basic FGF elicit differential responses in the adult spinal cord. Cell Transplant 5:191-204.

Nakamura F, Kalb RG, Strittmatter SM (2000) Molecular basis of semaphorin-mediated axon guidance. J Neurobiol 44:219-229.

Nakashima S, Morinaka K, Koyama S, Ikeda M, Kishida M, Okawa K, Iwamatsu A, Kishida S, Kikuchi A (1999) Small G protein Ral and its downstream molecules regulate endocytosis of EGF and insulin receptors. Embo J 18:3629-3642.

Neumann CJ, Cohen SM (1996) A hierarchy of cross-regulation involving Notch, wingless, vestigial and cut organizes the dorsal/ventral axis of the Drosophila wing. Development 122:3477-3485.

Nishina H, Bachmann M, Oliveira-dos-Santos AJ, Kozieradzki I, Fischer KD, Odermatt B, Wakeham A, Shahinian A, Takimoto H, Bernstein A, Mak TW, Woodgett JR, Ohashi PS, Penninger JM (1997) Impaired CD28-mediated interleukin 2 production and proliferation in stress kinase SAPK/ERK1 kinase (SEK1)/mitogen-activated protein kinase kinase 4 (MKK4)-deficient T lymphocytes. J Exp Med 186:941-953.

Nishiwaki K, Hisamoto N, Matsumoto K (2000) A metalloprotease disintegrin that controls cell migration in Caenorhabditis elegans. Science 288:2205-2208.

Nobes CD, Hall A (1995) Rho, rac, and cdc42 GTPases regulate the assembly of multimolecular focal complexes associated with actin stress fibers, lamellipodia, and filopodia. Cell 81:53-62.

Nusse R (1999) WNT targets. Repression and activation. Trends Genet 15:1-3.

Oda T, Wals P, Osterburg HH, Johnson SA, Pasinetti GM, Morgan TE, Rozovsky I, Stine WB, Snyder SW, Holzman TF, et al. (1995) Clusterin (apoJ) alters the aggregation of amyloid beta-peptide (A beta 1-42) and forms slowly sedimenting A beta complexes that cause oxidative stress. Exp Neurol 136:22-31.

Oguchi M, Gerth E, Fitzgerald B, Park JH (1973) Regulation of glyceraldehyde 3-phosphate dehydrogenase by phosphocreatine and adenosine triphosphate. IV. Factors affecting in vivo control of enzymatic activity. J Biol Chem 248:5571-5576.

Okazaki M, Kishida S, Hinoi T, Hasegawa T, Tamada M, Kataoka T, Kikuchi A (1997) Synergistic activation of c-fos promoter activity by Raf and Ral GDP dissociation stimulator. Oncogene 14:515-521.

Olson L (1993) NGF and the treatment of Alzheimer's disease. Exp Neurol 124:5-15.

Olson L (1997) Regeneration in the adult central nervous system: experimental repair strategies. Nat Med 3:1329-1335.

Orioli D, Klein R (1997) The Eph receptor family: axonal guidance by contact repulsion. Trends Genet 13:354-359.

Park J, Leong ML, Buse P, Maiyar AC, Firestone GL, Hemmings BA (1999) Serum and glucocorticoid-inducible kinase (SGK) is a target of the PI 3- kinase-stimulated signaling pathway. Embo J 18:3024-3033.

Parker JR, Parker JC, Jr., Overman JC (1990) Intracranial diffuse axonal injury at autopsy. Ann Clin Lab Sci 20:220-224.

Pasinetti GM, Johnson SA, Oda T, Rozovsky I, Finch CE (1994) Clusterin (SGP-2): a multifunctional glycoprotein with regional expression in astrocytes and neurons of the adult rat brain. J Comp Neurol 339:387-400.

Pasterkamp RJ, Giger RJ, Ruitenberg MJ, Holtmaat AJ, De Wit J, De Winter F, Verhaagen J (1999) Expression of the gene encoding the chemorepellent semaphorin III is induced in the fibroblast component of neural scar tissue formed following injuries of adult but not neonatal CNS. Mol Cell Neurosci 13:143-166.

Patapoutian A, Reichardt LF (2000) Roles of Wnt proteins in neural development and maintenance. Curr Opin Neurobiol 10:392-399.

Paxinos G, Watson C (1982) The rat brain in stereotaxic coordinates. Sydney: Academic Press.

Peifer M (1999) Signal transduction. Neither straight nor narrow. Nature 400:213-215.

Perou CM, Jeffrey SS, van de Rijn M, Rees CA, Eisen MB, Ross DT, Pergamenschikov A, Williams CF, Zhu SX, Lee JC, Lashkari D, Shalon D, Brown PO, Botstein D (1999) Distinctive gene expression patterns in human mammary epithelial cells and breast cancers. Proc Natl Acad Sci U S A 96:9212-9217.

Petrausch B, Jung M, Leppert CA, Stuermer CA (2000) Lesion-induced regulation of netrin receptors and modification of netrin-1 expression in the retina of fish and grafted rats. Mol Cell Neurosci 16:350-364.

Pettigrew DB, Crutcher KA (1999) White matter of the CNS supports or inhibits neurite outgrowth in vitro depending on geometry. J Neurosci 19:8358-8366.

Pinder JC, Baines AJ (2000) A protein accumulator. Nature 406:253-254.

Pollard TD, Blanchoin L, Mullins RD (2001) Actin dynamics. J Cell Sci 114:3-4.

Polleux F, Giger RJ, Ginty DD, Kolodkin AL, Ghosh A (1998) Patterning of cortical efferent projections by semaphorin-neuropilin interactions. Science 282:1904-1906.

Prinjha R, Moore SE, Vinson M, Blake S, Morrow R, Christie G, Michalovich D, Simmons DL, Walsh FS (2000) Inhibitor of neurite outgrowth in humans. Nature 403:383-384.

Puschel AW (1999) Semaphorins: repulsive guidance molecules show their attractive side. Nat Neurosci 2:777-778.

Quinn CC, Gray GE, Hockfield S (1999) A family of proteins implicated in axon guidance and outgrowth. J Neurobiol 41:158-164.

Raivich G, Jones LL, Kloss CU, Werner A, Neumann H, Kreutzberg GW (1998) Immune surveillance in the injured nervous system: T-lymphocytes invade the axotomized

mouse facial motor nucleus and aggregate around sites of neuronal degeneration. J Neurosci 18:5804-5816.

Ramer MS, Priestley JV, McMahon SB (2000) Functional regeneration of sensory axons into the adult spinal cord. Nature 403:312-316.

Ramon y Cajal S (1928) Degeneration and regeneration of the nervous system. London: Oxford University Press.

Ramon-Cueto A, Avila J (1998) Olfactory ensheathing glia: properties and function. Brain Res Bull 46:175-187.

Ramon-Cueto A, Plant GW, Avila J, Bunge MB (1998) Long-distance axonal regeneration in the transected adult rat spinal cord is promoted by olfactory ensheathing glia transplants. J Neurosci 18:3803-3815.

Ramon-Cueto A, Cordero MI, Santos-Benito FF, Avila J (2000) Functional recovery of paraplegic rats and motor axon regeneration in their spinal cords by olfactory ensheathing glia. Neuron 25:425-435.

Rapalino O, Lazarov Spiegler O, Agranov E, Velan GJ, Yoles E, Fraidakis M, Solomon A, Gepstein R, Katz A, Belkin M, Hadani M, Schwartz M (1998) Implantation of stimulated homologous macrophages results in partial recovery of paraplegic rats. Nat Med 4:814-821.

Redmond L, Oh SR, Hicks C, Weinmaster G, Ghosh A (2000) Nuclear Notch1 signaling and the regulation of dendritic development. Nat Neurosci 3:30-40.

Reier PJ, Perlow MJ, Guth L (1983) Development of embryonic spinal cord transplants in the rat. Brain Res 312:201-219.

Renaudin A, Lehmann M, Girault J, McKerracher L (1999) Organization of point contacts in neuronal growth cones. J Neurosci Res 55:458-471.

Reuther GW, Der CJ (2000) The Ras branch of small GTPases: Ras family members don't fall far from the tree. Curr Opin Cell Biol 12:157-165.

Richardson PM, McGuinness UM, Aguayo AJ (1980) Axons from CNS neurons regenerate into PNS grafts. Nature 284:264-265.

Ross DT, Scherf U, Eisen MB, Perou CM, Rees C, Spellman P, Iyer V, Jeffrey SS, Van de Rijn M, Waltham M, Pergamenschikov A, Lee JC, Lashkari D, Shalon D, Myers TG, Weinstein JN, Botstein D, Brown PO (2000) Systematic variation in gene expression patterns in human cancer cell lines. Nat Genet 24:227-235.

Sadot E, Simcha I, Shtutman M, Ben-Ze'ev A, Geiger B (1998) Inhibition of beta-catenin-mediated transactivation by cadherin derivatives. Proc Natl Acad Sci U S A 95:15339-15344.

Saunders PA, Chalecka-Franaszek E, Chuang DM (1997) Subcellular distribution of glyceraldehyde-3-phosphate dehydrogenase in cerebellar granule cells undergoing cytosine arabinoside-induced apoptosis. J Neurochem 69:1820-1828.

Savio T, Schwab ME (1990) Lesioned corticospinal tract axons regenerate in myelin-free rat spinal cord. Proc Natl Acad Sci U S A 87:4130-4133.

Sawa A, Khan AA, Hester LD, Snyder SH (1997) Glyceraldehyde-3-phosphate dehydrogenase: nuclear translocation participates in neuronal and nonneuronal cell death. Proc Natl Acad Sci U S A 94:11669-11674.

Schaden H, Stuermer CA, Bahr M (1994) GAP-43 immunoreactivity and axon regeneration in retinal ganglion cells of the rat. J Neurobiol 25:1570-1578.

Schimmoller F, Simon I, Pfeffer SR (1998) Rab GTPases, directors of vesicle docking. J Biol Chem 273:22161-22164.

Schlaepfer DD, Hunter T (1998) Integrin signalling and tyrosine phosphorylation: just the FAKs? Trends Cell Biol 8:151-157.

Schlaepfer DD, Jones KC, Hunter T (1998) Multiple Grb2-mediated integrin-stimulated signaling pathways to ERK2/mitogen-activated protein kinase: summation of both c-Src- and focal adhesion kinase-initiated tyrosine phosphorylation events. Mol Cell Biol 18:2571-2585.

Schnell L, Schwab ME (1993) Sprouting and regeneration of lesioned corticospinal tract fibres in the adult rat spinal cord. Eur J Neurosci 5:1156-1171.

Schnell L, Schneider R, Kolbeck R, Barde YA, Schwab ME (1994) Neurotrophin-3 enhances sprouting of corticospinal tract during development and after adult spinal cord lesion [see comments]. Nature 367:170-173.

Schober A, Huber K, Fey J, Unsicker K (1998) Distinct populations of macrophages in the adult rat adrenal gland: a subpopulation with neurotrophin-4-like immunoreactivity. Cell Tissue Res 291:365-373.

Schroeder WO, Wunderlich G, Mueller HW (1989) The postcommissural fornix in the rat brain: new aspects of its connections applying antero- and retrograde WGA-HRP-tracing in combination with hypothalamic fornix transection. (unpublished).

Schulze H, Schuler A, Stuber D, Dobeli H, Langen H, Huber G (1993) Rat brain glyceraldehyde-3-phosphate dehydrogenase interacts with the recombinant cytoplasmic domain of Alzheimer's beta-amyloid precursor protein. J Neurochem 60:1915-1922.

Schwaiger FW, Schmitt GH, Horvat A, Hager G, Streif R, Spitzer C, Gamal S, Breuer S, Brook GA, Nacimiento W, Kreutzberg GW (2000) Peripheral but not central axotomy induces changes in Janus kinases (JAK) and signal transducers and activators of transcription (STAT). Eur J Neurosci 12:1165-1176.

Segal JL, Pathak MS, Hernandez JP, Himber PL, Brunnemann SR, Charter RS (1999) Safety and efficacy of 4-aminopyridine in humans with spinal cord injury: a long-term, controlled trial. Pharmacotherapy 19:713-723.

Seidensticker MJ, Behrens J (2000) Biochemical interactions in the wnt pathway. Biochim Biophys Acta 1495:168-182.

Seidl EC (2000) Promising pharmacological agents in the management of acute spinal cord injury. Pharm Pract Manag Q 20:21-27.

Selkoe DJ (1999) Translating cell biology into therapeutic advances in Alzheimer's disease. Nature 399:A23-31.

Selkoe DJ (2000) Notch and presenilins in vertebrates and invertebrates: implications for neuronal development and degeneration. Curr Opin Neurobiol 10:50-57.

Sestan N, Artavanis-Tsakonas S, Rakic P (1999) Contact-dependent inhibition of cortical neurite growth mediated by notch signaling. Science 286:741-746.

Shibata H (1989) Descending projections to the mammillary nuclei in the rat, as studied by retrograde and anterograde transport of wheat germ agglutinin-horseradish peroxidase. J Comp Neurol 285:436-452.

Short DJ, El Masry WS, Jones PW (2000) High dose methylprednisolone in the management of acute spinal cord injury - a systematic review from a clinical perspective. Spinal Cord 38:273-286.

Shu T, Valentino KM, Seaman C, Cooper HM, Richards LJ (2000) Expression of the netrin-1 receptor, deleted in colorectal cancer (DCC), is largely confined to projecting neurons in the developing forebrain. J Comp Neurol 416:201-212.

Simcha I, Shtutman M, Salomon D, Zhurinsky J, Sadot E, Geiger B, Ben-Ze'ev A (1998) Differential nuclear translocation and transactivation potential of beta-catenin and plakoglobin. J Cell Biol 141:1433-1448.

Simons K, Zerial M (1993) Rab proteins and the road maps for intracellular transport. Neuron 11:789-799.

Sirover MA (1999) New insights into an old protein: the functional diversity of mammalian glyceraldehyde-3-phosphate dehydrogenase. Biochim Biophys Acta 1432:159-184.

Skaper SD, Walsh FS (1998) Neurotrophic molecules: strategies for designing effective therapeutic molecules in neurodegeneration. Mol Cell Neurosci 12:179-193.

Skene JH, Willard M (1981) Characteristics of growth-associated polypeptides in regenerating toad retinal ganglion cell axons. J Neurosci 1:419-426.

Skene JHP (1989) Axonal growth-associated proteins. Annual Review in Neuroscience 12:127-156.

Smith GM, Hale JH (1997) Macrophage/Microglia regulation of astrocytic tenascin: synergistic action of transforming growth factor-beta and basic fibroblast growth factor. J-Neurosci 17:9624-9633.

Song H, Ming G, He Z, Lehmann M, Tessier Lavigne M, Poo M (1998) Conversion of neuronal growth cone responses from repulsion to attraction by cyclic nucleotides Science 281:1515-1518.

Song HJ, Ming GL, Poo MM (1997) cAMP-induced switching in turning direction of nerve growth cones [published erratum appears in Nature 1997 Sep 25;389(6649):412]. Nature 388:275-279.

Stallcup WB, Beasley LL, Levine JM (1985) Antibody against nerve growth factor-inducible large external (NILE) glycoprotein labels nerve fiber tracts in the developing rat nervous system. J-Neurosci 5:1090-1101.

Stein E, Zou Y, Poo M, Tessier-Lavigne M (2001) Binding of DCC by netrin-1 to mediate axon guidance independent of adenosine A2B receptor activation. Science 291:1976-1982.

Steuer H, Fadale R, Muller E, Muller HW, Planck H, Schlosshauer B (1999) Biohybride nerve guide for regeneration: degradable polylactide fibers coated with rat Schwann cells. Neurosci Lett 277:165-168.

Stichel CC, Mueller HW (1994) Relationship between injury-induced astrogliosis, laminin expression and axonal sprouting in the adult rat brain. Journal of Neurocytology 23:615-630.

Stichel CC, Muller HW (1994) Extensive and long-lasting changes of glial cells following transection of the postcommissural fornix in the adult rat. Glia 10:89-100.

Stichel CC, Singer W, Zilles K (1990) Ultrastructure of PkC(II/III)-immunopositive structures in rat primary visual cortex. Exp Brain Res 82:575-584.

Stichel CC, Wunderlich G, Schwab ME, Mueller HW (1995a) Clearance of myelin constituents and axonal sprouting in the transected postcommissural fornix of the adult rat. European Journal of Neuroscience 7:401-411.

Stichel CC, Lips K, Wunderlich G, Mueller HW (1996) Reconstruction of transected postcommissural fornix in adult rat by Schwann cell suspension grafts. Experimental Neurology 140:21-36.

Stichel CC, Kappler J, Junghans U, Koops A, Kresse H, Mueller HW (1995b) Differential expression of the small chondroitin/dermatan sulfate proteoglycans decorin and biglycan after injury of the adult rat brain. Brain Research 704:263-274.

Stichel CC, Niermann H, D'Urso D, Lausberg F, Hermanns S, Muller HW (1999a) Basal membrane-depleted scar in lesioned CNS: characteristics and relationships with regenerating axons. Neuroscience 93:321-333.

Stichel CC, Hermanns S, Luhmann HJ, Lausberg F, Niermann H, D'Urso D, Servos G, Hartwig HG, Muller HW (1999b) Inhibition of collagen IV deposition promotes regeneration of injured CNS axons. Eur J Neurosci 11:632-646.

Strittmatter SM, Vartanian T, Fishman MC (1992) GAP-43 as a plasticity protein in neuronal form and repair. Journal of Neurobiology 23:507-520.

Stromberg I, Bygdeman M, Almqvist P (1992) Target-specific outgrowth from human mesencephalic tissue grafted to cortex or ventricle of immunosuppressed rats. J Comp Neurol 315:445-456.

Su QN, Namikawa K, Toki H, Kiyama H (1997) Differential display reveals transcriptional up-regulation of the motor molecules for both anterograde and retrograde axonal transport during nerve regeneration. Eur J Neurosci 9:1542-1547.

Sunaga K, Takahashi H, Chuang DM, Ishitani R (1995) Glyceraldehyde-3-phosphate dehydrogenase is over-expressed during apoptotic death of neuronal cultures and is recognized by a monoclonal antibody against amyloid plaques from Alzheimer's brain. Neurosci Lett 200:133-136.

Takahashi T, Fournier A, Nakamura F, Wang LH, Murakami Y, Kalb RG, Fujisawa H, Strittmatter SM (1999) Plexin-neuropilin-1 complexes form functional semaphorin-3A receptors. Cell 99:59-69.

Tanabe K, Nakagomi S, Kiryu-Seo S, Namikawa K, Imai Y, Ochi T, Tohyama M, Kiyama H (1999) Expressed-sequence-tag approach to identify differentially expressed genes following peripheral nerve axotomy. Brain Res Mol Brain Res 64:34-40.

Tatagiba M, Brosamle C, Schwab ME (1997) Regeneration of injured axons in the adult mammalian central nervous system. Neurosurgery 40:541-546; discussion 546-547.

Tatemoto K, Mutt V (1980) Isolation of two novel candidate hormones using a chemical method for finding naturally occurring polypeptides. Nature 285:417-418.

Tavares AT, Tsukui T, Izpisua Belmonte JC (2000) Evidence that members of the Cut/Cux/CDP family may be involved in AER positioning and polarizing activity during chick limb development. Development 127:5133-5144.

Tessier Lavigne M, Goodman CS (1996) The molecular biology of axon guidance. Science 274:1123-1133.

Tigyi G, Fischer DJ, Sebok A, Yang C, Dyer DL, Miledi R (1996) Lysophosphatidic acid-induced neurite retraction in PC12 cells: control by phosphoinositide-Ca2+ signaling and Rho. J Neurochem 66:537-548.

Tomatsuri M, Okajima S, Ide C (1993) Sprout formation at nodes of Ranvier of crush-injured peripheral nerves. Restorat Neurol Neurosci 5:275-282.

Tonkiss J, Rawlins JN (1992) Mammillary body lesions and restricted subicular output lesions produce long-lasting DRL performance impairments in rats. Exp Brain Res 90:572-582.

Torres R, Firestein BL, Dong H, Staudinger J, Olson EN, Huganir RL, Bredt DS, Gale NW, Yancopoulos GD (1998) PDZ proteins bind, cluster, and synaptically colocalize with Eph receptors and their ephrin ligands Neuron 21:1453-1463.

Touraine RL, Attie Bitach T, Manceau E, Korsch E, Sarda P, Pingault V, Encha Razavi F, Pelet A, Auge J, Nivelon Chevallier A, Holschneider AM, Munnes M, Doerfler W, Goossens M, Munnich A, Vekemans M, Lyonnet S (2000) Neurological phenotype in Waardenburg syndrome type 4 correlates with novel SOX10 truncating mutations and expression in developing brain. Am J Hum Genet 66:1496-1503.

Trapp BD, Ransohoff R, Rudick R (1999) Axonal pathology in multiple sclerosis: relationship to neurologic disability. Curr Opin Neurol 12:295-302.

Tseng CC, Jarboe LA, Landau SB, Williams EK, Wolfe MM (1993) Glucose-dependent insulinotropic peptide: structure of the precursor and tissue-specific expression in rat. Proc Natl Acad Sci U S A 90:1992-1996.

Tuszynski MH, Weidner N, McCormack M, Miller I, Powell H, Conner J (1998) Grafts of genetically modified Schwann cells to the spinal cord: survival, axon growth, and myelination. Cell-Transplant 7:187-196.

Tzeng SF, Kahn M, Liva S, De Vellis J (1999) Tumor necrosis factor-alpha regulation of the Id gene family in astrocytes and microglia during CNS inflammatory injury. Glia 26:139-152.

Usdin TB, Mezey E, Button DC, Brownstein MJ, Bonner TI (1993) Gastric inhibitory polypeptide receptor, a member of the secretin-vasoactive intestinal peptide receptor family, is widely distributed in peripheral organs and the brain. Endocrinology 133:2861-2870.

Varga ZM, Bandtlow CE, Erulkar SD, Schwab ME, Nicholls JG (1995) The critical period for repair of CNS of neonatal opossum (Monodelphis domestica) in culture: correlation with development of glial cells, myelin and growth-inhibitory molecules. Eur J Neurosci 7:2119-2129.

Venter JC, Adams MD, Myers EW, Li PW, Mural RJ, Sutton GG, Smith HO, Yandell M, Evans CA, Holt RA, Gocayne JD, Amanatides P, Ballew RM, Huson DH, Wortman JR, Zhang Q, Kodira CD, Zheng XH, Chen L, Skupski M, Subramanian G, Thomas PD, Zhang J, Gabor Miklos GL, Nelson C, Broder S, Clark AG, Nadeau J, McKusick VA, Zinder N, Levine AJ, Roberts RJ, Simon M, Slayman C, Hunkapiller M, Bolanos R, Delcher A, Dew I, Fasulo D, Flanigan M, Florea L, Halpern A, Hannenhalli S, Kravitz S, Levy S, Mobarry C, Reinert K, Remington K, Abu-Threideh J, Beasley E, Biddick K, Bonazzi V, Brandon R, Cargill M, Chandramouliswaran I, Charlab R, Chaturvedi K, Deng Z, Di Francesco V, Dunn P, Eilbeck K, Evangelista C, Gabrielian AE, Gan W, Ge W, Gong F, Gu Z, Guan P, Heiman TJ, Higgins ME, Ji RR, Ke Z, Ketchum KA, Lai Z, Lei Y, Li Z, Li J, Liang Y, Lin X, Lu F, Merkulov GV, Milshina N, Moore HM, Naik AK, Narayan VA, Neelam B, Nusskern D, Rusch DB, Salzberg S, Shao W, Shue B, Sun J, Wang Z, Wang A, Wang X, Wang J, Wei M, Wides R, Xiao C, Yan C, et al. (2001) The sequence of the human genome. Science 291:1304-1351.

Viollet C, Doherty P (1997) CAMs and the FGF receptor: an interacting role in axonal growth. Cell Tissue Res 290:451-455.

Virshup DM (2000) Protein phosphatase 2A: a panoply of enzymes. Curr Opin Cell Biol 12:180-185.

Volenec A, Bhogal RK, Moorman JM, Leslie RA, Flanigan TP (1997) Differential expression of DCC mRNA in adult rat forebrain. Neuroreport 8:2913-2917.

Wahl S, Barth H, Ciossek T, Aktories K, Mueller BK (2000) Ephrin-A5 induces collapse of growth cones by activating Rho and Rho kinase. J Cell Biol 149:263-270.

Walton M, Young D, Sirimanne E, Dodd J, Christie D, Williams C, Gluckman P, Dragunow M (1996) Induction of clusterin in the immature brain following a hypoxic-ischemic injury. Brain Res Mol Brain Res 39:137-152.

Wang KL, Roufogalis BD (1999) Ca2+/calmodulin stimulates GTP binding to the ras-related protein ral-A. J Biol Chem 274:14525-14528.

Wang LH, Strittmatter SM (1996) A family of rat CRMP genes is differentially expressed in the nervous system. J Neurosci 16:6197-6207.

Wang LH, Strittmatter SM (1997) Brain CRMP forms heterotetramers similar to liver dihydropyrimidinase. J Neurochem 69:2261-2269.

Wear MA, Schafer DA, Cooper JA (2000) Actin dynamics: assembly and disassembly of actin networks. Curr Biol 10:R891-895.

Webster MK, Goya L, Ge Y, Maiyar AC, Firestone GL (1993) Characterization of sgk, a novel member of the serine/threonine protein kinase gene family which is transcriptionally induced by glucocorticoids and serum. Mol Cell Biol 13:2031-2040.

Weidner N, Blesch A, Grill RJ, Tuszynski MH (1999) Nerve growth factor-hypersecreting Schwann cell grafts augment and guide spinal cord axonal growth and remyelinate central nervous system axons in a phenotypically appropriate manner that correlates with expression of L1. J Comp Neurol 413:495-506.

Weinmaster G (2000) Notch signal transduction: a real rip and more. Curr Opin Genet Dev 10:363-369.

White KP, Rifkin SA, Hurban P, Hogness DS (1999) Microarray analysis of Drosophila development during metamorphosis. Science 286:2179-2184.

Whittemore SR (1999) Neuronal replacement strategies for spinal cord injury. J Neurotrauma 16:667-673.

Wictorin K, Brundin P, Gustavii B, Lindvall O, Bjorklund A (1990) Reformation of long axon pathways in adult rat central nervous system by human forebrain neuroblasts. Nature 347:556-558.

Willert K, Shibamoto S, Nusse R (1999) Wnt-induced dephosphorylation of axin releases beta-catenin from the axin complex. Genes Dev 13:1768-1773.

Wilson MA, Gaze RM, Goodbrand IA, Taylor JS (1992) Regeneration in the Xenopus tadpole optic nerve is preceded by a massive macrophage/microglial response. Anat Embryol (Berl) 186:75-89.

Woerly S, Petrov P, Sykova E, Roitbak T, Simonova Z, Harvey AR (1999) Neural tissue formation within porous hydrogels implanted in brain and spinal cord lesions: ultrastructural, immunohistochemical, and diffusion studies. Tissue Eng 5:467-488.

Wolthuis RM, Bos JL (1999) Ras caught in another affair: the exchange factors for Ral. Curr Opin Genet Dev 9:112-117.

Wong JT, Wong ST, O'Connor TP (1999) Ectopic semaphorin-1a functions as an attractive guidance cue for developing peripheral neurons. Nat Neurosci 2:798-803.

Woodbury D, Schwarz EJ, Prockop DJ, Black IB (2000) Adult rat and human bone marrow stromal cells differentiate into neurons. J Neurosci Res 61:364-370.

Wunderlich G, Stichel CC, Schroeder WO, Muller HW (1994) Transplants of immature astrocytes promote axonal regeneration in the adult rat brain. Glia 10:49-58.

Xie XY, Barrett JN (1991) Membrane resealing in cultured rat septal neurons after neurite transection: evidence for enhancement by Ca(2+)-triggered protease activity and cytoskeletal disassembly. J Neurosci 11:3257-3267.

Xu XM, Zhang SX, Li H, Aebischer P, Bunge MB (1999) Regrowth of axons into the distal spinal cord through a Schwann-cell-seeded mini-channel implanted into hemisected adult rat spinal cord. Eur J Neurosci 11:1723-1740.

Yang X, Khosravi-Far R, Chang HY, Baltimore D (1997) Daxx, a novel Fas-binding protein that activates JNK and apoptosis. Cell 89:1067-1076.

Yao GL, Kiyama H, Tohyama M (1992) Distribution of GAP-43 (B50/F1) mRNA in the adult rat brain by in situ hybridization using alkaline phosphatase labeled probe. Molecular Brain Research 18:1-16.

Yao R, Yoshihara M, Osada H (1997) Specific activation of a c-Jun NH2-terminal kinase isoform and induction of neurite outgrowth in PC-12 cells by staurosporine. J Biol Chem 272:18261-18266.

Yip RG, Wolfe MM (2000) GIP biology and fat metabolism. Life Sci 66:91-103.

Yong VW, Krekoski CA, Forsyth PA, Bell R, Edwards DR (1998) Matrix metalloproteinases and diseases of the CNS. Trends Neurosci 21:75-80.

Zagrebelsky M, Buffo A, Skerra A, Schwab ME, Strata P, Rossi F (1998) Retrograde regulation of growth-associated gene expression in adult rat Purkinje cells by myelin-associated neurite growth inhibitory proteins. J Neurosci 18:7912-7929.

Zhang JH, Cerretti DP, Yu T, Flanagan JG, Zhou R (1996) Detection of ligands in regions anatomically connected to neurons expressing the Eph receptor Bsk: potential roles in neuron-target interaction. J Neurosci 16:7182-7192.

Zhang MQ (1999) Large-scale gene expression data analysis: a new challenge to computational biologists. Genome Res 9:681-688.

Zhang Q, Mason CA (1998) Developmental regulation of mossy fiber afferent interactions with target granule cells. Dev Biol 195:75-87.

Zhang Y, Roslan R, Lang D, Schachner M, Lieberman AR, Anderson PN (2000) Expression of CHL1 and L1 by neurons and glia following sciatic nerve and dorsal root injury. Mol Cell Neurosci 16:71-86.

Zheng JQ (2000) Turning of nerve growth cones induced by localized increases in intracellular calcium ions. Nature 403:89-93.

Zhou J, Liyanage U, Medina M, Ho C, Simmons AD, Lovett M, Kosik KS (1997) Presenilin 1 interaction in the brain with a novel member of the Armadillo family. Neuroreport 8:1489-1494.

Zhou L, Connors T, Chen DF, Murray M, Tessler A, Kambin P, Saavedra RA (1999) Red nucleus neurons of Bcl-2 over-expressing mice are protected from cell death induced by axotomy. Neuroreport 10:3417-3421.

Zhou Q, Wang S, Anderson DJ (2000) Identification of a novel family of oligodendrocyte lineage-specific basic helix-loop-helix transcription factors. Neuron 25:331-343.

Zhou R (1997) Regulation of topographic projection by the Eph family receptor Bsk (EphA5) and its ligands. Cell Tissue Res 290:251-259.

Zhou R, Copeland TD, Kromer LF, Schulz NT (1994) Isolation and characterization of Bsk, a growth factor receptor-like tyrosine kinase associated with the limbic system. J Neurosci Res 37:129-143.

Zisch AH, Pasquale EB (1997) The Eph family: a multitude of receptors that mediate cell recognition signals. Cell-Tissue-Res 290:217-226.

Ziv NE, Spira ME (1997) Localized and transient elevations of intracellular Ca2+ induce the dedifferentiation of axonal segments into growth cones. J Neurosci 17:3568-3579.

Zuo J, Ferguson TA, Hernandez YJ, Stetler Stevenson WG, Muir D (1998) Neuronal matrix metalloproteinase-2 degrades and inactivates a neurite-inhibiting chondroitin sulfate proteoglycan. J Neurosci 18:5203-5211.

7. ABBREVIATIONS

AD	Alzheimers disease
ADAM	A Disintegrin And Metalloprotease
BDNF	brain derived neurotrophic factor
CA	cornu ammonis
CAM	cell adhesion molecules
CaMKII	calcium/calmodulin-dependent protein kinase II
cAMP	cyclic-adenosinemonophosphate
cc	corpus callosum
cdk 5	cyclin-dependent kinase 5
cDNA	copy desoxyribonucleic acid
cGMP	cyclic-guanosinemonophosphate
CN	calcineurin
CNS	central nervous system
CRMP-4	collapsin response mediator protein 4
CSPG	chondroitinsulphate proteoglycan
d	day(s)
DCC	deleted in colorectal cancer
DEPC	diethyl-pyrogencarbonate
DG	dentate gyrus
DPY	2,2'-dipyridyl
DRG	dorsal root ganglia
ECM	extracellular matrix
FGF	fibroblast growth factor
Fig.	figure
GAP-43	growth associated protein 43 kDa
GAPDH	glyceraldehyde-3-phosphate
GPI	glycosylphosphatidyl-inositol
HiF	hippocampal formation
Hif	hippocampal formation
MAP2	microtubule associated protein 2
MD	multiple sclerosis
MMP-2	matrix metalloprotease 2
mRNA	messenger ribonucleic acid
MS	multiple sclerosis
NCAM	nerve CAM
NP-1/2	neuropilin-1/2
NT-3	neurotrophin-3
PAM	pan-axonal marker
PB	phosphate buffer
PBS	phosphate buffered saline
PKA	protein kinase A
PKC	protein kinase C
PL	post lesion
PLC γ	phospholipase C γ
Plex 1	Plexin 1
PMO	plasma membrane oxidoreductase
PNS	peripheral nervous system

rMDC15	rat metalloprotease/disintegrin/cystein-rich 15
RT-PCR	reverse transcription-polymerase chain reaction
RZPD	resource center/primary database
S	subicular complex
SCI	spinal cord injury
SH2/3	Src-homology-2/3
SSC	saline-sodium citrate
TGF-β1	transforming growth factor-β1
TOAD	turned on after division
Ulip	Unc-like-protein
w	weeks

8. APPENDICES

Appendix A

+2SD-list stage (i) -acute lesion, 1d PL-

+2SDcutoff	%maxRVal
10,77	29,92

avRVal		SD	%SD	%maxRVal
2,97	+/-	3,90	131	8,26

#genes
32

RVal	POS	NEG	Coord.	av REG	SD av REG	genes
12	4	16	A05e	-5,0	7,0	Jun-B; c-jun-related transcription factor
14	18	4	A06g	3,8	4,1	DNA-binding protein inhibitor ID1
14	14	0	A14k	3,6	1,1	phospholipid hydroperoxide glutathione peroxidase
13	14	1	B07d	2,6	1,9	high affinity L-proline transporter
13	16	3	B14g	9,7	12,9	nonspecific lipid-transfer protein precursor (NSL-TP)
13	16	3	C01n	5,6	6,3	rab GDI, beta species, ras related GTPase
12	15	3	C02a	2,2	3,8	Rab GDI alpha; Rab GDP-dissociation inhibitor alpha; GDI-1
11	14	3	C08f	2,8	3,6	aldehyde dehydrogenase 2, retinaldehyde-specific
12	12	0	C09g	3,1	0,8	dopa/tyrosine sulfotransferase
11	12	1	C10c	4,6	4,4	ceruloplasmin precursor (CP); ferroxidase
13	1	14	C12e	-19,5	25,2	mitochondrial elongation factor G precursor (MEF-G)
12	1	13	D05m	-4,1	2,8	5-hydroxytryptamine 5A receptor (5HT5A; HTR5A); serotonin receptor; REC17
11	2	13	D07l	-2,5	2,3	melanocortin receptor 4
14	6	20	D08n	-1,3	5,3	N-methyl-D-aspartate receptor (NMDAR1)
11	0	11	D12n	-34,6	37,0	glutamate receptor, metabotropic 4
11	5	16	D13m	-3,9	6,6	neurokinin B precursor (neuromedin K)
13	0	13	E01m	-3,3	1,2	neurotrophin 3 precursor (NTF3); (NGF2); NT3
14	0	14	E05m	-3,5	2,0	insulin-like growth factor-binding protein 5 precursor (IGFBP5)
13	0	13	E10n	-5,6	3,8	serine/threonine kinase PCTAIRE2 (PCTK2)
14	0	14	E14j	-2,8	0,6	rab15, ras related GTPase
12	2	14	E14k	-2,3	1,9	rab14, ras related GTPase
14	2	16	E14l	-4,5	4,9	rab16, ras related GTPase
13	2	15	F03j	-8,1	9,4	calbindin D28; avian- type vitamin D-dependent calcium-binding protein (CABP)
13	2	15	F03l	-1,9	1,6	Calcineurin B subunit
14	0	14	F03n	-3,5	1,4	NVP; neural visinin-like Ca2+-binding protein
12	0	12	F05m	-2,9	0,4	ADP-ribosylation factor 3 (ARF3)
13	0	13	F09l	-4,5	2,0	proteasome component C3
14	5	19	F09m	-5,5	6,6	proteasome component C8
11	0	11	F11l	-3,5	1,3	Cak tyrosine-protein kinase; EDDR1; Trk-E; Ptk-3; discoidin receptor
12	1	13	F13k	-5,9	6,5	plectin
14	1	15	F14h	-5,7	2,6	replication protein A 32-kDa subunit (RPA); replication factor-A protein 2 (RPA2)
14	1	15	G31	-8,1	6,7	ornithine decarboxylase (ODC)

Appendix B

+2SD-list stage (ii) -axonal outgrowth, 7d PL-

+2SDcutoff	%maxRVal
4,86	30,36

avRVal		SD	%SD	%maxRVal
1,34	+/-	1,76	131	8,40

#genes
52

RVal	POS	NEG	Coord.	av REG	SD av REG	genes
5	1	6	A01h	-2,3	2,2	CD9, surface glycoprotein, platelet
5	0	5	A02n	-2,5	0,5	BIG-1 ; neural cell adhesion protein; neurite outgrowth-promotor
5	0	5	A03i	-10,5	8,5	CD8, 37 kDa membrane protein, thymocyte
5	1	6	A04a	-2,6	2,4	tumor necrosis factor receptor 1 (TNF-R1; 55 kDa)
6	0	6	A04c	-2,8	0,7	interleukin-6 receptor ligand binding chain
5	5	0	A10g	124,4	120,7	c-fos proto-oncogene
5	5	0	A11g	4,2	1,9	DCC; netrin receptor
6	1	7	B05l	-2,7	2,2	potassium channel drk1, delayed rectifier
5	0	5	B06i	-2,7	0,6	potassium channel, voltage gated, KV3.1; RAW2; KV4; NGK2; KCNC1
5	6	1	B07d	2,4	2,1	high affinity L-proline transporter
6	0	6	B07n	-2,5	0,4	neuronal high-affinity glutamate transporter; nerve injury-inducible ; EAAC1
5	0	5	B08h	-2,3	0,2	sodium/hydrogen exchange protein 4
5	5	0	B10g	5,4	2,0	ATPase, hydrogen-potassium, alpha 2a subunit
5	5	0	B10i	3,3	1,0	ATPase, sodium/potassium, alpha(+) isoform catalytic subunit
5	0	5	B12k	-2,9	0,8	MYELIN BASIC PROTEIN S (MBP S)
6	6	0	B14e	5,1	1,2	fatty acid-binding protein (heart; H-FABP)
5	0	5	C01a	-2,6	0,4	syntaxin 5 (STX5)
6	6	0	C02i	4,3	1,7	aldolase C
6	7	1	C03d	2,3	3,1	testis-specific cytochrome C (CYCT)
5	0	5	C03g	-53,6	54,3	ATPase, subunit F, vacuolar (vatf)
5	8	3	C03k	4,6	7,7	cytochrome c oxidase, subunit VIIa
5	5	0	C04d	5,7	2,4	ATP synthase, H+, alpha subunit, mitochondrial
6	8	2	C07e	3,0	3,7	cytochrome P450 2C7 (CYP2C7); P450F; PTF1
5	5	0	C07k	2,5	0,5	cytochrome P-450 2J3
6	7	1	C08k	2,5	2,2	cytosolic thymidine kinase (TK1)
5	6	1	C09d	4,5	4,6	glutamate-cysteine ligase regulatory subunit (GLCLR)
5	6	1	C10g	6,2	6,6	11-beta-hydroxysteroid dehydrogenase 2
5	5	0	C11j	6,4	2,7	ribosomal protein L12
5	1	6	C12e	-1,8	2,2	mitochondrial elongation factor G precursor (MEF-G)
6	1	7	C12h	-15,6	18,6	bcl-2-associated death promoter (BAD)
6	7	1	D01j	6,3	7,0	interleukin-4 receptor
5	5	0	D01k	3,9	1,6	interleukin-1 receptor type I (IL-1R-1); P80
6	6	0	D04f	2,8	1,0	serotonin 5HT2 receptor
5	0	5	D07i	-3,1	0,8	galanin receptor 1
5	5	0	D14a	2,7	0,4	gastrin-releasing peptide precursor (GRP); neuromedin C
5	0	5	E03e	-5,4	2,4	prolactine like protein A (rPLP-A)
5	6	1	E03f	5,3	5,9	somatostatin
5	5	0	E04b	2,8	0,6	thyroid stimulating hormone, beta
5	0	5	E10h	-2,7	0,6	serum/glucocorticoid-regulated serine/threonine protein kinase (SGK)
5	5	0	E13c	3,1	1,0	transducin beta-1 subunit; GTP-binding protein G(i)/G(s)/G(t) beta subunit 1
5	0	5	E13k	-5,3	2,8	guanine nucleotide-binding protein G(I)/G(S)/G(O) gamma-7 subunit (GNG7)
5	0	5	E14h	-3,1	0,9	Rab-11A; Ras p21-like small GTP-binding protein; 24KG; YL8
5	5	0	F01h	4,7	2,3	phospholipase C gamma 1 9PLC gamma-1); PLC-II; PLC-148
6	0	6	F01k	-3,3	1,1	FKBP-rapamycin-associated protein (FRAP); rapamycin target protein (RAFT1)
5	5	0	F03a	2,5	0,5	adenylyl cyclase 4
6	6	0	F04b	2,6	0,7	NVP-3; neural visinin-like Ca2+-binding protein
5	8	3	F06b	2,7	4,6	ADP-ribosylation factor 6 (ARF6)
5	5	0	F06g	2,5	0,6	phospholipase A-2-activating protein (PLAP)
6	6	0	F08i	3,4	1,2	membrane-type matrix metalloproteinase MT3-MMP
5	5	0	F10g	3,5	1,6	26S protease regulatory subunit 7 (P26S7); MSS1; PSMC2
5	6	1	F13b	2,3	2,2	G protein coupled receptor, putative, GPR12
5	5	0	G27	8,4	4,1	glyceraldehyde 3-phosphate dehydrogenase (GAPDH)

Appendix C

+2SD-list stage (iii) -axonal growth arrest, 3w PL-

+2SDcutoff			%maxRVal
10,37			28,82

avRVal		SD	%SD	%maxRVal
2,80	+/-	3,79	135	7,78

#genes
44

RVal	POS	NEG	Coord.	av REG	SD av REG	genes
11	16	5	A03f	1,8	5,7	leukocyte surface antigen CD53; leukocyte antigen MRC-OX44
12	12	0	A05d	6,9	3,2	fos-related antigen 2 (FRA-2); FOSL2
12	12	0	A07c	2,5	0,5	G1/S-specific cyclin D3 (CCND3)
13	14	1	A08e	2,5	1,6	prothymosin-alpha (PTMA)
11	12	1	A10l	3,3	2,4	c-ets-1 proto-oncogene protein; p54
12	12	0	A10n	4,4	0,7	Rb; pp105; retinoblastoma susceptibility-associated protein; tumor suppressor gene
14	14	0	A12d	21,3	21,7	casein kinase II beta subunit (CKII; CSNK2B; CK2N); phosvitin
12	12	0	A13a	3,1	0,6	ras-GTPase-activating protein (GAP); ras p21 protein activator; p120GAP
13	13	0	A13e	3,5	1,1	NF-2; moesin-ezrin-radixin-like protein (MERLIN); shwannomin
11	11	0	A14b	24,4	21,6	thioredoxin peroxidase 1 (TDPX1); thioredoxin-dependent peroxide reductase 1
11	12	1	A14e	2,3	1,4	glutathione S-transferase Yb subunit; GST subunit 4 mu (GSTM2)
14	1	15	A14k	-3,5	2,4	phospholipid hydroperoxide glutathione peroxidase
14	14	0	B06c	6,1	3,4	potassium channel RB-IRK2, inward rectifier
11	11	0	B08b	2,5	0,3	fibroblast ADP/ATP carrier protein; ADP/ATP translocase 2
13	17	4	B09c	7,2	10,5	sodium/dicarboxylate cotransporter
12	12	0	B10d	3,6	1,3	sodium/potassium-transporting ATPase beta 2 subunit (ATP1B2)
11	12	1	B10i	7,5	7,0	ATPase, sodium/potassium, alpha(+) isoform catalytic subunit
11	11	0	B12d	3,5	1,5	organic anion transporter
14	14	0	B14g	2,7	0,5	nonspec. lipid-transfer protein prec. (NSL-TP); sterol carrier protein 2 (SCP2)
12	13	1	C07a	3,9	3,0	3-beta-hydroxysteroid dehydrogenase/delta-5-->-4 isomerase, type I
13	15	2	C08g	3,5	2,6	lysophospholipase
12	12	0	C12d	2,6	0,4	elongation factor 2 (EF2)
13	13	0	C14e	3,0	0,9	TRK-B; BDNF/NT-3 growth factor tyrosine kinase receptor
13	2	15	D01e	-4,2	4,5	LCR-1; put. chemokine and HIV coreceptor homolog; G protein-coupled receptor
11	12	1	D06g	3,0	2,0	opioid receptor-like orphan receptor
11	0	11	D12n	-4,0	2,4	glutamate receptor, metabotropic 4
12	0	12	E01m	-3,3	1,5	neurotrophin 3 precursor (NTF3); neurotrophic factor; NT3
13	3	16	E03i	-3,4	3,9	thymosin beta-like protein
11	2	13	E05n	-2,3	2,0	cocaine/amphetamine-induced rat transcript, CART
13	2	15	E06g	-7,2	9,6	F-spondin; secreted; promotes neural cell adhesion and neurite extension
12	0	12	E06n	-2,5	0,5	protein arginine N-methyltransferase 1
12	12	0	E08g	2,6	0,4	dual-specificity mitogen-activated protein kinase kinase 1 (MAPKK1)
11	2	13	E08m	-3,1	3,2	focal adhesion protein-tyrosine kinase (FAK)
12	12	0	E10c	6,7	2,8	Ctk; non-receptor protein tyrosine kinase (batk)
13	0	13	E11e	-4,4	2,4	cyclin-dependent kinase 4 (CDK4); cell division protein kinase 4; PSK-J3
12	0	12	E11k	-7,8	6,1	Syp; SH-PTP2; adaptor protein tyrosine phosphatase
12	1	13	E11n	-2,1	1,3	nuclear tyrosine phosphatase; PRL-1; affects cell growth
11	2	13	E12l	-2,0	1,9	phosphatase 2A, catalytic subunit, isotype alpha
14	0	14	E13n	-2,8	0,7	Ras-related GTPase, ARF-like 5
12	12	0	F01e	3,2	0,7	RalGDSB; GTP/GDP dissociation stimulator for a ras-related GTPase
14	14	0	F01g	5,8	4,0	RIN1; interacts directly with Ras and competes with Raf1
12	1	13	F05j	-2,7	1,7	PDGF-associated protein
12	2	14	F13k	-2,8	2,8	plectin
13	0	13	F13n	-2,5	0,4	cofilin

Appendix D

+3SD-list 1d PL KvsK (15)

+3SDcutoff	%maxRVal
9,43	62,86

avRVal		SD	%SD	%maxRVal
1,86	+/-	2,52	135	12,42

avRVal+3SD			
10,65	+/-	0,86	8

avRVal-stage(i)			
4,24	+/-	1,53	36

#genes
17

RVal	POS	NEG	Coord.	av REG	SD av REG	RVal-stage(i)
11	12	1	A02d	14,5	22,4	8
10	10	0	A08e	6,6	5,9	10
11	11	0	B08a	5,4	4,0	4
10	10	0	B10g	6,3	3,2	2
12	12	0	C01j	6,1	4,0	2
10	11	1	C02j	3,9	3,0	2
11	11	0	C09n	4,0	2,4	2
11	11	0	D01a	6,7	6,1	2
10	10	0	D01c	3,8	2,0	6
10	10	0	D02h	4,6	1,9	4
10	10	0	D05k	5,1	2,4	0
10	10	0	E01n	5,2	2,2	2
11	11	0	E08d	22,6	39,3	2
10	11	1	E09e	10,0	12,4	10
11	11	0	E09n	6,1	4,8	5
13	13	0	E14c	7,1	6,8	10
10	10	0	F08h	4,2	2,3	1

Appendix E

+3SD-list 3w PL KvsK (15)

+3SDcutoff	%maxRVal
6,84	45,61

avRVal		SD	%SD	%maxRVal
1,24	+/-	1,87	150	8,28

avRVal+3SD			
7,93	+/-	1,17	15

avRVal-stage(iii)			
4,54	+/-	0,58	13

#genes
28

RVal	POS	NEG	Coord.	av REG	SD av REG	RVal-stage(iii)
8	0	8	A02a	-16,0	15,2	2
9	9	0	A02f	4,9	1,7	1
8	0	8	A02g	-8,4	3,1	0
7	0	7	A05f	-4,2	1,9	1
8	1	9	A08b	-3,4	2,6	16
8	0	8	A12i	-5,3	1,5	1
8	8	0	A14m	2,9	0,8	2
7	0	7	B02c	-7,6	4,7	4
9	1	10	B04c	-6,3	4,8	10
7	9	2	B05h	2,3	2,9	3
8	2	10	B13d	-16,1	19,7	7
7	0	7	B14g	-3,0	0,7	14
8	9	1	B14l	6,2	5,0	0
8	0	8	C05n	-32,4	28,8	2
8	0	8	C08k	-7,2	4,6	9
8	0	8	D03n	-64,0	62,8	6
12	0	12	D05k	-4,9	3,1	5
8	0	8	D06n	-20,3	16,0	3
7	8	1	D08j	3,5	2,6	4
7	7	0	D09k	17,4	19,3	1
10	10	0	D13k	5,0	2,7	0
8	9	1	E05h	10,0	7,4	4
7	1	8	E12c	-4,2	2,7	8
7	2	9	F01j	-29,0	46,1	1
7	7	0	F09e	2,8	0,7	5
8	0	8	F10l	-3,0	0,9	2
7	1	8	F13g	-4,7	4,6	8
8	8	0	F14h	3,6	1,0	8

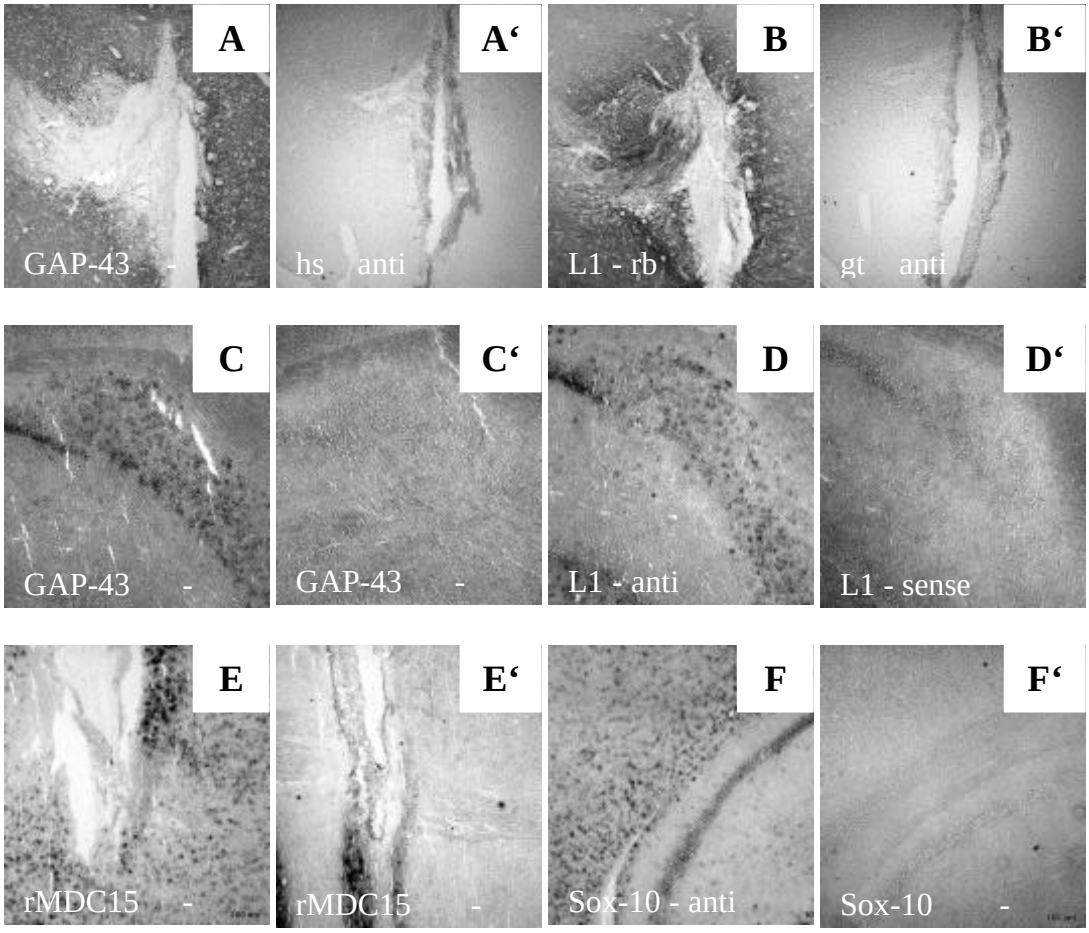

Appendix F. Negative controls. Demonstration of specificity of histological stainings. Pairs of adjacent histological sections are shown, which were either labeled by immunohistochemistry (A, A‘, B, B‘) or in situ hybridization (C-F‘). For immunolabelings the employed antibody and its host organism are specified (A, B) or the host of the secondary antibody and origin of the antigen (A‘, B‘) are indicated. For in situ hybridizations the employed antisense cRNA probes (C, D, E, F) and the respective sense controls (C‘, D‘, E‘, F‘) are indicated. Negative controls in A‘ and B‘ were treatet like the positive controls, except for omitting the primary antibody. In analogy, conditions for the negative controls C‘, D‘, E‘ and F‘ were identical to their positive counterparts, except for using the DIG-labeled sense strand.

The negative controls for immunohistochemical labelings (A‘, B‘) are also representative for the other primary antibodies used (calbindin, parvalbumin, pan axon marker and clusterin). Panel pairs A/A‘, B/B‘ and E/E‘ show the lesion site, C/C‘, D/D‘ show the dorsal subiculum and F/F‘ show the corpus callosum and part of the hippocampal CA1/2 region. All sections were made in the sagittal plane.

9. ACKNOWLEDGEMENTS

I am indepted to Prof. Hans Werner Müller for giving me the opportunity to work in his group and his support.

I am especially grateful to Dr. Patrick Küry for taking over responsibilities in part B, his excellent supervision, encouragement and friendship.

I want to thank the members of the Molecular Neurobiology Laboratory in Düsseldorf, for the friendly and motivating working atmosphere.

To all my friends, who believed in me during that catastrophe of my life, thank you for being there, when I needed you.

All my love to my family, my mom and dad for their love, encouragement, support and respect; my brother and sister for standing by my side during all this time; my greater family for their love and believing in me.

Julia, words cannot express how your love helps me. It couldn't be better than having a family with you.